WHITE LIGHT INTERFEROMETRIC SENSOR SYSTEMS

by

Dong Ning WANG

A Thesis Submitted for the Degree of
Doctor of Philosophy

CITY UNIVERSITY

Department of Electrical, Electronic
and Information Engineering

February 1995

To My Father

Table of Contents

List of Figures

List of Tables

Acknowledgements

Declaration

The author hereby grants powers of discretion to the City University Librarian to allow this thesis to be copied in whole or in part without further reference to him. This permission covers only single copies made for study purposes, subject to normal conditions of acknowledgement.

Abstract

Optical fibre sensor technology has been developed extensively over the past decade. It provides a means of measurement which is flexible, accurate, free of electromagnetic interference and non-destructive and is suitable for a chemically hazardous environment.

Among various kinds of optical fibre sensors explored so far, the interferometric type has received much attention as it exhibits the highest level of sensitivity. However, conventional interferometric optical fibre sensors have only limited unambiguous range. To overcome this difficulty, white light interferometry has been developed, which provides the possibility of performing an absolute and unambiguous measurement of physical parameters.

This thesis represents a study of the light sources, scanning techniques and applications of white light interferometric sensor systems.

As a technique of using non-monochromatic light sources, white light interferometry is based on coherence theory which is introduced in Chapter 2. The main low coherence light sources and scanning techniques currently used are also discussed.

Multimode laser diodes have become more and more popular in white light interferometry because of their large output power and good coupling efficiency into optical fibres, but they have relatively long coherence lengths, which may cause some difficulties in identifying the central fringe in the output fringe pattern as such a fringe provides a reliable reference position thus posessing crucial importance in performing high precision measurement.

It can be seen from Chapter 3 and Chapter 4 that, by the use of two wavelength or multiwavelength combination source techniques, especially when the wavelengths are optimized, the central fringe identification becomes relatively straightforward. The methods of selecting the optimum wavelength combinations are also demonstrated, with the help of computer simulations.

The price paid for the adoption of two wavelength or multiwavelength combination sources is an increased system complexity and alignment difficulty. As demonstrated in Chapter 5, an Ar-ion laser pumped Sm^{3+}-doped fibre provides an efficient and flexible means to generate a "pseudo" two wavelength and multiwavelength combination source without any additional difficulties in alignment. The fibre fluorescent sources may become highly competitive if a laser diode pumped system can be realized.

A conventional remote sensing white light interferometric system consists of two interferometers, of which one has to be scanned to recover the signals. An alternative optical scanning technique has been developed in Chapter 6, which shows distinct advantages over existing techniques by offering the possibility of eliminating one of the interferometers and thus simplifing the whole sensor system.

A simple optical sensor for eye length measurement is presented in Chapter 7, to explore the applications of white light interferometry. The principles of the system and the preliminary measurement results carried out on a simulated eye are presented.

Finally, the whole study is summarized and future research work is suggested.

Chapter 1

Introduction

1.1 Introduction

Optical fibre sensors have been a booming research area over the past decade, owing to their precise and non-destructive measurement capability and a series of advantages offered by the optical fibres, discussed in detail elsewhere [1-8]. The emergence of optical fibre sensors is due to the rapid development of optical fibre communications, which has made various kinds of optical fibre products and opto-electronic devices become commercially available.

An optical fibre sensor is an optical device in which the optical signal is modulated to follow the change of a measurand, usually physical or chemical, and the optical fibre is used either as a transmission medium or as a sensing element itself.

Since the optical fibre has small size and light weight and is made from dielectric and corrosion resistant material, the optical fibre sensor is normally mechanically flexible, intrinsically safe, immune to electromagnetic interference and suitable for a chemically hazardous environment. In addition, remote sensing can be realized, i.e. the light sources, detectors and signal processing electronics may be situated at different locations with respect to the sensor head. As a result, a wide range of optical fibre sensors has been explored in industrial, consumer, medical and military applications. Various kinds of physical and chemical measurands have been investigated [1-8].

In the early days of optical fibre sensor development, the research interests were dominated by the intensity modulated sensors because of their simplicity and low cost [1], [9-10]. However, this type of sensor is likely to be most affected by any power fluctuation of the light source and a variation of the transmission and connection losses

1

in the optical fibres, and for an accurate measurement, a reliable referencing scheme is always needed which may increase the system complexity as well as its cost.

In recent years, phase modulated or interferometric optical fibre sensors have been receiving considerable attention [11-15], as they have a high **sensitivity**, i.e. the response of the sensor to a change of measurand, and an accurate measurement can be readily achieved.

1.2 Interferometric Optical Fibre Sensors

Interference is a well-known optical phenomenon which occurs when two or more optical waves from the same source, travelling along different paths, are superposed in the same spatial region, resulting in a spatial intensity distribution variation. This phenomenon is a result of applying the **principle of superposition** [16] to the optical waves, which states that when two or more waves of the same nature pass through a point at the same time, the resultant amplitude is the sum of the amplitudes of the individual waves. According to this principle, if two monochromatic waves of the same frequency with electrical fields E_1 and E_2 respectively are overlapped at a given point in space, the result is also a monochromatic wave of the same frequency with electrical field

$$E = E_1 + E_2 \qquad (1.2.1)$$

The electrical field of a monochromatic light wave can be described by a real function of spatial position, **r**, and time, t, as

$$E(\mathbf{r}, t) = \mathbf{E}_0 \cos[\omega t - \mathbf{k} \cdot \mathbf{r} + \varphi(\mathbf{r})]$$

$$= \text{Re}\{\mathbf{E}_0 \exp\{i[\omega t - \mathbf{k} \cdot \mathbf{r} + \varphi(\mathbf{r})]\}\} \qquad (1.2.2)$$

where $\text{Re}\{\cdot\}$ denotes the real part of $\{\cdot\}$, $\mathbf{E}_0$ is a constant vector whose magnitude, E_0, is referred to as the **amplitude**, $\omega = 2\pi v$ is **angular frequency**, **k** is the **wave vector** or

2

propagation vector and $|\mathbf{k}| = 2\pi n/\lambda$, where n is the **refractive index** of the transmission medium and λ is the **wavelength** of the optical wave, and $\varphi(\mathbf{r})$ is the **initial phase**.

In the case of a scalar wave, the **complex wave function**

$$E(\mathbf{r}, t) = E_0 \exp\{i[\omega t - \mathbf{k} \cdot \mathbf{r} + \varphi(\mathbf{r})]\}$$

$$= E(\mathbf{r}) \exp(i\omega t) \qquad\qquad (1.2.3)$$

can be used to describe the wave completely as the wave function $E(\mathbf{r}, t)$ is simply the real part of $E(\mathbf{r}, t)$, i.e. $\mathrm{Re}\{E(\mathbf{r}, t)\} = E(\mathbf{r}, t)$, where $E(\mathbf{r}) = E_0 \exp\{-i[\mathbf{k} \cdot \mathbf{r} - \varphi(\mathbf{r})]\}$ is referred to as the **complex amplitude**.

For a monochromatic wave, the optical intensity is the absolute square of its complex amplitude, which does not vary with time, i.e.

$$I(\mathbf{r}) = |E(\mathbf{r})|^2 \qquad\qquad (1.2.4)$$

At a fixed spatial position, it can be written as

$$I = |E|^2 = E\, E^*$$

$$= (E_1 + E_2)(E_1 + E_2)^*$$

$$= |E_1|^2 + |E_2|^2 + E_1^*\, E_2 + E_1\, E_2^* \qquad\qquad (1.2.5)$$

where E^* represents the complex conjugate of E, which means that if $E = A + iB$, then $E^* = A - iB$, and E_1 and E_2 are the complex amplitudes of the two constituent waves respectively. Substituting

$$E_1 = E_{01} \exp\{-i[\mathbf{k_1} \cdot \mathbf{r} - \varphi_1(\mathbf{r})]\} \qquad\qquad (1.2.6)$$

$$E_2 = E_{02} \exp\{-i[\mathbf{k_2} \cdot \mathbf{r} - \varphi_2(\mathbf{r})]\} \qquad\qquad (1.2.7)$$

where E_{01} and E_{02} are the amplitudes, $\mathbf{k_1}$ and $\mathbf{k_1}$ are the propagation vectors and $\varphi_1(\mathbf{r})$ and $\varphi_2(\mathbf{r})$ are the initial phases of the two waves respectively. Hence

$$I = I_1 + I_2 + 2(I_1 I_2)^{1/2} \cos\varphi(\mathbf{r}) \qquad\qquad (1.2.8)$$

where $I_1 = |E_{01}|^2$, $I_2 = |E_{02}|^2$ and $\varphi(\mathbf{r}) = (\mathbf{k_1} - \mathbf{k_2}) \cdot \mathbf{r} - + \varphi_2(\mathbf{r}) - \varphi_1(\mathbf{r})$ is the **optical phase difference** between the two waves. Equation (1.2.8) is known as the **interference**

equation of the two monochromatic waves, and the last term of the equation, $2(I_1I_2)^{1/2}$ $\cos\varphi(\mathbf{r})$, is called the **interference term.**

According to the interference equation (1.2.8), the total intensity of the two superposed monochromatic waves is the sum of their individual intensities plus the interference term of the two waves. Since the interference term is dependent on the value of $\varphi(\mathbf{r})$, the total intensity also varies with $\varphi(\mathbf{r})$, and when

$$|\varphi(\mathbf{r})| = 2n\pi \qquad\qquad (n = 0, 1, 2, ...)$$

the total intensity becomes the maximum

$$I_{max} = I_1 + I_2 + 2(I_1I_2)^{1/2} \qquad\qquad (1.2.9)$$

and when $\qquad\qquad |\varphi(\mathbf{r})| = (2n + 1)\pi \qquad\qquad (n = 0, 1, 2, ...)$

the minimum value of the total intensity

$$I_{min} = I_1 + I_2 - 2(I_1I_2)^{1/2} \qquad\qquad (1.2.10)$$

can be observed.

As the phase difference $\varphi(\mathbf{r})$ is dependent on the spatial position, $\mathbf{r}$, the total intensity is also dependent on $\mathbf{r}$, and a periodic spatial distribution of optical intensity occurs, this being the **interference fringe**.

The interference effect can be generated by the use of an **interferometer** in which the optical waves from the same source are split into two waves, where each wave travels along a different path and then the two waves are recombined to enable the intensity of their superposition to be detected.

Since the output fringe intensity from the interferometer is sensitive to the optical phase difference between the two waves travelling along the different paths, the interferometer can be used as a means of optical sensing.

One of the simplest interferometers being explored for the sensor applications and also used in this research work, a Michelson interferometer, is illustrated in Fig.1.1, in both bulk optic and fibre versions respectively.

4

In the bulk optic configuration, as shown in Fig.1.1(a), the optical beam from the light source is split by a beam splitter into two, propagating along the sensing arm and the reference arm respectively. After travelling the length of the arms, the two beams are reflected back through the same arms by the corresponding mirrors, and then recombined by the same beam splitter. Finally, the recombined beam is received by a photodetector. This version is simple and suitable for use in the laboratory to demonstrate the principles of operation of a sensor system.
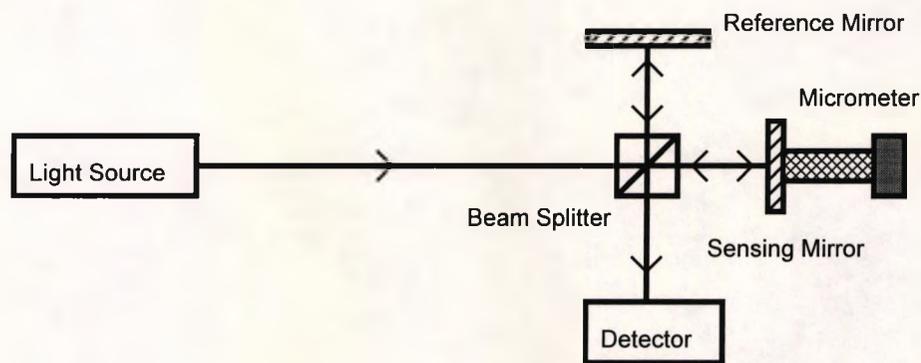
(a)
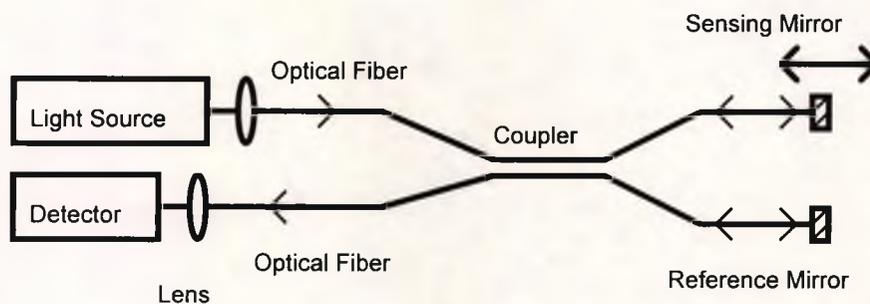
(b)

Fig.1.1 Michelson Interferometer Arrangement

(a) Bulk Optic Type

(b) Optical Fibre Type

In Fig.1.1(b), the light beam from the source is launched through a microscope objective lens into a single mode optical fibre in which only one propagation path or

mode of light beam can be supported. The light is then split into two beams of equal intensity by a coupler, where one of the beams is travelling along the sensing arm and is reflected back by the sensing mirror, and the other is sent through the reference arm and reflected back by the reference mirror. The two reflected beams are then recombined by the same coupler and received by the detector through another microscope objective lens. The optical fibre version provides a high mechanical flexibility for various system configurations and ease of alignment and hence this version is particularly suitable for a remote sensing optical system.

For the sake of simplicity, only the bulk optic Michelson interferometer is utilized in the investigations of this research work. However, the optical fibre version is also applicable and, in principle, the results are not dependent on the version adopted.

For a Michelson interferometer, if the light beam intensity from a monochromatic source is I_0, then in an ideal situation, i.e. without considering any optical losses, the output signal intensity from the interferometer, according to equation (1.2.8), can be simplified as [14]:

$$I = (I_0/2) \, (1 + \cos \varphi) \tag{1.2.11}$$

where φ is the optical phase difference between the two beams of the interferometer.

The optical phase difference can be written as

$$\varphi = 2\pi n l/\lambda \tag{1.2.12}$$

where n is the refractive index of the transmission medium, λ is the wavelength of the light source and l is the path difference between the sensing and reference arms. The product

$$x = nl \tag{1.2.13}$$

is referred to as the **optical path difference** (OPD) of the interferometer. Hence the optical phase difference becomes

$$\varphi = 2\pi x/\lambda \tag{1.2.14}$$

and

$$I = (I_0/2) [1 + \cos (2\pi x/\lambda)] \qquad\qquad (1.2.15)$$

By moving the sensing mirror position, i.e. changing the OPD between the two arms of the interferometer, x, the output fringe intensity from the interferometer will be changed accordingly. If x changes by a source wavelength, λ, resulting in a phase change of 2π, this will lead to a shift of one fringe. Hence, the distance moved by the sensing mirror can be readily determined in terms of the degree of fringe shift experienced.

For a stable monochromatic light source, the variation of OPD is given by

$$\Delta\varphi = (2\pi/\lambda) (n \, \Delta l + l \, \Delta n) \qquad\qquad (1.2.16)$$

which is related to the variation of refractive index and the path difference in an interferometer. The variation can then be designed to be stimulated by a desired physical measurand, and the output signal intensity will be varied accordingly. Therefore, an optical sensor system can be established by the use of an interferometer as the essential element of the device.

Interferometric optical fibre sensors exhibit extremely high sensitivity, especially when using a small wavelength light source, have a large **dynamic range**, i.e. the ratio of measurement range to **resolution**, where the resolution is the smallest change in a measurand to which the sensor can respond, and can be used for efficient multiplexing, i.e. the simultaneous transmission of several information channels along a common path or a fibre link in this case [8] [11]. A conventional interferometric optical fibre sensor utilizes a monochromatic, highly coherent light source such as a He-Ne laser, the output interference signals thus exhibiting a limited unambiguous phase range of 2π radians, equivalent to an OPD change of a wavelength of the light source used, owing to the periodic nature of the interferometer transfer function as indicated by the equation (1.2.11). Although by means of fringe counting or through the phase tracking technique [3], the unambiguous range can be significantly increased, a problem occurs when the measurement process is shutdown or interrupted by accident as the fringe order information may be lost. In this case, the measurement system has to be re-initialized.

Considerable efforts have been made to find more efficient methods to extend the unambiguous range [14-15] [17-29].

One solution is to use a highly birefringent (Hi-Bi) fibre as the sensing element [17], from which two optical outputs may be derived, each corresponding to one orthogonal linear polarization eigenmode of the fibre, and because of these different refractive indices, the two beams have a mutual phase delay when received by two photodetectors. The unambiguous range can be extended since it is now restricted by the condition that the change of phase delay is less than 2π radian. The performance of such a system, to a large extent, depends on the material properties of the optical fibres utilized, in which the birefringence may be difficult to be maintained as a constant.

Another approach is dual wavelength interferometric technique [18-21], which uses two light sources of different wavelengths, λ_1 and λ_2 respectively, to illuminate simultaneously an interferometer. The resultant interference fringe pattern possesses an **equivalent wavelength**, λ_{eq}, given by [18]

$$\lambda_{eq} = \lambda_1 \lambda_2 / |\lambda_1 - \lambda_2| \qquad (1.2.17)$$

The unambiguous range of the system can be determined by λ_{eq}, or is increased by a factor of $\lambda_2 / |\lambda_1 - \lambda_2|$ when compared with the case that only a single wavelength source λ_1 is used in the interferometer. As shown in the examples illustrated in the work of Kersey *et al* [20-21], the phase shifts induced by the variation of physical measurand are different for different wavelength sources, where the difference in the phase shift can then be determined by the interferometer path difference and the wavelength difference. This technique is flexible as the unambiguous range can in principle be controlled by selecting a suitable equivalent wavelength or wavelength difference of the two light sources. Furthermore, by means of the use of an appropriate signal processing technique [22], a direct detection of the phase difference, which is only sensitive to the equivalent wavelength can also be achieved, thus facilitating the measurement process, but with a decreased measurement resolution. Dual wavelength interferometry suffers a practical drawback that as the interferometer output is sensitive to the source wavelength drift,

the error introduced may become significant when the OPD generated by the measurand in the interferometer is considerably large.

On the other hand, the unambiguous range can also be extended by the use of wavelength tuning methods in which one laser diode is used as the light source, whose emitting wavelength can be controlled by the changing of the injection current. Since the variation of the optical phase difference between the two interfering beams is proportional to the wavelength shift and the OPD generated by the interferometer, then by examining the value of the wavelength shift and the phase difference change, the value of the OPD in the interferometer can be determined. However, the measurement resolution achieved is relatively low (~3μm) [23]. Alternatively, a tunable, double wavelength heterodyne detection interferometer may be employed to perform a high precision measurement with an extended unambiguous range by subsequently measuring two different synthetic wavelengths, the price paid being a considerably more complex system configuration [24].

In addition, another method, the frequency modulated continuous wave (FMCW) technique has also been used for the purpose of increasing the unambiguous range [25-28]. In this approach, the light source frequency is continuously modulated through a small amplitude by varying the driving current. Because of the time delay that exists between the reference beam and the sensing beam, a beat frequency is created, which is proportional to the OPD of the interferometer. Hence the OPD information can be obtained by the measurement of the beat frequency. However, the FMCW methods also suffer the disadvantage of relatively poor resolution (~ 2μm) [29].

It then becomes clear that although the unambiguous range can be significantly increased by the use of above techniques, there are associated problems which are clearly evident. Hence it is desirable to find a simple technique that can perform high precision measurement with a large unambiguous range where the results obtained are not affected by the source wavelength fluctuation and the property of the optical materials employed.

One of the suitable candidates for such an application is the method of white light interferometry [30-34]. The key to success for this technique lies in the fact that there exists a zero OPD position which can be used as a reliable reference point.

1.3 White Light Interferometry

When compared with conventional interferometric sensor systems, white light interferometry possesses the distinctive feature of employing a broadband light source which implies a short coherence length, as will be discussed in detail in the next Chapter. Consequently, the interference fringe obtained can only be observed when the OPD generated by the interferometer becomes nearly zero or less than the coherence length of the light source. Hence, in a simple one-interferometer sensor system, if a physical measurand-induced optical path length change is introduced to one of the arms of the balanced white light interferometer, the other arm has to be scanned to recover the signal. When the optical path lengths of the two arms are matched, the interference fringes appear, as shown schematically in Fig.1.2 (a). Thus the variation of the physical measurand can be determined from the scanning distance experienced by the interferometer. This technique has a much greater unambiguous measurement range and the result is not affected by the wavelength fluctuation, optical fibre transmission and connection loss, fibre material properties and possible system interruption, as a zero OPD position provides a reliable reference throughout the whole measurement process. A high precision measurement can also be achieved by the determination of the central fringe position (corresponding to the zero OPD) in the output interference fringe pattern of the interferometer.

Hence, white light interferometry opens up an efficient way to extend the system unambiguous range. Furthermore, this technique enables remote sensing to be done with a compact and passive sensor head [34-35], and to implement the concept of absolute position measurement [35].
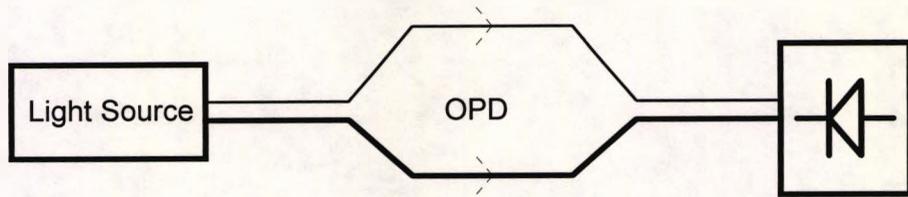
Interference fringe appears when OPD is within the coherence length

(a)
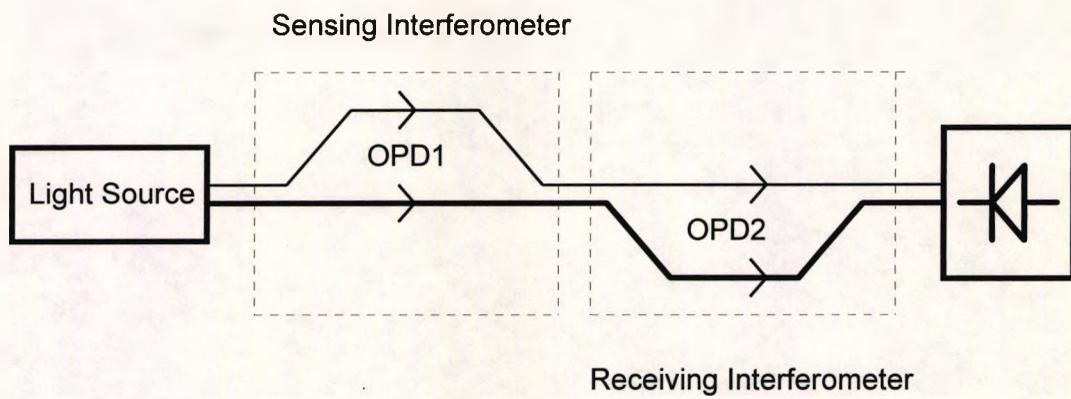
Maximum interference fringe appears when OPD1 - OPD2 = 0

(b)

Fig.1.2 Schematic of a White Light Interferometer

(a) Single Interferometer System

(b) Dual Interferometer System

A commonly used remote sensing white light interferometric system consists of a broadband light source, a sensing interferometer which transfers the measurand into OPD information and a local receiving interferometer to recover the signal by means of a scanning mechanism [32] [34]. When the absolute value of the OPD in the receiving interferometer can match that of the sensing interferometer as shown in Fig1.2 (b), a series of interference fringes can be seen. Since at the position corresponding to a balanced receiving interferometer, the interference fringes also appear, an absolute measurement can then be realized in this system in which the balanced position of the receiving interferometer becomes a readily determined absolute "zero" position. Hence, position can now be measured instead of displacement, thus extending the sensor applications [36]. The price paid, however, is the need for an extra interferometer to achieve remote sensing with a passive sensor head.

The advantages shown by white light interferometry have led to a number of applications, such as the measurement of temperature [37-38], strain [39-40], pressure [41-42], refractive index [43], dispersion [44] as well as position and displacement as mentioned above [36] [45]. An exploration has also been made in coherence multiplexing system, using such techniques [30] [46-50].

The challenges to white light interferometry also remain, such as to find new light sources and appropriate methods to identify efficiently the central fringe in the output fringe pattern of an interferometer, in order to achieve high precision measurement or, in the case of remote sensing, to eliminate the extra receiving interferometer thus simplifying the system configuration and to explore a wide range of white light interferometric sensor applications.

The significance of an investigation of white light interferometry is thus evident, and forms a major part of the work of this thesis.

1.4 About The Thesis

In summary, it is the intention of this thesis to study the performance and characteristics of several white light interferometric sensor systems, to make efforts to increase the system measurement precision, to reduce system complexity and to explore the possible system applications which result.

1.4.1 Aims and Objectives of This Thesis

The aims and objectives of this thesis are:

1. To develop the multiwavelength combination source technique that can readily and efficiently identify the central fringe position in the output interference fringe pattern of a white light interferometric system and hence increase the overall measurement precision.

2. To verify the existence of optimum wavelength combinations for a two wavelength combination source and a multiwavelength combination source. It will be shown that at this optimum wavelength combination, the minimum signal-to-noise ratio required by the system to identify the central fringe can reach its lowest possible value, and the work will aim to explain the method of selecting the optimum wavelength combinations for a given light source.

3. To explore the use of a Sm^{3+}-doped fibre as a low coherence light source for white light interferometry, which provides an alternative means to produce a two wavelength combination source, without additional alignment difficulty.

4. To develop an optical scanning technique as an alternative scanning mechanism to white light interferometry, which offers the possibility of eliminating the receiving interferometer in some cases and thus provide the potential to simplify the overall system configuration.

5. To present, as an application, a simple white light interferometric sensor for eye length measurement to show the possible uses of white light interferometry in one important medical system.

1.4.2 Structure of This Thesis

The structure of this thesis is as follows:

Chapter 1 gives a brief historic background to the emergence of white light interferometry which, as a powerful tool to overcome the ambiguity problem associated with conventional interferometric optical fibre sensor systems, becomes the prime concern of this thesis. The major advantages and existing problems of white light interferometry and the explanation of the structure and aims and objectives of this thesis are also provided by this Chapter.

The theoretical background of white light interferometry is included in Chapter 2. In order to understand the principle of white light interferometry which utilizes non-monochromatic light sources, the essential coherence theory required is introduced, followed by a detailed description of white light interferometric sensor system operation. The main white light sources and scanning mechanisms currently used are also discussed.

In Chapter 3, detailed discussions for the characteristics of the two wavelength combination sources are made and the method of selecting the optimum wavelength combinations is developed. Theoretical analysis, computer simulations and experimental verifications constitute a systematic investigation undertaken here.

An investigation of the characteristics and optimization of multiwavelength combination sources is carried out in Chapter 4. A comparison and assessment of single wavelength, two wavelength and three wavelength combination sources in terms of the minimum signal-to-noise ratio required by the corresponding system to identify the central fringe is also given, with a view to their optimization in a sensor system.

Chapter 5 presents a novel, efficient, and flexible means to produce a two wavelength combination source, i.e. to use an Ar-ion laser pumped Sm^{3+}-doped fibre. The spectral characteristics of Sm^{3+}-doped fibre are investigated and experimental results on its use in such a white light system are reported.

A new scanning technique as an alternative to white light interferometric sensing is described in Chapter 6. The principle of operation of this technique is described through appropriate theoretical analysis, followed by the necessary experimental confirmation.

In order to explore the possible applications in medicine, a dual Michelson white light interferometer configuration has been investigated for eye length measurement. Some preliminary experimental results carried out in a model eye are presented in Chapter 7. A brief review of previous work carried out in this field is also made, to set this application in context.

Finally, in Chapter 8, the totality of the work is summarized, major conclusions are made and some further studies are suggested.

References

1. T. G. Giallorenzi, J. A. Bucaro, A. Dandridge, G. H. Sigel, Jr., J. H. Cole, S. C. Rashleigh and R. G. Priest, "Optical Fiber Sensor Technology", IEEE Journal of Quantum Electronics, Vol.QE-18, No.4, pp.626-665, April 1982

2. B. E. Jones, "Optical Fiber Sensors and Systems for Industry", Journal of Physics E, Vol.18, pp.770-781, 1985

3. D. A. Jackson and J. D. C. Jones, "Fiber Optic Sensors", Optica Acta, Vol.33, No.12, pp.1469-1503,1986

4. T. G. Giallorenzi, J. A. Bucaro, A. Dandridge and J. H. Cole, "Optical-Fiber Sensors Challenge the Competition", IEEE Spectrum, pp.44-49, September 1986

5. K. T. V. Grattan, "Recent Advances in Fibre Optic Sensors", Measurement, Vol.5, No.3, pp.122-134, July-September 1987

6. K. T. V. Grattan, "New Developments in Sensor Technology — Fibre and Electro-Optics", Measurement + Control, Vol.22, pp.165-175, July/August 1989

7. J. D. C. Jones and J. Barton, "Rugged Optical Sensors Are Ready for Industry", Opto & Laser Europe, Issue 1, pp.26-33, September 1992

8. E. Udd, "Optical Fiber Sensors", Fiber and Integrated Optics, Vol.11, pp.319-336, 1992

9. B. Culshaw, "Optical Fibre Sensing and Signal Processing", Peter Peregrinus Ltd., 1984

10. R. S. Medlock, "Fibre Optic Intensity Modulated Sensors", NATO Series E: Applied Science, No.132, pp.131-142, Martinus Nijhoff Publishers, 1987

11. D. A. Jackson, "Monomode Fibre Optic Interferometers and Their Application in Sensing Systems", NATO ASI Series E: Applied Sciences, No. 132, pp.1-33, Martinus Nijhoff Publishers, 1987

12. D. A. Jackson and J. D. C. Jones, "Interferometers", in "Optical Fiber Sensors: Systems and Applications", Edited by B. Culshaw & J. Dakin, pp.329-380, Artech House, Inc., 1989

13. A. D. Kersey, "Recent Progress in Interferometric Fiber Sensor Technology", Proceedings of SPIE, Vol.1367, pp.1-12, 1990

14. A. Dandridge, "Fiber Optical Sensors Based on the Mach-Zender and Michelson Interferometers", in "Fiber Optic Sensors: An Introduction for Engineers and Scientists", Edited by E. Udd, pp.271-323, John Wiley & Sons, Inc., 1991

15. D. A. Jackson, "Recent Progress in Monomode Fiber-Optic Sensors", Measurement Science and Technology, Vol.5, pp.621-638, June 1994

16. E. Hecht and A. Zajac, "Optics", Second Edition, pp.242-243, Addison-Wesley Publishing Company, 1987

17. P. A. Leilabady, J. D. C. Jones, M. Corke and D. A. Jackson, "A Dual Interferometer Implemented in Parallel on a Single Birefringent Monomode Optical Fibre", Journal of Physics E, Vol.19, pp.143-146, 1986

18. J. C. Wyant, "Testing Aspherics Using Two-Wavelength Holography", Applied Optics, Vol.10, No.9, pp.2113-2118, September 1971

19. C. Polhemus, "Two Wavelength Interferometry", Applied Optics, Vol.12, No.9, pp.2071-2074, September 1973

20. A. D. Kersey, A. Dandridge and W. K. Burns, "Two-Wavelength Fibre Gyroscope with Wide Dynamic Range", Electronics Letters, Vol.22, No.18, pp.935-937, 28th August 1986

21. A. D. Kersey and A. Dandridge, "Dual-Wavelength Approach to Interferometric Sensing", Proceedings of SPIE., Vol.798, pp.176-181, 1987

22. R. Dändliker, R. Thalmann and D. Prongué, "Two Wavelength Laser Interferometry Using Superheterodyne Detection", Optics Letters, Vol.13, No.5, pp.339-341, May 1988

23. H.Kikuta, K. Iwata and R. Nagata, "Distance Measurement by the Wavelength Shift of Laser Diode Light", Applied Optics, Vol.25, No.17, pp.2976-2980, 1 September 1986

24. E. Gelmini, U. Minoni and F. Docchio, "Tunable, Double-Wavelength Heterodyne Detection Interferometer for Absolute-Distance Measurements", Optics Letters, Vol.19, No.3, pp.213-215, February 1, 1994

25. I. P. Giles, D. Uttam, B. Culshaw and D. E. N. Davies, "Coherent Optical-Fibre Sensors with Modulated Laser Sources", Electronics Letters, Vol.19, No.1, pp.14-15, 6th January 1983

26. G. Beheim and K. Fritsch, "Remote Displacement Measurements Using a Laser Diode", Electronics Letters, Vol.21, No.3, pp.93-94, 31st January 1985

27. D. Uttam and B. Culshaw, "Precision Time Domain Reflectometry in Optical Fiber System Using a Frequency Modulated Continuous Wave Ranging Technique", IEEE/OSA Journal of Lightwave Technology, Vol.LT-3, No.5, pp.971-977, May 1985

28. D. J. Webb, R. M. Taylor, J. D. C. Jones and D. A. Jackson, "Interferometric Optical Path Difference Measurement Using Sinusoidal Frequency Modulation of a Diode Laser", Optics Communications, Vol.66, No.5,6, pp.245-248, 15 May 1988

29. D J. Webb, J. D. C. Jones, R. M. Taylor and D. A. Jackson, "Extended Range Monomode Fibre-optic Sensors: Spectral and Polarisation Techniques", International Journal of Optoelectronics, Vol.3, No.3, pp.213-224, 1988

30. S. A. Al-Chalabi, B. Culshaw and D. E. N. Davies, "Partially Coherent Sources in Interferometric Sensors", Proceedings of the First International Optical Fiber Sensors Conference, pp.132-135, London, U.K., 1983

31. Th. Bosselmann and R. Ulrich, "High Accuracy Position Sensing with Fiber-coupled White Light Interferometers", Proceedings of the Second International Optical Fiber Sensors Conference, pp.361-365, Stuttgart, Germany, 1984

32. Th. Bosselmann, "Multimode-fiber Coupled White-Light Interferometric Position Sensor", NATO ASI Series E: Applied Science, No.132, pp.429-432, Martinus Nijhoff Publishers, 1987

33. R. Ulrich, "Interferometric and Polarimetric Sensors Using White-Light Interferometry", Proceedings of the 6th International Optical Fiber Sensors Conference, pp.62-77, Paris, France, September 18-20, 1989

34. H. C. Lefèvre, "White Light Interferometry in Optical Fiber Sensors", Proceedings of the 7th International Optical Fiber Sensors Conference, pp.345-351, Sydney, Australia, December 2-6, 1990

35. A. S. Gerges, F. Farahi, T. P. Newson, J. D. C. Jones and D. A. Jackson, "Fibre-Optic Interferometric Sensors Using a Low Coherence Source: Dynamic Range Enhancement", International Journal of Optoelectronics", Vol.3, No.4, pp.311-322, 1988

36. A. Koch and R. Ulrich, "Fiber-Optic Displacement Sensor with 0.02 μm Resolution by White-Light Interferometry", Sensors and Actuators A, 25-27, pp.201-207, 1991

37. C. Mariller and M. Lequime, "Fiber-Optic White-Light Birefringent Temperature Sensor", Proceedings of SPIE., Vol.798, pp.121-130, 1987

38. C. E. Lee and H. F. Taylor, "Fiber-Optic Fabry-Perot Temperature Sensor Using a Low-Coherence Light Source", IEEE/OSA Journal of Lightwave Technology, Vol.9, No.1, pp.129-134, January 1991

39. C. Belleville and G. Duplain, "White-Light Interferometric Multimode Fiber-Optic Strain Sensor", Optics Letters, Vol.18, No.1, pp.78-81, January 1, 1993

40. W. J. Bock, W. Urbanczyk and M. B. Zaremba, "Electronically Scanned White-Light Interferometric Strain Sensor Employing Highly Birefringent Fibers", Optics Communications, Vol.101, No.3,4, pp.157-162, 15 August 1993

41. M. T. Velluet, P. Graindorge and H. J. Arditty, "Fiber Optic Pressure Sensor Using White Light Interferometry", Proceedings of SPIE., Vol.838, pp.78-83, 1987

42. W. J. Bock and W. Urbanczyk, "Electronically Scanned White-Light Interferometric Sensor for High Hydrostatic Pressure Measurements", Proceedings of the 9th International Optical Fiber Sensors Conference, pp.135-138, Firenze, Italy, May 4-6, 1993

43. D. Trouchet, F. X. Desforges, P. Graindorge and H. C. Lefèvre, "Remote Fiber Optic Measurement of Air Index with White Light Interferometry", Proceedings of the 8th International Optical Fiber Sensors Conference, pp.57-60, Montery, USA, January 29-31, 1992

44. H. T. Shang, "Chromatic Dispersion Measurement by White-Light Interferometry on Metre-Length Single-Mode Optical Fibres", Electronics Letters, Vol.17, No.17, pp.603-605, 20th August 1981

45. A. Koch and R. Ulrich, "Displacement Sensor with Electronically Scanned White Light Interferometer", Proceedings of SPIE., Vol.1267, pp.126-133, 1990

46. J. L. Brooks, R. H. Wentworth, R. C. Youngquist, M. Tur, B. Y. Kim and H. J. Shaw, "Coherence Multiplexing of Fiber-Optic Interferometric Sensors", IEEE/OSA Journal of Lightwave Technology, Vol.LT-3, No.5, pp.1062-1072, October 1985

47. T. Y. Liu, J. Cory and D. A. Jackson, "Partially Multiplexing Sensor Network Exploiting Low Coherence Interferometry", Applied Optics, Vol.32, No.7, pp.1100-1103, 1 March 1990

48. S. Chen, B. T. Meggitt and A. J. Rogers, "Novel Electronic Scanner for Coherence Multiplexing in a Quasi-Distributed Pressure Sensor", Electronics Letters, Vol.26, No.17, pp.1367-1369, 16th August 1990

49. A. D. Kersey, "Distributed and Multiplexed Fiber Optical Sensors", in "Fiber Optic Sensors: An Introduction for Engineers and Scientists", Edited by E. Udd, pp.325-367, John Wiley & Sons, Inc., 1991

50. J. L. Santos and D. A. Jackson, "Coherence Sensing of Time-Addressed Optical-Fiber Sensors Illuminated by a Multimode Laser Diode", Applied Optics, Vol.30, No.34, pp.5068-5076, 1 December 1991

Chapter 2

Principles of White Light Interferometry

This Chapter introduces the basic coherence theory needed to study the interference effect generated by using a non-monochromatic light source in an interferometer. Based on this theory, the principles of white light interferometry are explained in terms of spectral domain analysis. The main low coherence light sources and the current scanning mechanisms employed in white light interferometry are also discussed.

2.1 Introduction

A commonly used white light interferometer has two distinct features when compared with a conventional interferometer in that it utilizes a non-monochromatic, broadband instead of a monochromatic light source and has an extra receiving interferometer to achieve remote sensing with a passive sensor head, by means of a scanning mechanism. Because of these features, an unambiguous, high precision and absolute position measurement can be realized in such a system and the results obtained from it are not perturbed by the system interruption, source wavelength drift and fibre transmission and link loss variations.

In contrast to a monochromatic light source which possesses only a single frequency or wavelength in its optical spectrum and a time-independent optical intensity, the non-monochromatic light sources usually have a specific spectral intensity distribution and to a certain extent, random light intensity fluctuations. This causes a significant effect on

the interference observed, which becomes a major concern of **optical coherence theory** [1-5]. Broadly speaking, such an optical coherence theory is expressed as a statistical description of the optical field fluctuations, considered in terms of correlation functions. As a technique of using non-monochromatic light sources, white light interferometry cannot be properly described without resorting to coherence theory.

In this Chapter, a basic optical coherence theory is introduced to meet the needs of studying white light interferometry. The principle of white light interferometry is explained in detail, in order to understand the system clearly and to consider how to make further possible improvements. The characteristics of different kinds of non-monochromatic, broadband light sources used in white light interferometry and the major receiving interferometer scanning techniques as the means to detect the measurand variations are also discussed.

2.2 Basic Coherence Theory

Coherence theory was developed first as a description of interference phenomena. If the two light beams can interfere, they are said to be **coherent**, which means that they have a fixed phase relationship one to the other. **Coherence** is a measure of the ability to interfere or, in other words, the extent to which the phase relationship can be maintained. **Temporal coherence** means that a fixed, time-independent phase relationship is existing between, for example, two points along the light beam, whilst **spatial coherence** means that the above relationship is maintained between two points across the light beam. The time interval during which the phase of the light wave is predictable is called the **coherence time**, and the corresponding distance is known as the **coherence length**.

Considering the scalar wave description, the electrical field of a non-monochromatic light wave can be represented by a Fourier integral

$$E(\mathbf{r}, t) = \int_{-\infty}^{\infty} E_v(\mathbf{r}) \exp(i2\pi vt)dv \qquad (2.2.1)$$

where

$$E_v(\mathbf{r}) = \int_{-\infty}^{\infty} E(\mathbf{r}, t) \exp(-i2\pi vt)dt \qquad (2.2.2)$$

is the Fourier transform of $E(\mathbf{r}, t)$ and the other terms have been defined in the previous chapter.

Since $E(\mathbf{r}, t)$ is a real function, $E_v(\mathbf{r})$ must be symmetric, i.e. $E_{-v}(\mathbf{r}) = E_v{}^*(\mathbf{r})$ and

$$\int_{-\infty}^{0} E_v(\mathbf{r}) \exp(i2\pi vt)dv$$

$$= \int_{0}^{\infty} E_{-v}(\mathbf{r}) \exp(-i2\pi vt)dv$$

$$= \int_{0}^{\infty} E_v{}^*(\mathbf{r}) \exp(-i2\pi vt)dv \qquad (2.2.3)$$

it follows that

$$E(\mathbf{r}, t) = \int_{0}^{\infty} [E_v(\mathbf{r}) \exp(i2\pi vt) + E_v{}^*(\mathbf{r}) \exp(-i2\pi vt)]dv \qquad (2.2.4)$$

The complex wave function for a non-monochromatic light wave may be defined as

$$E(\mathbf{r}, t) = 2 \int_{0}^{\infty} E_v(\mathbf{r}) \exp(i2\pi vt)dv \qquad (2.2.5)$$

hence the electrical field can be written as

$$E(\mathbf{r}, t) = Re\{E(\mathbf{r}, t)\} = (1/2) [E(\mathbf{r}, t) + E^*(\mathbf{r}, t)] \qquad (2.2.6)$$

The complex wave function defined above, $E(\mathbf{r}, t)$, is also known as the **analytic signal** associated with the optical wave of the electrical field, $E(\mathbf{r}, t)$. The advantage of

utilizing the complex wave function lies in the possibility of simplifying the calculations involved with the optical wave.

The optical wave, represented by $E(\mathbf{r}, t)$, is a random function, the average intensity of which may be defined as

$$I(\mathbf{r}, t) = \langle |E(\mathbf{r}, t)|^2 \rangle \qquad (2.2.7)$$

$\langle \cdot \rangle$ stands for an ensemble average over different realizations of the function, which is an average carried out from one possible wave function to another at a fixed time and position.

Assuming that the optical wave is stationary and ergodic (which means that the ensemble average of the optical wave is time-independent and in particular, equal to the corresponding time average of a typical member of the ensemble), then the average intensity can be determined by the time average over a long time interval

$$I(\mathbf{r}, t) = I(\mathbf{r}) = \langle |E(\mathbf{r}, t)|^2 \rangle = \lim_{T \to \infty} \frac{1}{T} \int_{-T/2}^{T/2} |E(\mathbf{r}, t)|^2 \, dt \qquad (2.2.8)$$

where T is the detection time interval of the optical wave.

Considering the light wave at a fixed spatial position as a function of time, it usually can be written that: $E(\mathbf{r}, t) = E(t)$ and $I(\mathbf{r}) = I$.

Without losing generality, two optical waves arriving at a point in space with a mutual time delay, τ, have a resultant average intensity given as

$$I = \langle |E_1(t + \tau) + E_2(t)|^2 \rangle$$

$$= \langle [E_1(t + \tau) + E_2(t)] \, [E_1(t + \tau) + E_2(t)]^* \rangle$$

$$= \langle E_1(t + \tau) \, E_1^*(t + \tau) \rangle + \langle E_2(t) \, E_2^*(t) \rangle$$

$$+ \langle E_1(t + \tau) \, E_2^*(t) \rangle + \langle E_1^*(t + \tau) \, E_2(t) \rangle \qquad (2.2.9)$$

For a stationary random process,

$$I_1 = \langle E_1(t) \, E_1^*(t) \rangle = \langle E_1(t + \tau) \, E_1^*(t + \tau) \rangle \qquad (2.2.10)$$

$$I_2 = \langle E_2(t) \, E_2^*(t) \rangle \qquad (2.2.11)$$

and

$$\langle E_1(t + \tau) E_2^*(t)\rangle + \langle E_1^*(t + \tau) E_2(t)\rangle = 2\text{Re}[\langle E_1(t + \tau) E_2^*(t)\rangle]$$

$$= 2\text{Re}[\Gamma_{12}(\tau)] \qquad (2.2.12)$$

where

$$\Gamma_{12}(\tau) = \langle E_1(t + \tau) E_2^*(t)\rangle \qquad (2.2.13)$$

is referred to as the **mutual coherence function**, and its normalized form

$$\gamma_{12}(\tau) = \Gamma_{12}(\tau) / [(\Gamma_{11}(0)\Gamma_{22}(0))]^{1/2} = \Gamma_{12}(\tau) / [I_1 I_2]^{1/2} \qquad (2.2.14)$$

is known as the **complex degree of mutual coherence**, where $\Gamma_{11}(0) = I_1$, $\Gamma_{22}(0) = I_2$ are also called the **self coherence function**.

Therefore,

$$I = I_1 + I_2 + 2\text{Re}[\Gamma_{12}(\tau)]$$

$$= I_1 + I_2 + 2(I_1 I_2)^{1/2} \text{Re}[\gamma_{12}(\tau)]$$

$$= I_1 + I_2 + 2(I_1 I_2)^{1/2} |\gamma_{12}(\tau)|\cos[\theta(\tau)] \qquad (2.2.15)$$

where $\theta(\tau)$ is the **optical phase difference** between the two light waves and equation (2.2.15) is known as the **interference equation** of the two non-monochromatic waves.

The **visibility** of the interference fringe pattern is often used to measure the strength of interference and is defined by

$$V = (I_{max} - I_{min}) / (I_{max} + I_{min}) \qquad (2.2.16)$$

where I_{max} and I_{min} are the maximum and minimum intensities of the interference fringes respectively. In terms of the interference equation, the visibility can be written as

$$V = 2(I_1 I_2)^{1/2} |\gamma_{12}(\tau)| / [I_1 + I_2] \qquad (2.2.17)$$

If the two optical waves are identical, $E_1(t) = E_2(t) = E(t)$, then the autocorrelation function, $\Gamma(\tau) = \langle E(t + \tau) E^*(t)\rangle$ is called the **temporal coherence function** (or **complex self coherence function**), and its normalized form,

$$\gamma(\tau) = \Gamma(\tau) / \Gamma(0)$$

$$= \langle E(t + \tau) \, E^*(t) \rangle \, / \, \langle E(t) \, E^*(t) \rangle \qquad (2.2.18)$$

is known as the **complex degree of temporal coherence**.

In general, the **coherence time**, τ_c, is defined by the width of $\gamma(\tau)$ as

$$\tau_c = \int_{-\infty}^{\infty} |\gamma(\tau)|^2 \, d\tau \qquad (2.2.19)$$

The corresponding **coherence length** is then

$$L_c = c\tau_c \qquad (2.2.20)$$

Assuming that a stationary optical wave, represented by the analytic signal E(t), is also an ergodic random process, then the amplitude associated with a frequency, ν, can be expressed in terms of the Fourier integral as

$$e(\nu) = \int_{-\infty}^{\infty} E(t) \exp(-i2\pi\nu t) dt \qquad \text{when } \nu \geq 0,$$

$$= 0 \qquad\qquad\qquad \text{when } \nu < 0 \qquad (2.2.21)$$

Introducing a truncate function, defined by

$$E_T(t) = E(t) \qquad \text{when } |t| \leq T/2$$

$$= 0 \qquad\qquad \text{when } |t| > T/2 \qquad (2.2.22)$$

then the truncated Fourier transform

$$e_T(\nu) = \int_{-T/2}^{T/2} E(t) \exp(-i2\pi\nu t) dt$$

$$= \int_{-\infty}^{\infty} E_T(t) \exp(-i2\pi\nu t) dt \qquad (2.2.23)$$

hence

$$\int_{-\infty}^{\infty} E_T^*(t) E_T(t + \tau) dt = \int_{-\infty}^{\infty} E_T^*(t) \{ \int_{-\infty}^{\infty} e_T(\nu) \exp[i2\pi\nu(t + \tau)] d\nu \} dt$$

$$= \int_{-\infty}^{\infty} e_T^*(\nu)e_T(\nu)\exp(i2\pi\nu\tau)d\nu$$

$$= \int_{-\infty}^{\infty} |e_T(\nu)|^2 \exp(i2\pi\nu\tau)d\nu \qquad (2.2.24)$$

The temporal coherence function

$$\Gamma(\tau) = \langle E(t+\tau)\, E^*(t) \rangle$$

$$= \lim_{T\to\infty}(1/T) \int_{-T/2}^{T/2} E(t+\tau)E^*(t)dt$$

$$= \lim_{T\to\infty}(1/T) \int_{-T/2}^{T/2} |e_T(\nu)|^2 \exp(i2\pi\nu\tau)d\nu$$

$$= \int_{-\infty}^{\infty} \lim_{T\to\infty} (|e_T(\nu)|^2/T)\exp(i2\pi\nu\tau)d\nu$$

$$= \int_{-\infty}^{\infty} S(\nu)\exp(i2\pi\nu\tau)d\nu \qquad (2.2.25)$$

where $S(\nu) = \lim_{T\to\infty}\dfrac{|e_T(\nu)|^2}{T}$ is known as the **power spectral density**, or **power spectrum**.

Therefore, the power spectrum and temporal coherence function form a Fourier transform pair as follows

$$\Gamma(\tau) = \int_{-\infty}^{\infty} S(\nu)\exp(i2\pi\nu\tau)d\nu \qquad (2.2.26)$$

This relation is known as **Wiener-Khinchin theorem** from which the average light intensity can be obtained as

$$I = \langle E(t)E^*(t) \rangle = \Gamma(0)$$

$$= \int_0^{\infty} S(\nu)d\nu \qquad (2.2.27)$$

27

as no negative frequency exists in the power spectrum.

From the characteristics of Fourier transform, the **spectral width** of $S(v)$ is inversely related to the width of $\gamma(\tau)$ and so is the coherence time, if the spectral width is defined by [5]

$$\Delta v_c = (\int_0^\infty S(v)dv)^2 / (\int_0^\infty S^2(v)dv) \qquad (2.2.28)$$

then a simple relation

$$\Delta v_c = 1/\tau_c \qquad (2.2.29)$$

can be obtained. It shows that the coherence time and hence the coherence length is inversely proportional to the source spectral width, or in other words, a broadband light source has a small coherence time and consequently, has a short coherence length.

For a Michelson interferometer illuminated by a non-monochromatic light source, $E_1(t) = E_2(t) = (1/2)E(t)$, $I_1 = I_2 = I_0/4$, where $I_0 = E_0^2/2$ is the source intensity. The interference equation (2.2.15) becomes

$$I = (I_0/2)\{1 + Re[\gamma(\tau)]\} \qquad (2.2.30)$$

Since

$$\gamma(\tau) = \Gamma(\tau) / I_0 = (1/I_0) \int_0^\infty S(v)\exp(i2\pi v\tau)dv \qquad (2.2.31)$$

and $\qquad I_0 = \int_0^\infty S(v)dv \qquad (2.2.32)$

then from equation (2.2.30), it follows that

$$I = (1/2) \int_0^\infty S(v)[1 + \cos(2\pi v\tau)]dv \qquad (2.2.33)$$

This equation shows the relation between the output interference intensity and the source power spectrum, which possesses crucial importance and forms the basis of the principles of white light interferometry, as will be seen in the next Section.

2.3 Principles of White Light Interferometry

A white light interferometric system may be considered as a spectral encoding and decoding system of the physical measurand. In such a system, the light beam from a broadband source is launched, usually through an optical fibre, into a sensing interferometer where the physical measurand is encoded into the power spectrum of the transmitted light and then sent to a receiving interferometer. The receiving interferometer is used to decode the spectrum and to recover the measurand [6-10].

In order to illustrate the principle, a typical white light interferometric position sensor system is shown in Fig.2.1, which uses two Michelson interferometers.
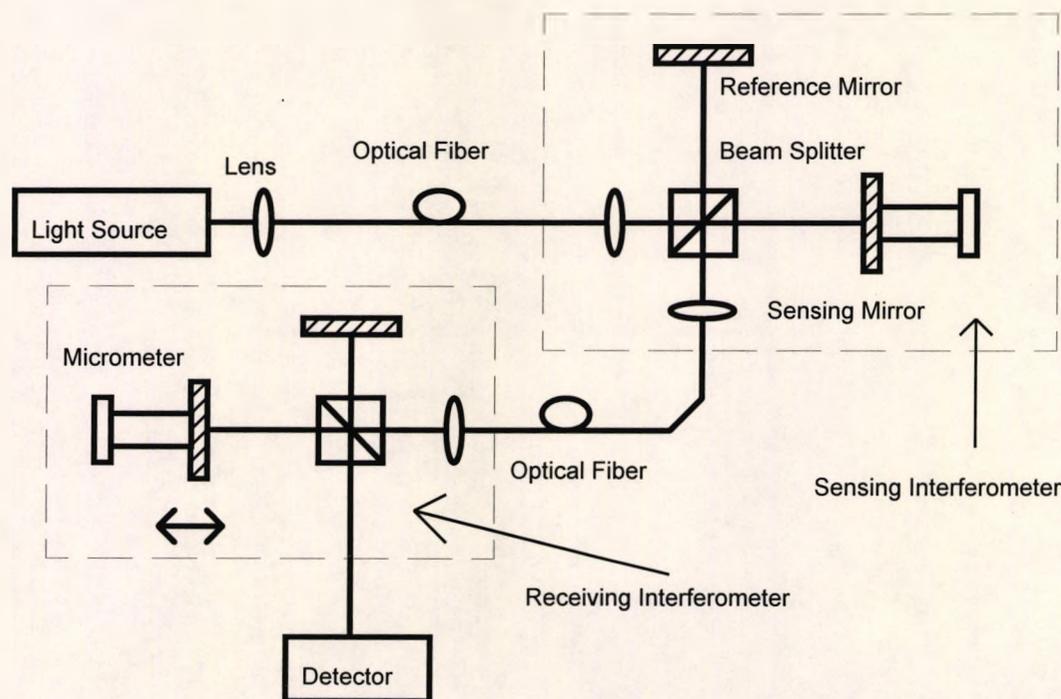
Fig.2.1 White Light Interferometric Position Sensor System

Assuming that the power spectrum of the light source is $S(\sigma)$, where σ is optical spatial frequency measured in **wavenumbers**, then

$$\sigma = 1/\lambda \qquad\qquad (2.3.1)$$

where λ is the wavelength of the light source. By equation 2.2.33, the output power spectrum from the sensing interferometer is

$$S_1(\sigma, x) = [S(\sigma)/2] [1 + \cos(2\pi\sigma x)] \qquad\qquad (2.3.2)$$

where x is the OPD introduced by the sensing interferometer. In the system operation, the measurand is first transferred into the OPD information, x, and then encoded into the output power spectrum of the interferometer, $S_1(\sigma, x)$.

The sensing interferometer can be considered as a spectral filter with a transmission function

$$T_1(\sigma, x) = (1/2) [1 + \cos(2\pi\sigma x)] \qquad\qquad (2.3.3)$$

It is a periodic function, with the **periodicity** defined by

$$D_1 = 1/|x| \qquad\qquad (2.3.4)$$

The measurand is hence encoded, through the OPD information, into the periodicity of the spectral transmission function.
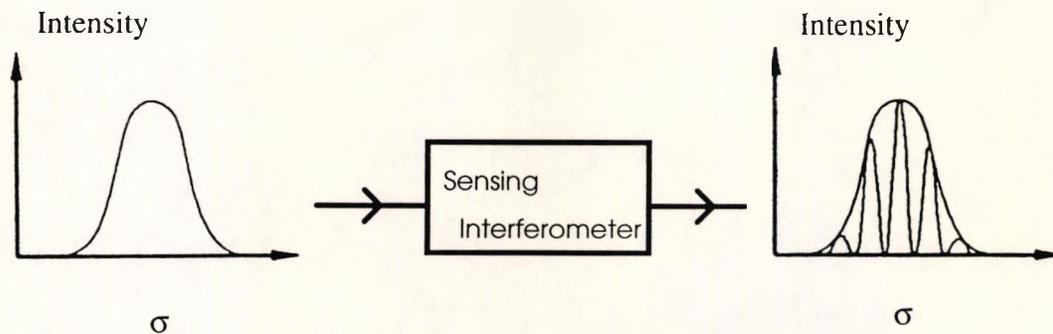
Fig.2.2 Schematic Description of Encoding Process Showing a

Spectrum Transformation

When the source spectrum is much wider than the periodicity of the sensing interferometer, D_1, the output power from the interferometer will have a comb-like spectrum, as a result of the sinusoidal modulation [8] [10]. This process is depicted in Fig.2.2, in which a broadband source spectrum is transferred into a comb-like spectrum through an interferometer.

In order to recover the signal, a spectrum analysis method may be used to determine the frequency or the periodicity of the sinusoidal modulation introduced by the sensing interferometer, so that the measurand encoded in the spectral transmission function can be retrieved [6-7] [11-13]. However, since a large number of spectral points is involved, the computation process using this method is time consuming [9].

In general, a receiving interferometer is preferred to perform a direct "decoding" process [9]. The spectral transmission function of the receiving interferometer can also be expressed as

$$T_2(\sigma, y) = (1/2) [1 + \cos(2\pi\sigma y)] \qquad (2.3.5)$$

where y is the OPD generated by the receiving interferometer. Similarly, $T_2(\sigma, y)$ is a periodic function and has a periodicity

$$D_2 = 1/|y| \qquad (2.3.6)$$

The output interference signal power spectrum then becomes

$$S_2(\sigma, x, y) = S(\sigma) T_1(\sigma, x) \ T_2(\sigma, y)$$

$$= (1/4) S(\sigma) [1 + \cos(2\pi\sigma x)] [1 + \cos(2\pi\sigma y)] \qquad (2.3.7)$$

hence the total output signal intensity

$$I(x, y) = (1/4) \int_0^\infty S(\sigma)[1 + \cos(2\pi\sigma x)][1 + \cos(2\pi\sigma y)]d\sigma \qquad (2.3.8)$$

which can be written as

$$I(x, y) = I_0 + I_1 + I_2 + I_3 + I_4 \qquad (2.3.9)$$

where

$$I_0 = (1/4) \int_0^\infty S(\sigma) d\sigma \qquad (2.3.10)$$

$$I_1 = (1/4) \int_0^\infty S(\sigma) \cos(2\pi\sigma x) d\sigma \qquad (2.3.11)$$

$$I_2 = (1/4) \int_0^\infty S(\sigma) \cos(2\pi\sigma y) d\sigma \qquad (2.3.12)$$

$$I_3 = (1/8) \int_0^\infty S(\sigma) \cos[2\pi\sigma(x+y)] d\sigma \qquad (2.3.13)$$

$$I_4 = (1/8) \int_0^\infty S(\sigma) \cos[2\pi\sigma(x-y)] d\sigma \qquad (2.3.14)$$

Assuming a broadband light source has a Gaussian power spectrum, thus for $\sigma > 0$

$$S(\sigma) = \{2P_0 / [\Delta\sigma(\pi)^{1/2}]\} \exp\{-[(\sigma - \sigma_0)/\Delta\sigma]^2\} \qquad (2.3.15)$$

where σ_0 is the central wavenumber of the light source, $\Delta\sigma$ is the spectral width and P_0 is the optical power launched into the system. In addition, the coherence length is inversely proportional to the source spectral width, i.e.

$$L_c \sim 1 / \Delta\sigma \qquad (2.3.16)$$

By the well-known integration result

$$\int_{-\infty}^\infty \exp(-a^2 x^2) dx = (\pi)^{1/2} / a \qquad (2.3.17)$$

can be seen. For an optical wave, σ_0 exhibits a large value and for a quasi-monochroatic light source such as LEDs and multimode laser diodes, the condition: $\Delta\sigma \ll \sigma_0$ can be satisfied, then

$$I_0 = (1/4) \int_0^\infty S(\sigma) d\sigma$$

$$= (1/2) \int_0^\infty \frac{P_0}{\sqrt{\pi}\,\Delta\sigma} \exp\{-[(\sigma - \sigma_0) / \Delta\sigma]^2\} d\sigma$$

$$= (1/4) \int_{-\infty}^{\infty} \frac{P_0}{\sqrt{\pi}\,\Delta\sigma} \exp[-(\sigma'/\Delta\sigma)^2]d\sigma' \quad \text{(where } \sigma' = \sigma - \sigma_0)$$

$$= P_0/4 .\qquad\qquad\qquad\qquad\qquad\qquad (2.3.18)$$

Therefore, I_0 is a DC term, standing for a uniform intensity background.

Since

$$\int_0^{\infty} \frac{2P_0}{\sqrt{\pi}\,\Delta\sigma} \exp\{-[(\sigma - \sigma_0)/\Delta\sigma]^2\}\exp(i2\pi\sigma x)d\sigma$$

$$= \int_{-\infty}^{\infty} \frac{P_0}{\sqrt{\pi}\,\Delta\sigma} \exp(i2\pi\sigma_0 x)\exp\{-[(\sigma'/\Delta\sigma) - i\pi\Delta\sigma x]^2\}\exp[-(\pi\Delta\sigma x)^2]d\sigma'$$

$$= P_0\exp[-(\pi\Delta\sigma x)^2]\exp(i2\pi\sigma_0 x) \qquad\qquad (2.3.19)$$

and similarly

$$\int_0^{\infty} \frac{2P_0}{\sqrt{\pi}\,\Delta\sigma} \exp\{-[(\sigma - \sigma_0)/\Delta\sigma]^2\}\exp(-i2\pi\sigma x)d\sigma$$

$$= P_0\exp[-(\pi\Delta\sigma x)^2]\exp(-i2\pi\sigma_0 x) \qquad\qquad (2.3.20)$$

so that

$$I_1 = (P_0/4)\exp[-(\pi\Delta\sigma x)^2]\cos(2\pi\sigma_0 x) \qquad\qquad (2.3.21)$$

when $|x| > L_c$ where $L_c \sim 1/\Delta\sigma$, then $I_1 \approx 0$, as in the usual case of remote sensing white light interferometric operation, this term vanishes.

For the same reason

$$I_2 = (P_0/4) \exp[-(\pi\Delta\sigma y)^2] \cos(2\pi\sigma_0 y) \qquad\qquad (2.3.22)$$

$$I_3 = (P_0/8) \exp\{-[\pi\Delta\sigma(x+y)]^2\} \cos[2\pi\sigma_0(x+y)] \qquad (2.3.23)$$

$$I_4 = (P_0/8) \exp\{-[\pi\Delta\sigma(x-y)]^2\} \cos[2\pi\sigma_0(x-y)] \qquad (2.3.24)$$

When $|y| < L_c$, I_2 exists and is the central set of the output interference fringe pattern. If $|x + y| < L_c$ or $|x - y| < L_c$, I_3 or I_4 will appear as a side set of the fringe pattern respectively.

The scanning mechanism in the receiving interferometer allows the value of y to be changed continuously. When y = -x, the periodicities of the two interferometers become equal, so their spectral transmission functions are identical, in other words, the OPD produced by the sensing interferometer can now be compensated by that of the receiving interferometer. As the consequence, a set of interference fringes, I_3, can be observed in the interferogram. If y changes to zero, fringes with even higher intensities can be seen. In this case, the sensing interferometer has no influence on the output signal intensity, I_2, as indicated by equation (2.3.22), and it is totally transparent. The position y = 0 is considered to be the central set fringes position. A further increase of y will lead to the appearance of another set of fringes, given by I_4, which corresponds the situation of y = x, and the fringes possess the same intensities as those when y = -x. The interferogram of the system is shown in Fig.2.3.
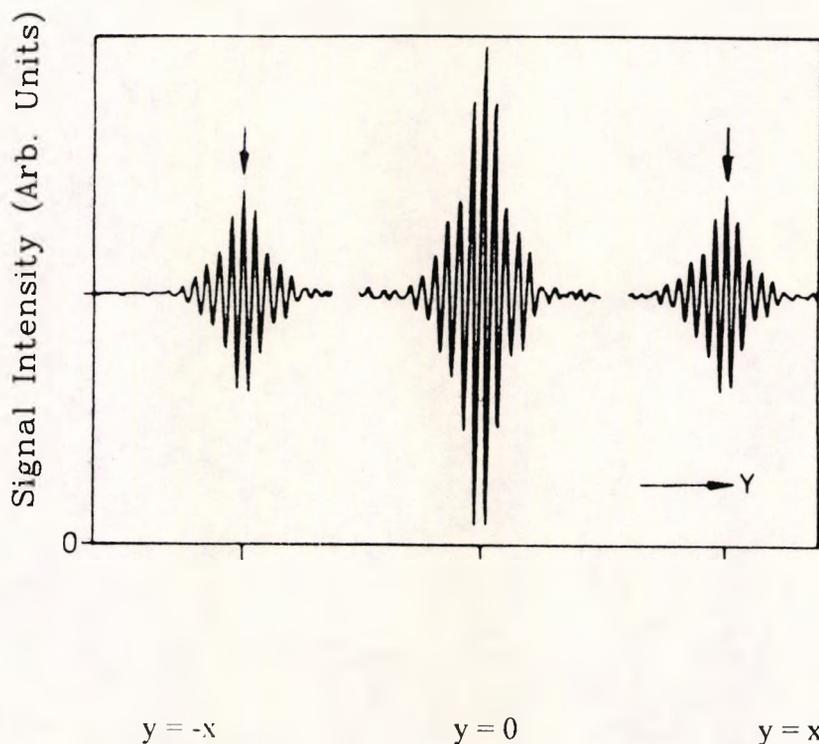
Fig. 2.3 Interferogram of the Receiving Interferometer

Therefore, by scanning the OPD of the receiving interferometer, the measurand that encoded into the periodicity, $1/|x|$, of the spectral transmission function of the sensing interferometer can be recovered when the receiving interferometer has the same periodicity or in other words, when the OPDs generated by the two interferometers are matched. This is the principle of white light interferometry. The advantages of white light interferometry are manifold, and are discussed below.

Since the measurand is entirely encoded into the periodicity, i.e. the phase term of the spectral transmission function, and decoded by matching the periodicity of the sensing interferometer with that of the receiving interferometer, the signal obtained is obviously not disturbed by the output power variation caused by the transmission and connection losses and is insensitive to the source wavelength drift. The power variation and the source wavelength drift may affect the total output power or the fringe shape, but will not change the fringe frequency. Provided that the ratio of the source spectral width and the periodicity, $\Delta\sigma/D_1 = \Delta\sigma|x|$, is larger enough so that $\Delta\sigma|x| \gg 1$, or $|x| \gg L_c$, a full recovery of signals can be realised. Therefore, white light interferometry is a powerful tool for unambiguous and reliable measurement. Moreover, a white light interferometer may operate with the multimode fibre through which the periodicity encoded signal is not disturbed [6] [9] and, as a relatively large signal power can be transmitted along such a fibre, a significant advantage over the single mode system thus becoming evident.

As a result of using a short coherence length light source, a high resolution can be achieved with the white light interferometric measurement. At the same time, considering the large scanning range usually available in the system, a large dynamic range can be obtained. Moreover, white light interferometry can be used to implement the absolute measurement as a reference position, $y = 0$, always exists in the operation process. This position will not be changed in the situation such as the interruption or power breakdown in the system, thus paving the way for measuring the position instead of the displacement. In addition, as inexpensive broadband light sources and multimode fibres can be used, white light interferometry is promising for industrial use and thus is potentially competitive in the sensor market.

2.4 Light Sources for White Light Interferometry

As mentioned before, broadband, short coherence length light sources have to be used in white light interferometric operation, such light sources thus playing an important role in determining the fundamental performance of the whole system. For an efficient operation, the light sources used should also have good spatial coherence, large output power as well as high coupling efficiency into optical fibres. Various light sources have been explored for this purpose [14-15].

2.4.1 Incandescent Lamps

At the early development stage of white light interferometry, an incandescent lamp was the natural choice of the "white light " source [6] [8], because of its extremely short coherence length, as required.
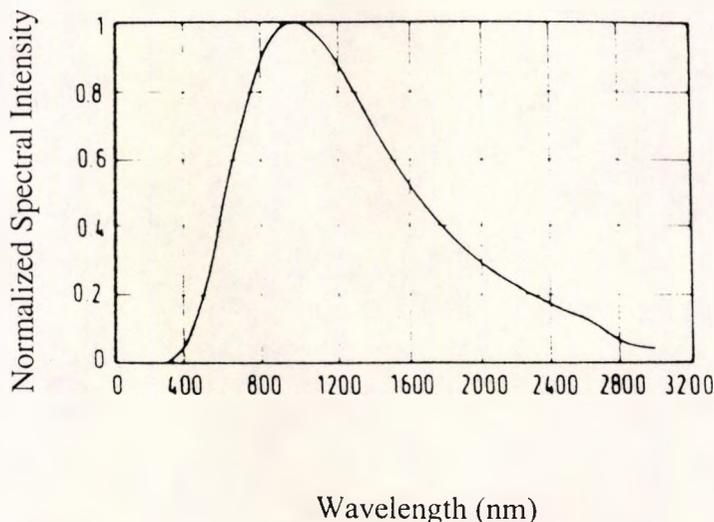
Wavelength (nm)

Fig.2.4 Spectrum of a Tungsten Lamp [14]

36

The emission spectrum of an incandescent lamp can be expressed by Planck's law as [14]

$$L = (2hc^2/\lambda^5) / [\exp(hc/\lambda kT) - 1] \qquad (2.4.1)$$

where L is the spectral radiance, h is the Planck's constant, c is the speed of light, λ is the source wavelength, k is the Boltzmann constant and T is the absolute temperature. An example is shown in Fig.2.4 which corresponds to a typical tungsten lamp operated at 2850K and has a spectral bandwidth of nearly 1000nm, implying a coherence length of less than 1μm.

Although a high resolution can be obtained by using this type of broadband sources, the coherence lengths of which are very short, a number of serious drawbacks exist. For example, low spatial coherence may deteriorate the interference fringe quality, poor coupling efficiency into optical fibres limits its fibre applications, their large physical size usually causes light collimation difficulty and a relatively short lifetime. These also result in inconvenience in the system operation. For this reason, much effort has been made to investigate the use of other suitable sources.

2.4.2 Light Emitting Diodes (LEDs)

One of the most suitable candidates is the light emitting diode (LED) which is widely used in white light interferometry at present due to its compact size, good reliability and also its short coherence length [11] [16-18].

An LED is essentially a semiconductor p-n junction operated under forward bias. In this condition, the major carriers from both sides of the p-n junction are injected to the other side where they become minority. The relatively large local minority carrier population close to the junction leads to a minority carrier concentration gradient. As a consequence, the excess minority carriers will diffuse away from the junction, recombine with majority carriers and emit photons as illustrated in Fig.2.5 [19].
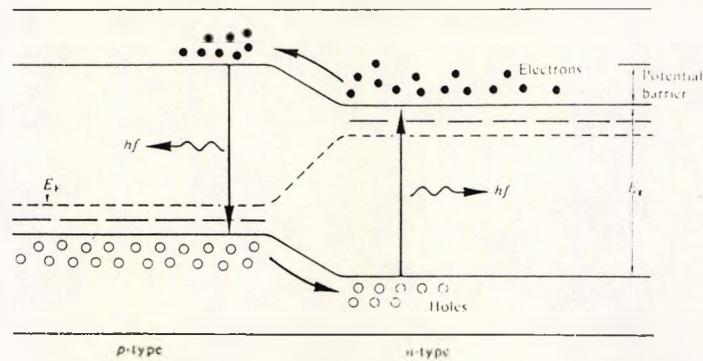
Fig.2.5 The p-n Junction with Forward Bias Giving

Spontaneous Emission of Photons [19]

An emitted photon has an energy

$$E_g = h\nu \qquad (2.4.2)$$

where ν is the optical frequency, h denotes Planck's constant and E_g is the energy difference between the conduction band and the valence band. The emitted optical wavelength then is

$$\lambda = c/\nu = hc / E_g \qquad (2.4.3)$$

where c is the speed of light. Hence the emitted optical wavelength is determined by the energy gap between the conduction band and the valence band. Since different materials have different energy gaps, E_g, the emitted wavelengths also become different.

In LEDs, the dominant photon generation is **spontaneous emission** in which the electron drops to the lower energy level in an entirely random way. Because of the wide energy distribution, the emitted photons are mutually independent and as a result, the output spectrum becomes considerably wide. An example of a typical spectrum is shown in Fig.2.6 [20].

38

Wavelength (nm)
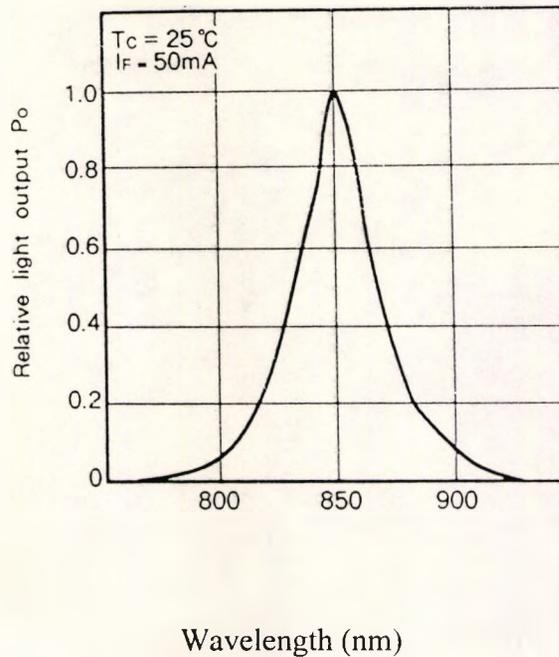
Fig.2.6 A Typical LED Emission Spectrum [20]

Due to the nature of the spontaneous emission process, an LED has a short coherence length and high insensitivity to optical feedback effects which means a low noise level. Other advantages include low cost, good reliability and wide availability.

However, the low output power and the poor coupling efficiency into optical fibres are the main problems in the use of LEDs in white light interferometry.

2.4.3 Superluminescent Diodes (SLDs)

Another alternative light source is the superluminescent diode (SLD) which exhibits a larger output power and better coupling efficiency into optical fibres when compared with the LED [21-25].

In a superluminescent diode, while a high level of spontaneous emission is still maintained, substantial **stimulated emission** also occurs. The stimulated emission means that an emitted photon can stimulate the emission of another photon and the

newly created photon will have the same phase, wavelength and polarization state with the initial photon. Hence, both the coherence and output power can be increased in such a process.

A typical spectrum of a superluminescent diode is shown in Fig.2.7.
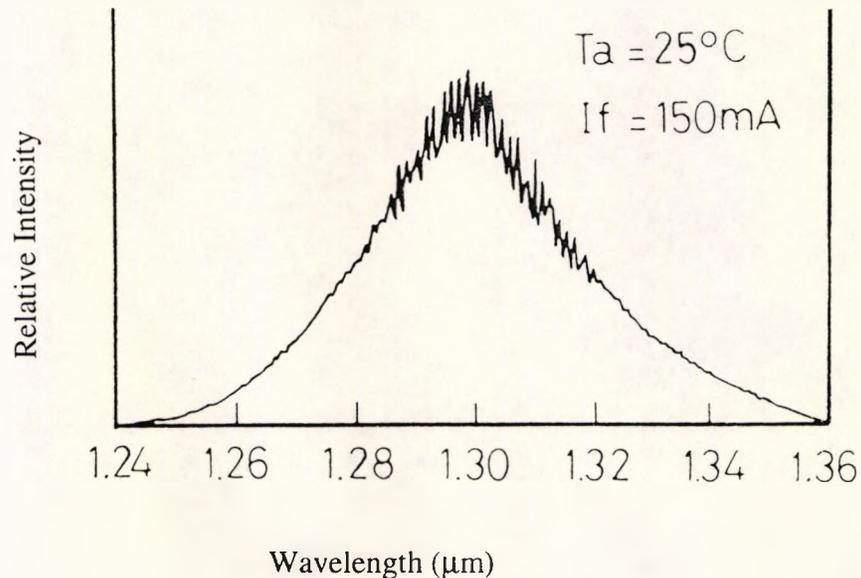
Fig.2.7 Emission Spectrum of a Superluminescent Diode [25]

Superluminescent diodes are more coherent and hence more sensitive to temperature changes than LEDs and they have a major drawback of a relatively higher price.

2.4.4 Multimode Laser Diodes

In recent years, multimode laser diodes have received increasing attention in the white light interferometry field as possessing large output power, good coupling efficiency into optical fibres and with reasonable price [26-29]. In a multimode laser diode, carriers are injected into a small area where the photons generated are confined, in order that the light intensity can exceed the necessary level for stimulated emission. Consequently, the stimulated emission becomes dominant.
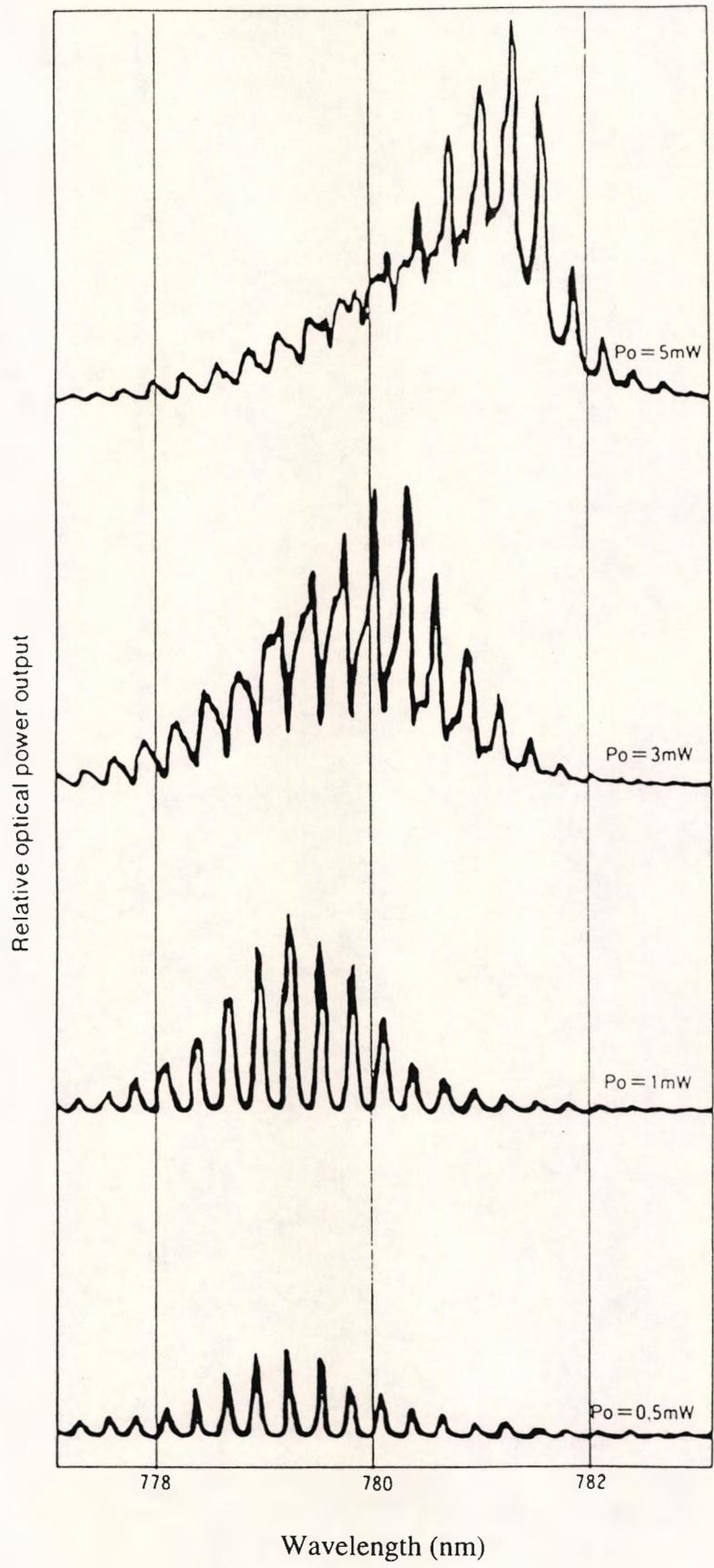
Fig.2.8 Emission Spectrum of a Multimode Laser Diode [31]

The emission spectrum of a typical multimode laser diode, as shown in Fig.2.8, consists of a series of wavelength peaks corresponding to the presence of different longitudinal modes. An individual spectral line of a multimode laser diode typically shows a Lorentzian shape while the whole envelope has a Gaussian profile [30]. Since the Fourier transform of a Gaussian function is still a Gaussian function and the Lorentzian function and the exponential function form a Fourier transform pair, the output signals from a simple Michelson interferometer operated with a multimode laser diode, in the time domain, are composed of a series of fringe packets, where each fringe packet corresponds to an individual spectral line or mode, and the overall envelope of the whole fringe packets is an exponential, but for each fringe packet, the envelope is defined by a Gaussian profile.

Compared with LEDs, multimode laser diodes have also higher spatial coherence. In addition, since a multimode laser diode can be operated below its threshold, and function as a LED, flexibility exists within the system. However, multimode laser diodes have relatively long coherence lengths, thus limiting their applications in high precision measurement. It is in this aspect in particular that some efforts have been made in Chapter 3 and Chapter 4 for the system improvement, the details of which will be discussed later.

2.4.5 Fibre Fluorescent Sources

The most recent development in white light sources is the emergence of fibre fluorescent sources (the basis of fibre laser) which are compatible with other fibre components and hence have excellent coupling efficiency, high spatial coherence, mechanical flexibility and thus are becoming one of the most promising light sources for future white light interferometric uses [32-35].

A fibre fluorescent source is most readily realized using a rare-earth-doped fibre. When pumped by a laser source of suitable wavelength and appropriate output power, the rare-earth elements can absorb the short wavelength photons and re-emit longer

wavelength photons. The output of a fibre fluorescent source has a broadband power spectrum and hence can act as a low temporal coherence light source. A fluorescent spectrum for a typical source, a Nd-doped fibre is shown in Fig.2.9.

Wavelength (nm)
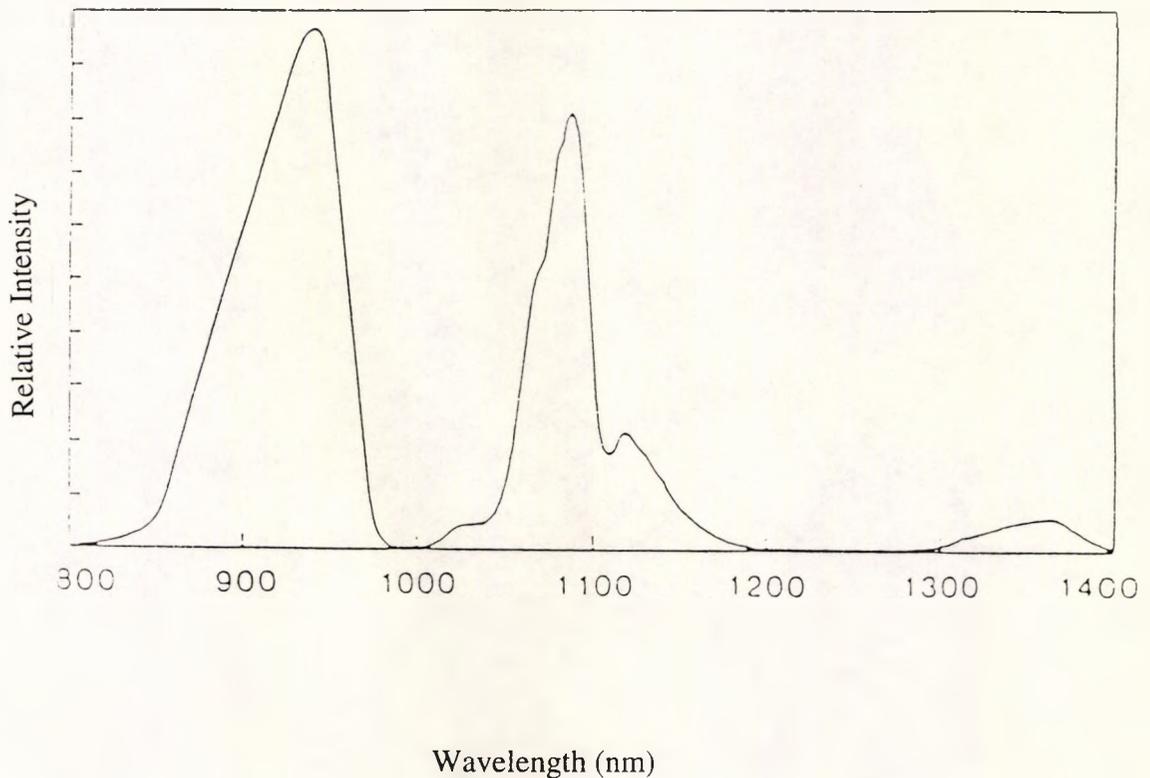
Fig.2.9 A Typical Fluorescence Spectrum [36]

Since a rare-earth-doped fibre may have several fluorescent peaks in its spectrum, a novel application for white light interferometry can be achieved, which will be described in Chapter 5, using a Sm^{3+}-doped fibre. At present, the price for the pump laser is still high, the exploration for the use of fibre fluorescent sources in white light interferometry has only started and a full investigation remains to be done of their long term value.

2.5 White Light Interferometry Scanning Techniques

As discussed previously, in a white light interferometric remote sensing system, in order to recover the variation of the measurand encoded in the output spectrum of the sensing interferometer, a receiving interferometer is introduced, one of the arms of which has to be scanned to follow the OPD changes in the sensing interferometer. Mechanical and electronic scans are the main techniques used at present to achieve this [9-10].

2.5.1 Mechanical Scanning Technique

In a typical Michelson type mechanical scanning mechanism, the sensing mirror in the receiving interferometer is mounted on a moving mechanical device such as a micrometer or a translation stage as shown in Fig.2.10.
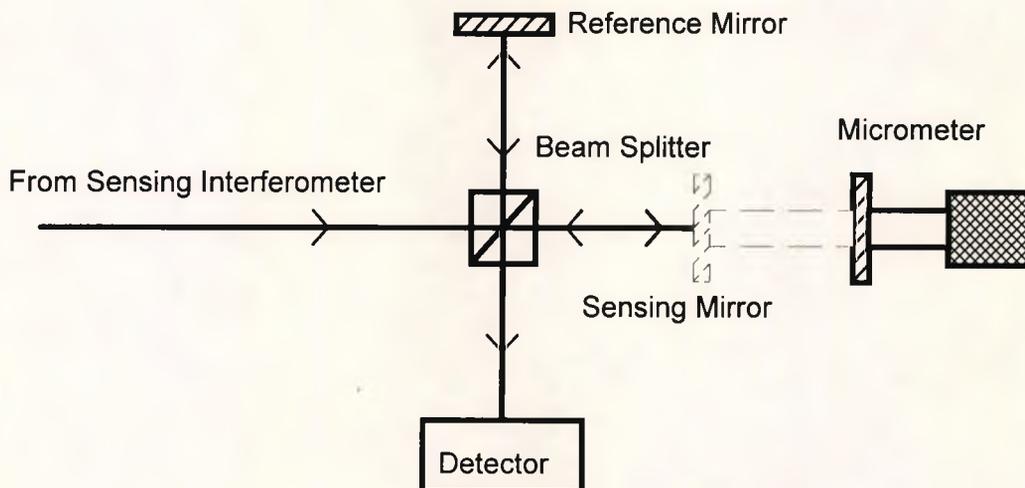
Fig.2.10 Mechanical Scanning System

The scanning distance and the measurement accuracy of the system are then determined by that of the moving mechanical device. Obviously, this technique is simple and convenient and a large scanning distance or operating range can easily be achieved. However, the price paid is a large system dimension, critical demand on mechanical device quality and possible long term mechanical stability problems.

Hence, although this technique is widely used at present, it is still not considered to be a good solution in all sensor cases, and alternatives must be investigated.

2.5.2 Electronic Scanning Technique

Recently, electronic scanning techniques have attracted much attention [13] [37-40]. In this technique, as shown in Fig.2.11, which also corresponds to a typical Michelson type scanner, by slightly tilting one of the mirrors, the expanded and collimated light beams from the two arms of the receiving interferometer are overlapped at a small angle on a CCD array, which is actually an array of photodiodes that can convert incident light intensity into an electrical signal. As a result of the tilt angle, the two light beams arrive at each photodiode of the array with an OPD one with respect to the other, and an equivalent spatial scan can then be obtained from the output of the CCD array. Hence the operating range of the electronically scanned interferometer is limited by the configuration of the CCD array, i.e. the total number of effective pixels and the sampling rate which is defined as the number of pixels per fringe.

Obviously, the measurement resolution of this technique is also dependent on the spatial sampling rate of the CCD array, and if only a low sampling rate can be obtained, the recorded position of the maximum signal intensity may not correspond to the actual fringe peak, some signal processing then becomes necessary in such a situation [41-42]. In the electronic scanning technique, since there are no moving elements involved, the system may enjoy small size, compact structure, good mechanical stability and high scanning speed, but its operating range is usually limited [10] [40] [43], as explained above.

An alternative electronic scanner may simply consist of a diffraction grating and a CCD array, the output of which is sent to a computer to be used to analyze the spectrum [11] [44]. However, as mentioned in Section 2.3, this spectrum analysis process is time consuming as a large number of spectral points are involved.

In Chapter 6, an optical scanning technique is proposed as an alternative to the current scanning mechanism for white light interferometric sensor use. In this technique, a white light interferometric sensor can be realized without resorting to the receiving interferometer in some cases, thus offering the potential of a simple system, the corresponding details of which will be discussed.
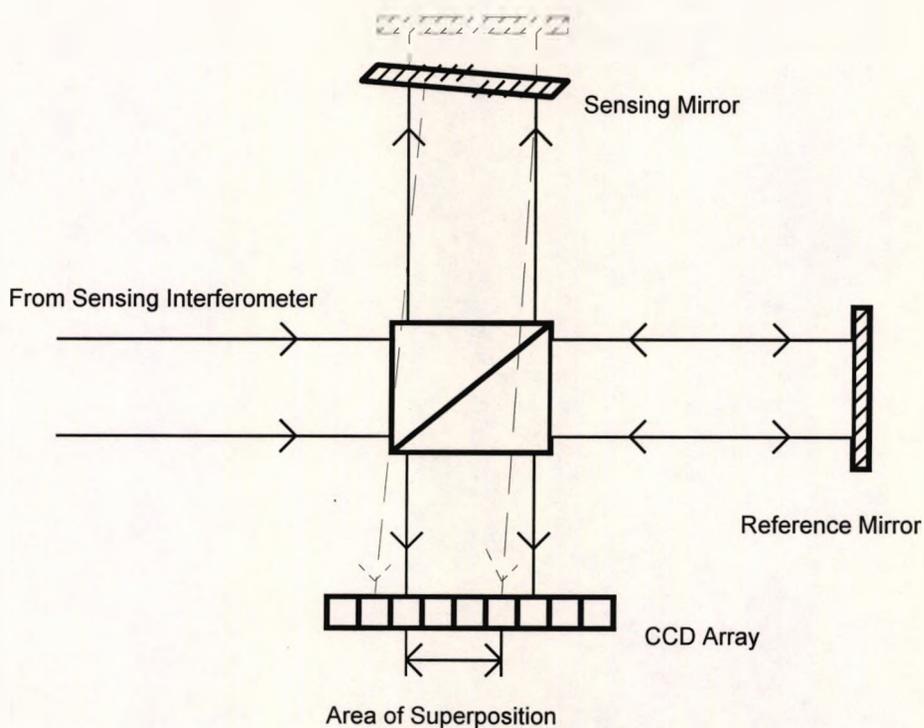
Fig.2.11 Electronic Scanning System

2.6 Summary

For an interferometer illuminated by a non-monochromatic, broadband light source, the output signal intensity is determined by the interference equation deduced from simple coherence theory. In principle, an interferometer can be considered as a spectral filter and so that its output spectrum is the product of the source spectrum and the interferometer spectral transmission function. In white light interferometry, the physical measurand is encoded by a sensing interferometer into its output spectrum and then decoded by a receiving interferometer by means of a scanning mechanism. LEDs and multimode laser diodes are the main broadband sources currently used and as far as a scanning mechanism is concerned, mechanical scanning and electronic scanning are the two main choices at present.

Multimode laser diodes have large output power and good coupling efficiency into optical fibres when compared with LEDs, however, they have larger coherence lengths, which causes a severe problem in performing high precision measurements in white light interferometry, as the absolute reference position, i.e. the central fringe position (corresponding to a zero OPD) in the interference fringe pattern may be determined only with great difficulty, especially when a high noise level exists in the system. An efficient technique to solve this problem is to use a two wavelength combination source [28] [45-46]. The method for selecting an optimum wavelength combination for such a source is an important subject of study and the efforts will be made, as discussed in the next Chapter, to solve this problem.

References

1. M. Born and E. Wolf, "Principle of Optics", Sixth Edition, pp.491-508, Pergamon Press, 1983

2. L. Mandel and E. Wolf, "Coherence Properties of Optical Fields", Reviews of Modern Physics, Vol.37, No.2, pp.231-287, April 1965

3. E. Hecht and A. Zajac, "Optics", Second Edition, pp.516-537, Addison-Wesley Publishing Company, 1987

4. W. H. Steel, "Interferometry", Second Edition, pp.72-88, Cambridge University Press, 1983

5. B. E. A. Saleh and M. C. Teich, "Fundamentals of Photonics", pp.342-384, John Wiley & Sons, Inc., 1991

6. Th. Bosselmann and R. Ulrich, "High Accuracy Position-Sensing with Fiber-Coupled White Light Interferometers", Proceedings of the 2nd International Optical Fiber Sensors Conference", pp.361-365, Stuttgart, Germany, 1984

7. R. Ulrich, "Theory of Spectral Encoding for Fiber-Optic Sensors", NATO ASI Series E: Applied Science, No.132, pp.72-130, Martinus Nijhoff Publishers, 1987

8. Th. Bosselmann, "Multimode-fiber Coupled White-Light Interferometric Position Sensor", NATO ASI Series E: Applied Science, No.132, pp.429-432, Martinus Nijhoff Publishers, 1987

9. H. C. Lefèvre, "White Light Interferometry in Optical Fiber Sensors", Proceedings of the 7th International Optical Fiber Sensors Conference, pp.345-351, Sydney, Australia, December 2-6, 1990

10. A. Koch and R. Ulrich, "Fiber-Optic Displacement Sensor with 0.02 μm Resolution by White-light Interferometry", Sensors and Actuators A, 25-27, pp.201-207, 1991

11. M. T. Velluet, P. Graindorge and H. J. Arditty, "Fiber Optic Pressure Sensor Using White Light Interferometry", Proceedings of SPIE., Vol. 838, pp. 78-83, 1987

12. C. Lecot and M. Lequime, "A New Spectral Detection Method for Fiber-Coupled Interferometers", Proceedings of SPIE., Vol.1169, pp.73-79, 1989

13. D. Trouchet, B. Laloux and P. Graindorge, "Prototype Industrial Multi-Parameter F. O. Sensor Using White Light Interferometry, Proceedings of the 6th International Optical Fiber Sensors Conference, pp.227-233, Paris, France, September 18-20, 1989

14. R. Kist, "Sources and Detectors for Fiber-Optic Sensors", NATO ASI Series E: Applied Science, No.132, pp.267-298, Martinus Nijhoff Publishers, 1987

15. E. Udd, "Light Sources", in "Fiber Optic Sensors: An Introduction for Engineers and Scientists", Edited by E. Udd, pp.37-68, John Wiley & Sons, Inc., 1991

16. C. Mariller and M. Lequime, "Fiber-Optic White-Light Birefringent Temperature sensor", Proceedings of SPIE., Vol.798, pp.121-130, 1987

17. R. Bohm and R. Ulrich,"High-Accuracy Fiber-Optic Refractometer for Fluids", Proceedings of the 7th International Optical Fiber Sensors Conference, pp.353-356, Sydney, Australia, December 1990

18. D. Trouchet, F. X. Desforges, P. Graindorge and H. C. Lefevre, "Remote Fiber Optic Measurement of Air Index with White Light Interferometry", Proceedings of the 8th International Optical Fiber Sensors Conference, pp.57-60, Montery, USA, January 29-31, 1992

19. J. M. Senior, "Optical Fiber Communications: Principles and Practice", p.248, Prentice-Hall International Inc., 1985

20. Mitsubishi LED ME1013, Mitsubishi Optoelectronics Data Book, 1992

21. S. A. Al-Chalabi, B. Culshaw and D. E. Davies, "Partially Coherent Sources in Interferometric Sensors", Proceedings of the First International Optical Fiber Sensors Conference, pp.132-135, London, U.K., 1983

22. C. B. Morrison, L. M. Zinkiewicz, J. Niesen and L. Figueroa, "High-Power Superluminescent Diode with Reduced Coherence Length", Electronics Letters, Vol.21, No.19, pp.840-841, 12th September 1985

23. P. Sansonetti, M. Lequime and H. Giovannini, "Interferometric Spectrally Encoded Sensor Using a Superadiant diode", Proceedings of the 6th International Optical Fiber Sensors Conference, pp.71-77, Paris, France, September 18-20, 1989

24. V. Gusmeroli and M. Martinelli, "High-Resolution Distance Measurement by Dynamical Spectral Filtering of a Superluminescent Source", Optics Letters, Vol.16, No.15, pp.1195-1197, August 1, 1991

25. Y. Kashima, A. Matoba and H. Takano, "Performance and Reliability of InGaAsP Superluminescent Diode", IEEE/OSA Journal of Lightwave Technology, Vol.10, No.11, pp.1644-1649, November 1992

26. Y. Ning, K. T. V. Grattan, B. T. Meggitt and A. W. Palmer, "Characteristics of Laser Diodes for Interferometric Use", Applied Optics, Vol.28, No.17, pp.3657-3661, 1 September 1989

27. A. S. Gerges, T. P. Newson and D. A. Jackson, "Coherence Tuned Fiber Optic Sensing System, with Self-Initialization, Based on a Multimode Laser Diode", Applied Optics, Vol.29, No.30, pp.4473-4480, 20 October 1990

28. B. K. Ward and K. Seta, "Quasimonochromatic White Light Fringe Interferometer", Applied Optics, Vol.30, No.1, pp.66-71, 1 January 1991

29. J. L. Santos and D. A. Jackson, "Coherence Sensing of Time-Addressed Optical-Fiber Sensors Illuminated by a Multimode Laser Diode", Applied Optics, Vol.30, No.34, pp.5068-5076, 1 December 1991

30. W. V. Etten and J. V. D. Plaats, "Fundamentals of Optical Fiber Communications", pp.153-154, Prentice Hall International, 1991

31. Sharp Laser Diode LT023, Sharp Data Book, 1992

32. K. Liu, M. Digonnet, H. J. Shaw, B. J. Ainslie and S. P. Craig, "10 mW Superfluorecent Single-Mode Fibre Source at 1060nm", Electronics Letters, Vol.23, No.24, pp.1320-1321, 19th November 1987

33. I. N. Duling III, W. K. Burns and L. Goldberg, "High-Power Superfluorescent Fiber Source", Optics Letters, Vol.12, No.1, pp.33-35, January 1, 1990

34. R. J. Mears and S. R. Baker, "Erbium Fibre Ampliers and Lasers", Optical and Quantum Electronics, Vol.24, No.5, pp.517-538, May 1992

35. P. F. Wysocki, M. J. F. Digonnet, B. Y. Kim and H. J. Shaw, "Characteristics of Erbium-Doped Superfluorescent Fiber Sources for Interferometric Sensor Applications", IEEE/OSA Journal of Lightwave Technology, Vol.12, No.3, pp.550-567, March 1994

36. York VSOP, "Neodymium-Doped Laser Fiber Data Book", 1987

37. A. Koch and R. Ulrich, "Displacement Sensor with Electronically Scanned White Light Interferometer", Proceedings of SPIE., Vol.1267, pp.126-133, 1990

38. S. Chen, A. J. Rogers and B. T. Meggitt, "Electronically Scanned Optical-Fiber Young's White-Light Interferometer", Optics Letters, Vol.16, No.10, pp.761-763, May 15, 1991

39. S. Chen, A. W. Palmer, K. T. V. Grattan, B. T. Meggitt and S. Martin, "Study of Electronically-Scanned Optical-Fibre White-Light Fizeau Interferometer", Electronics Letters, Vol.27, No.12, pp.1032-1034, 6th June 1991

40. W. J. Bock and W. Urbanczyk, "Electronically Scanned White-Light Interferometric Sensor for High Hydrostatic Pressure Measurements", Proceedings of the 9th International Optical Fiber Sensors Conference, pp. 135-138, Firenze, Italy, May 4-6, 1993

41. R. Dändliker, E. Zimmermann and G. Frosio, "Electronically Scanned White-Light Interferometry: A Noise-Resistant Signal Processing", Optics Letters, Vol.17, No.9, pp.679-681, May 1, 1992

42. S. Chen, A. W. Palmer, K. T. V. Grattan and B. T. Meggitt, "Digital Signal-Processing Techniques for Electronically-Scanned Optical-Fiber White-Light Fizeau Interferometry", Applied Optics, Vol.31, No.28, pp.6003-6010, 1 October 1992

43. S. Chen, B. T. Meggitt and A. J. Rogers, "Electronically Scanned White-Light Interferometry with Enhanced Dynamic Range", Electronics Letters, Vol.26, No.20, pp.1663-1665, 27th September, 1990

44. S. Taplin, A. Gh. Podoleanu, D. J. Webb and D. A. Jackson, "Displacement Sensor Using Channelled Spectrum Dispersed on a Linear CCD Array", Electronics Letters, Vol.29, No.10, pp.896-897, 13th May 1993

45. S. Chen, K. T. V. Grattan, B. T. Meggitt and A. W. Palmer, "Instantaneous Fringe-Order Identification Using Dual Broad-Band Sources with Widely Spaced Wavelengths", Electronics Letters, Vol.29, No.4, pp.334-335, 18th February 1993

46. Y. J. Rao, Y. N. Ning and D. A. Jackson, "Synthesized Source for White-Light Sensing Systems", Optics Letters, Vol.18, No.6, pp.462-464, March 15, 1993

Chapter 3

Two Wavelength Combination Sources

A two wavelength combination source can be used to enhance the measurement precision in a white light interferometric system. However, for efficient operation, an optimum wavelength combination has to be chosen. In this Chapter, the method of selecting the optimum wavelength combination of a two wavelength source is presented. The existence of such an optimum wavelength combination may be deduced from the theoretical analysis given. By the use of computer simulations of interference fringe patterns of such two wavelength combination sources, the optimum wavelength combination can be obtained for a light source of given wavelength, which is further confirmed by a series of experimental investigation carried out on a number of laser diodes.

3.1 Introduction

The main advantages of white light interferometry lie in the possibility of making high precision, unambiguous and absolute measurements, which are due to the use of a low coherence (short coherence length) light source in the system. As discussed in Chapter 2, LEDs and multimode laser diodes are the main low coherence light sources for use at present. LEDs are simple, compact, reliable and available at relatively low cost, but they exhibit low output power, poor coupling efficiency into optical fibres and low spatial coherence. This results in a severe disadvantage for their potential

53

applications in an optical fibre sensor system. By contrast, multimode laser diodes possess high output power, good coupling efficiency into optical fibres, high spatial coherence and are also available at reasonable price. However, the relatively long coherence length of multimode laser diodes may also cause a serious problem in pursuing high precision measurement applications.

For a white light interferometric system illuminated with a multimode laser diode, in order to perform an accurate measurement, the position of the central fringe in the central set (zero order set) fringe packet [1], which corresponds to the zero OPD position, must be precisely determined. This central fringe position acts as a reliable reference, and thus is of crucial importance in the system [2-4]. Due to the relatively large coherence length of the multimode laser diodes available, the intensity difference between the central fringe and its adjacent side fringes may become too small to be distinguished clearly, especially in the presence of noise in the system. To overcome this difficulty, various digital signal processing techniques have been proposed [5-6], but their accuracy is still limited and the process is time consuming as considerable computation work is involved. In addition, the total system cost may also be increased.

It is well known that a "beat" interference fringe pattern can be created when two light sources of different wavelengths illuminate an interferometer simultaneously. This phenomenon has been utilized as a technique to significantly extend the unambiguous measurement range as discussed in Chapter 1 [7-9], which can also be used to overcome the central fringe identification difficulty in a white light interferometric system as described above [10-12].

In [10], the output beams from two multimode laser diodes of wavelength 670nm were combined to illuminate an interferometer. By controlling the temperature difference between the two laser diodes, wavelength differences were achieved. As a result, the full width at half maximum (FWHM) value for the central set fringe packet can be reduced from 130μm to 63μm at a 0.6nm wavelength difference and to 27μm for a 1.5nm wavelength difference. However, such a reduction is still limited or in other words, the zero OPD position (central fringe position) still cannot be accurately

determined, due to the fact that there is only a small wavelength difference between the two laser diode sources.

A large wavelength difference was used in [11], where the two laser diode wavelengths were 670nm and 810nm respectively and their corresponding coherence lengths were about 20μm and 33μm respectively. When compared with one of the laser diodes (wavelength of 670nm), the minimum signal-to-noise ratio required by the system to identify directly the central fringe from the second largest side fringe, SNR_{min}, can be greatly reduced. Moreover, a number of SNR_{min} values corresponding to the different coherence lengths of the optical sources and different $\Delta\lambda/\lambda$ ratios, where $\Delta\lambda = \lambda_2 - \lambda_1$ is the wavelength difference between the two sources and $\lambda = (\lambda_1 + \lambda_2)/2$, were also computer simulated. The results demonstrate that a significant improvement in the SNR_{min} can be achieved by the use of a two wavelength combination source technique and the SNR_{min} value reduction varies with the $\Delta\lambda/\lambda$ values, but it was still difficult to decide the appropriate $\Delta\lambda/\lambda$ value in a certain coherence length region or in other words, an optimum wavelength combination in which the SNR_{min} can reach its lowest possible value remains to be determined.

Similar efforts to improve the central fringe identification by using a two wavelength combination source with a relatively large wavelength difference were also reported in [12], where the two laser diodes had wavelengths of 676nm and 784nm and coherence lengths of 45μm and 80μm respectively. The equivalent coherence length which is determined by the width of the central fringe packet was decreased to ~ 4μm or less than one tenth of that of either the individual light sources used. Since only one pair of multimode laser diode sources was investigated in this case, it was not possible to predict the variation of the equivalent coherence lengths for different wavelength combinations.

It then becomes clear that although through the use of the two wavelength combination source technique, the problem of central fringe identification can be eased, an optimum wavelength combination still has to be chosen in order to achieve a better signal-to-noise ratio in the white light interferometric system [13-14]. In addition, it is

also necessary to investigate the variation of the interference fringe patterns in a two wavelength source for different wavelength combinations.

In this Chapter, a method of selecting the optimum wavelength combinations of two multimode laser diode sources is presented. The development of this method is based on the theoretical analysis, computer simulations and appropriate experimental verification.

3.2 Theoretical Analysis

3.2.1 Single Wavelength Light Sources

As mentioned in section 2.4.4, the power spectrum of a multimode laser diode can be considered to have a Gaussian profile. Since the Fourier transform of a Gaussian function is still a Gaussian function, and by the Wiener-Khinchin theorem or equation (2.2.26), the temporal coherence function, $\Gamma(\tau)$, and consequently the normalized self coherence function, $\gamma(\tau)$, of a multimode laser diode, are both also Gaussian functions. When only the central set of fringe packets is considered, the output intensity from a Michelson interferometer illuminated by a multimode laser diode, according to the interference equation (2.2.15), can be expressed as:

$$I(x) = (I_0/2) [1 + |\gamma|\cos(2\pi x/\lambda)]$$

$$= (I_0/2)\{1 + \exp[-(2x/L_c)^2]\cos(2\pi x/\lambda)\} \qquad (3.2.1)$$

where I_0 is the light intensity, λ is the central wavelength, L_c is the coherence length of the laser diode source and x is the OPD introduced by the interferometer.

As shown in equation (3.2.1), the output consists of a dc term which corresponds to a uniform intensity background and an ac term which represents the interference signal.

The normalized ac signal intensity can be written as

$$I_{ac}(x) = \exp[-(2x/L_c)^2]\cos(2\pi x/\lambda) \qquad (3.2.2)$$
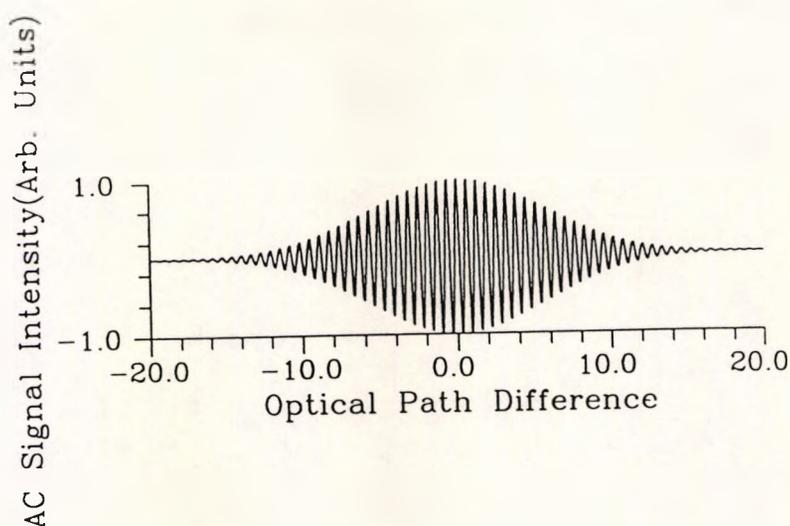
Fig.3.1 Interference Fringe Pattern for One Multimode Laser

Diode Source (λ = 635nm, L_c = 16μm)

As shown in Fig.3.1, the output ac signal is a cosine oscillation modulated by a Gaussian visibility function, V(x), which is given by

$$V(x) = |\gamma| = \exp[-(2x/L_c)^2] \qquad (3.2.3)$$

When x = 0, V = 1 is the maximum value which corresponds to the central fringe position. As implied by equation (3.2.3), for a given OPD, x, the visibility is determined by the coherence length of the light source, and when the coherence length is large, the visibility profile becomes relatively flat near the central fringe position.

In order to determine the position of the central fringe from its adjacent side fringes, the **visibility difference** between them should be as large as possible, which is given by

$$\Delta V = V(0) - V(\lambda)$$

$$= 1 - \exp[-(2\lambda/L_c)^2] \qquad (3.2.4)$$

Hence, for a given light source of wavelength λ, if the coherence length L_c is large, the visibility difference, ΔV, will be small, which means that the central fringe

identification is difficult. However, the situation can be changed favourably when combining two multimode laser diodes to form a two wavelength combination source.

3.2.2 Two Wavelength Combination Sources

According to coherence theory [15], light beams of a different frequency or wavelength are mutually incoherent, the resultant output intensity from a two wavelength combination source is simply the sum of the two output intensities produced by each light source individually. Thus the normalized output ac signal intensity obtained can be written as:

$$I_{ac}(x) = (1/2)\{\exp[-(2x/L_{c1})^2]\cos(2\pi x/\lambda_1) + \exp[-(2x/L_{c2})^2]\cos(2\pi x/\lambda_2)\}$$

$$(3.2.5)$$

where λ_1, λ_2 are the central wavelengths of the two laser diodes respectively and L_{c1}, L_{c2} are their corresponding coherence lengths.

Assuming that both laser diodes have the same coherence length, i.e. $L_c = L_{c1} = L_{c2}$, equation (3.2.5) then becomes:

$$I_{ac}(x) = (1/2)\exp[-(2x/L_c)^2][\cos(2\pi x/\lambda_1) + \cos(2\pi x/\lambda_2)]$$

$$= \exp[-(2x/L_c)^2]\cos(2\pi x/\lambda_m)\cos(2\pi x/\lambda_a) \qquad (3.2.6)$$

where $\lambda_m = 2\lambda_1\lambda_2/|\lambda_2 - \lambda_1|$ is the **modulation** or **beat wavelength** of the two laser sources and $\lambda_a = 2\lambda_1\lambda_2/(\lambda_1 + \lambda_2)$ is known as the **average wavelength**. When compared with the synthetic wavelength, λ_{eq}, shown in equation (1.2.17), the modulation wavelength, $\lambda_m = 2\lambda_{eq}$, is so defined as to maintain the symmetry with the average wavelength λ_a.

The corresponding visibility function is given by

$$V(x) = \exp[-(2x/L_c)^2]\ |\cos(2\pi x/\lambda_m)| \qquad (3.2.7)$$

AC Signal Intensity (Arb. Units)

1.0

0.0

−1.0

I_{00}
I_{01}
I_{10}
L_{ce}
L_c
V

−20.0   −10.0   0.0   10.0   20.0

Optical Path Difference (μm)
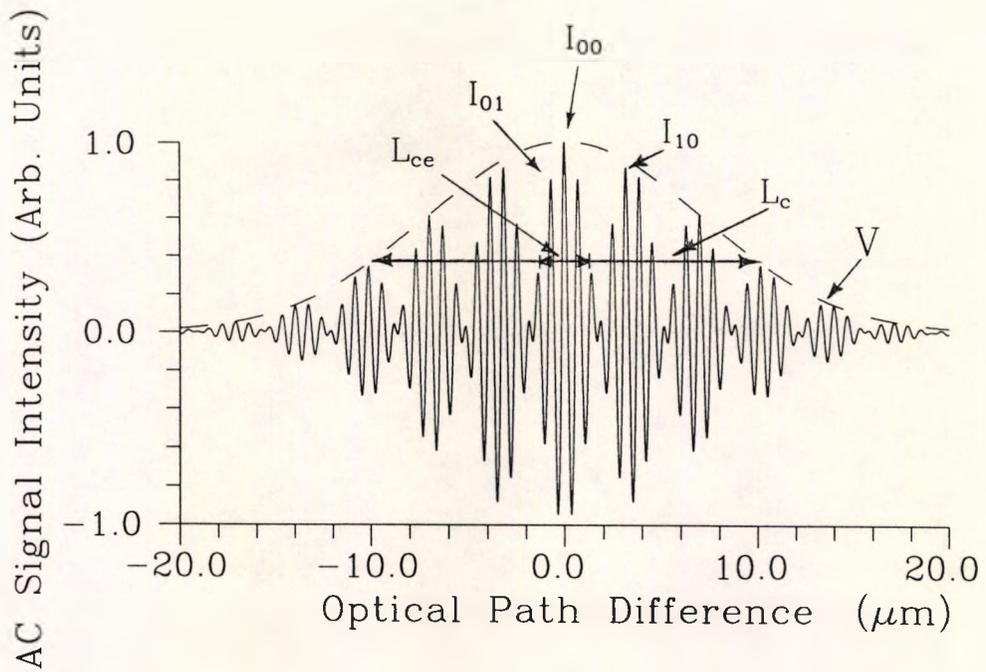
V — Fringe Visibility Curve of Single Laser Diode Source;

L_c — Coherence Length of Single Laser Diode Source;

L_{ce} — Equivalent Coherence Length (See Section 3.2.4);

I_{00} — Central Fringe (See Section 3.2.3);

I_{01} — First Side Fringe in the Central Fringe Packet (See Section 3.2.3);

I_{10} — Central Fringe in the First Side Fringe Packet (See Section 3.2.3)

Fig.3.2 Fringe Pattern for a two Wavelength Combination Source

As indicated in Fig.3.2, the visibility is now, itself, the absolute value of a cosine function modulated by a Gaussian profile. In such a situation, the visibility difference between the central fringe and its adjacent side fringes in the central fringe packet becomes

$$\Delta V = 1 - \exp[-(2\lambda_a/L_c)^2] \, |\cos(2\pi\lambda_a/\lambda_m)| \qquad (3.2.8)$$

When compared with the situation in equation (3.2.4), where only one laser diode is used, the visibility difference may be increased as long as the following condition can be satisfied

$$\exp[-(2\lambda_1/L_c)^2] - \exp[-(2\lambda_a/L_c)^2] \, |\cos(2\pi\lambda_a/\lambda_m)| > 0 \qquad (3.2.9)$$

As in the general case, suppose that $\lambda_1 < \lambda_2$, then

$$\lambda_a/\lambda_1 = 2\lambda_2/(\lambda_1 + \lambda_2) > 1 \qquad\qquad (3.2.10)$$

i.e. $\quad \lambda_a > \lambda_1$ $\qquad\qquad (3.2.11)$

This condition can always be satisfied.

Therefore, by using a two wavelength combination source, the visibility difference between the central fringe and its adjacent side fringes can be increased or in other words, the central fringe identification becomes relatively easier to perform.

For an efficient operation of the white light interferometric system, the wavelength combination used in such a two wavelength system has to be optimized, as discussed in the next part of this Section.

3.2.3 The Optimum Wavelength Combination

As shown in Fig.3.2, the central fringe intensity (peak-to-peak value), I_{00}, in the central fringe packet is given by

$$I_{00} = I_{ac}(0) - I_{ac}(\lambda_a/2)$$

$$= 1 + \exp[-(\lambda_a/L_c)^2]\cos(\pi\lambda_a/\lambda_m) \qquad\qquad (3.2.12)$$

Its adjacent or the first side fringe intensity (peak-to-peak value) in the same fringe packet then can be written as:

$$I_{01} = I_{ac}(\lambda_a) - I_{ac}(\lambda_a/2)$$

$$= \exp[-(2\lambda_a/L_c)^2]\cos(2\pi\lambda_a/\lambda_m) + \exp[-(\lambda_a/L_c)^2]\cos(\pi\lambda_a/\lambda_m) \qquad (3.2.13)$$

The normalized form of I_{01} can thus be written as :

$$I_{01n} = I_{01} / I_{00}$$

$$= \frac{\exp[-(2\lambda_a / L_c)^2]\cos(2\pi\lambda_a / \lambda_m) + \exp[-(\lambda_a / L_c)^2]\cos(\pi\lambda_a / \lambda_m)}{1 + \exp[-(\lambda_a / L_c)^2]\cos(\pi\lambda_a / \lambda_m)}$$

$$(3.2.14)$$

Assuming that the **wavelength difference** between the two laser diode sources is $\Delta\lambda$, i.e. $\Delta\lambda = \lambda_2 - \lambda_1$, and $\Delta\lambda > 0$, then as

$$\lambda_a = 2\lambda_1\lambda_2/(\lambda_1 + \lambda_2)$$

$$= 2\lambda_1[1 - \lambda_1/(2\lambda_1 + \Delta\lambda)], \qquad (3.2.15)$$

$$\lambda_m = 2\lambda_1\lambda_2/(\lambda_2 - \lambda_1)$$

$$= 2\lambda_1(1 + \lambda_1/\Delta\lambda) \qquad (3.2.16)$$

the following can be obtained

$$\lambda_m/\lambda_a = 1 + 2\lambda_1/\Delta\lambda \qquad (3.2.17)$$

i.e. I_{01n} is essentially a function of wavelength difference, $\Delta\lambda$.

Assuming that $\lambda_m/\lambda_a = 1 + 2\lambda_1/\Delta\lambda = t$ is a real quantity, then

$$\Delta\lambda = 2\lambda_1 / (t - 1) \qquad (3.2.18)$$

By equation (3.2.15)

$$\lambda_a = (t + 1)\lambda_1 / t \qquad (3.2.19)$$

The normalized fringe intensity obtained from equation (3.2.14) then becomes

$$I_{01n}(\Delta\lambda) = I_{01n}[2\lambda_1 / (t - 1)]$$

$$= \frac{\exp\{-[2(t+1)\lambda_1 / tL_c]^2\}\cos(2\pi / t) + \exp\{-[(t+1)\lambda_1 / tL_c]^2\}\cos(\pi / t)}{1 + \exp\{-[(t+1)\lambda_1 / tL_c]^2\}\cos(\pi / t)}$$

$$= 1 + \frac{\exp\{-[2(t+1)\lambda_1 / tL_c]^2\}\cos(2\pi / t) - 1}{1 + \exp\{-[(t+1)\lambda_1 / tL_c]^2\}\cos(\pi / t)} \qquad (3.2.20)$$

For a larger wavelength difference $\Delta\lambda' > \Delta\lambda$, and correspondingly, $\Delta\lambda' = 2\lambda_1 / (t' - 1)$, where t' is also assumed to be a real quantity, then $2\lambda_1 / (t' - 1) > 2\lambda_1 / (t - 1)$, which leads to $t' < t$, so

$$I_{01n}(\Delta\lambda') - I_{01n}(\Delta\lambda)$$

61

$$= \frac{\exp\{-[2(t'+1)\lambda_1 / t'L_c]^2\}\cos(2\pi / t') - 1}{1 + \exp\{-[(t'+1)\lambda_1 / t'L_c]^2\}\cos(\pi / t')} - \frac{\exp\{-[2(t+1)\lambda_1 / tL_c]^2\}\cos(2\pi / t) - 1}{1 + \exp\{-[(t+1)\lambda_1 / tL_c]^2\}\cos(\pi / t)}$$

$$(3.2.21)$$

If A is defined by

$$(\lambda_1/L_c)^2 = A \qquad (3.2.22)$$

and

$$I_{00}(\Delta\lambda) = 1 + \exp\{-[(t + 1)/t]^2 A\}\cos(\pi/t) \qquad (3.2.23)$$

equation (3.2.21) becomes

$$I_{01n}(\Delta\lambda') - I_{01n}(\Delta\lambda)$$

$$= [1/I_{00}(\Delta\lambda')I_{00}(\Delta\lambda)]\ \{\exp[-4A(t' + 1)^2/t'^2]\cos(2\pi/t') - \exp[-4A(t + 1)^2/t^2]\cos(2\pi/t)$$

$$+ \exp[-A(t' + 1)^2/t'^2]\cos(\pi/t') - \exp[-A(t + 1)^2/t^2]\cos(\pi/t)$$

$$+ \exp\{-[4A(t' + 1)^2/t'^2 + A(t + 1)^2/t^2]\}\cos(2\pi/t')\cos(\pi/t)$$

$$- \exp\{-[4A(t + 1)^2/t^2 + A(t' + 1)^2/t'^2]\}\cos(2\pi/t)\cos(\pi/t')\} \qquad (3.2.24)$$

Since $t > t' > 1$, then

$$\cos(\pi/t') < \cos(\pi/t) \qquad (3.2.25)$$

$$\exp[-A(t' + 1)^2/t'^2] = \exp[-A(1 + 1/t')^2]$$

$$< \exp[-A(1 + 1/t)^2] \qquad (3.2.26)$$

so that

$$\exp[-A(t' + 1)^2/t'^2]\cos(\pi/t') - \exp[-A(t + 1)^2/t^2]\cos(\pi/t) < 0 \qquad (3.2.27)$$

$$\exp[-4A(t' + 1)^2/t'^2]\cos(2\pi/t') - \exp[-4A(t + 1)^2/t^2]\cos(2\pi/t) < 0 \qquad (3.2.28)$$

Also from

$$2t + t' > 2t' + t \qquad (3.2.29)$$

$$2t - t' > 2t' - t \qquad (3.2.30)$$

the following can be written

$$\cos[(2t + t')\pi/tt')] < \cos[(2t' + t)\pi/tt')] \qquad (3.2.31)$$

62

$$\cos[(2t - t')\pi/tt')] < \cos[(2t' - t)\pi/tt')]$$ (3.2.32)

in the general situation, of $\lambda_1/\Delta\lambda' > 1$, the condition

$$(2t + t') / tt' < 1$$ (3.2.33)

and $$(2t - t') / tt' < 1$$ (3.2.34)

can be satisfied. Hence

$$\exp\{-[4A(t' + 1)^2/t'^2 + A(t + 1)^2/t^2]\}\cos(2\pi/t')\cos(\pi/t)$$

$$- \exp\{-[4A(t + 1)^2/t^2 + A(t' + 1)^2/t'^2]\}\cos(2\pi/t)\cos(\pi/t')$$

$$< \exp\{-[4A(t' + 1)^2/t'^2 + A(t + 1)^2/t^2]\}[\cos(2\pi/t')\cos(\pi/t) - \cos(2\pi/t)\cos(\pi/t')]$$

$$= (1/2)\exp\{-[4A(t' + 1)^2/t'^2 + A(t + 1)^2/t^2]\} [\cos(2\pi/t' + \pi/t) + \cos(2\pi/t' - \pi/t)$$

$$- \cos(2\pi/t + \pi/t') - \cos(2\pi/t - \pi/t')]$$

$$= (1/2)\exp\{-[4A(t' + 1)^2/t'^2 + A(t + 1)^2/t^2]\} \{\cos[(2t + t')\pi/tt'] + \cos[(2t - t')\pi/tt']$$

$$- \cos[(2t' + t)\pi/tt'] - \cos[(2t' - t)\pi/tt']\}$$

$$< 0$$ (3.2.35)

From equation (3.2.27), (3.2.28), (3.2.35) and the fact that $I_{00}(\Delta\lambda)\, I_{00}(\Delta\lambda') > 0$, it can be written that

$$I_{01n}(\Delta\lambda') - I_{01n}(\Delta\lambda) < 0$$ (3.2.36)

Therefore, for $\Delta\lambda' > \Delta\lambda$, it has $I_{01n}(\Delta\lambda') < I_{01n}(\Delta\lambda)$, i.e. $I_{01n}(\Delta\lambda)$ has been shown to be a monotonically decreasing function.

The normalized intensity difference between the central fringe and the first side fringe in the central fringe packet is:

$$\Delta I_{01n} = (I_{00} - I_{01})/I_{00}$$

$$= 1 - I_{01n}$$ (3.2.37)

In order to identify correctly the central fringe position in a white light interferometric system, the value of ΔI_{01n} should be larger than the system noise level, otherwise the output signal may be lost in the background noise. To facilitate the

process of quantitative evaluation, a minimum signal-to-noise ratio required by the system to identify the central fringe, SNR_{min}, is introduced, which is defined as:

$$SNR_{min} = 1/\Delta I_{0n} \qquad (3.2.38)$$

or, in terms of dB (in the electrical domain), it is given by

$$SNR_{min} (dB) = -20lg(\Delta I_{0n}) \qquad (3.2.39)$$

where ΔI_{0n} is the normalized intensity (peak-to-peak value) difference between the central fringe and the largest side fringe. The SNR_{min} value is thus used to describe the performance of the system, and a small SNR_{min} value is considered to correspond a high performance white light interferometric system for ease of identification of the central fringe.

Therefore, in order to identify efficiently the central fringe in the central fringe packet, the value

$$SNR_{min} = 1/\Delta I_{0n} = 1/\Delta I_{01n}$$

$$= 1/(1 - I_{01n}) \qquad (3.2.40)$$

or equivalently

$$SNR_{min} (dB) = -20lg(\Delta I_{0n}) = -20lg(\Delta I_{01n})$$

$$= -20lg(1 - I_{01n}) \qquad (3.2.41)$$

should be as small as possible. Because of the monotonically decreasing nature of the function $I_{01n}(\Delta\lambda)$, this value can be reduced provided that the wavelength difference between the laser diodes, $\Delta\lambda$, is increased.

However, the central fringe in the first side fringe packet should also be considered, as this may become the largest side fringe in the output fringe pattern as will be shown in the next Section, and consequently, the value of SNR_{min} in the system will be increased for the determination of the central fringe position.

To determine the near central fringe intensity (peak-to-peak value) in the first side fringe packet, it may be assumed that

$$\lambda_m/\lambda_a = n + \delta \tag{3.2.42}$$

where n is an integer, and δ is a real number given by $0 \le \delta < 1$, and thus equation (3.2.6) can be written as

$$I_{ac}(x) = \exp\left[-(2x/L_c)^2\right] \cos[2\pi x/(n+\delta)\lambda_a] \cos(2\pi x/\lambda_a) \tag{3.2.43}$$

The fringe peak positions are

$$x = m\lambda_a/2 \qquad (m = 0, \pm 1, \pm 2, ...) \tag{3.2.44}$$

Since the envelope peak position in the first side fringe packet is $\lambda_m/2 = (n + \delta)\lambda_a/2$, thus the possible near central fringe peak positions, in the first side fringe packet are given by

$$n\lambda_a/2,\ (n + 1)\lambda_a/2,\ (n + 2)\lambda_a/2 \text{ and } (n + 3)\lambda_a/2,$$

and the corresponding intensities are

$$I_{ac}(n\lambda_a/2) = \exp[-(n\lambda_a/L_c)^2] \cos[n\pi/(n + \delta)] \cos(n\pi)$$

$$= (-1)^{n+1} \exp[-(n\lambda_a/L_c)^2] \cos[\delta\pi/(n + \delta)] \tag{3.2.45}$$

Similarly,

$$I_{ac}[(n + 1)\lambda_a/2] = (-1)^n \exp\{-[(n + 1)\lambda_a/L_c]^2\} \cos[(1 - \delta)\pi/(n + \delta)] \tag{3.2.46}$$

$$I_{ac}[(n + 2)\lambda_a/2] = (-1)^{n+1} \exp\{-[(n + 2)\lambda_a/L_c]^2\} \cos[(2 - \delta)\pi/(n + \delta)] \tag{3.2.47}$$

$$I_{ac}[(n + 3)\lambda_a/2] = (-1)^n \exp\{-[(n + 3)\lambda_a/L_c]^2\} \cos[(3 - \delta)\pi/(n + \delta)] \tag{3.2.48}$$

By comparing the values of each pair of possible near central peak intensity of the same sign, it can be seen that

$$|I_{ac}(n\lambda_a/2)| - |I_{ac}[(n + 2)\lambda_a/2)|$$

$$= \exp[-(n\lambda_a/L_c)^2] \ |\cos[\delta\pi/(n + \delta)]| - \exp\{-[(n + 2)\lambda_a/L_c]^2\} \ \cos|[(2 - \delta)\pi/(n + \delta)]|$$

$$> \exp[-(n\lambda_a/L_c)^2] \ \{|\cos[\delta\pi/(n + \delta)]| - |\cos[(2 - \delta)\pi/(n + \delta)]|\}$$

When $n \ge 1$ and $(2 - \delta)/(n + \delta) < 1/2$,

$$\exp[-(n\lambda_a/L_c)^2] \ \{|\cos[\delta\pi/(n + \delta)]| - |\cos[(2 - \delta)\pi/(n + \delta)]|\}$$

$$= \exp[-(n\lambda_a/L_c)^2] \{\cos[\delta\pi/(n + \delta)] - \cos[(2 - \delta)\pi/(n + \delta)]\}$$

$$= 2 \exp[-(n\lambda_a/L_c)^2] \sin[\pi/(n + \delta)] \sin[(1 - \delta)\pi/(n + \delta)]$$

$$\geq 0 \tag{3.2.49}$$

When $n \geq 1$ and $1/2 < (2 - \delta)/(n + \delta) < 1$,

$$\exp[-(n\lambda_a/L_c)^2] \{|\cos[\delta\pi/(n + \delta)]| - |\cos[(2 -\delta)\pi/(n + \delta)]|\}$$

$$= \exp[-(n\lambda_a/L_c)^2] \{\cos[\delta\pi/(n + \delta)] + \cos[(2 -\delta)\pi/(n + \delta)]\}$$

$$= 2 \exp[-(n\lambda_a/L_c)^2] \cos[\pi/(n + \delta)] \cos[(1 - \delta)\pi/(n + \delta)]$$

$$\geq 0 \tag{3.2.50}$$

Hence, when $n \geq 2$

$$|I_{ac}(n\lambda_a/2)| \geq |I_{ac}[(n + 2)\lambda_a/2)| \tag{3.2.51}$$

Using the same method, it can be seen that, when $n > 3$

$$|I_{ac}[(n + 1)\lambda_a/2)| > |I_{ac}[(n + 3)\lambda_a/2)| \tag{3.2.52}$$

Therefore, in the general situation of $n > 3$, the near central fringe intensity (peak-to-peak value) in the first side fringe packet can be expressed as

$$I_{10} = |\ I_{ac}(n\lambda_a/2) - I_{ac}[(n+1)\lambda_a/2]|$$

$$= \exp[-(n\lambda_a/L_c)^2]\cos[\delta\pi/(n+\delta)] + \exp\{-[(n+1)\lambda_a/L_c]^2]\cos[(1-\delta)\pi/(n+\delta)]\} \tag{3.2.53}$$

The normalized form of I_{10} is

$$I_{10n} = I_{10} / I_{00}$$

$$= \frac{\exp[-(n\lambda_a / L_c)^2]\cos[\delta\pi / (n + \delta)] + \exp\{-[(n+1)\lambda_a / L_c]^2\}\cos[(1 - \delta)\pi / (n + \delta)]}{1 + \exp[-(\lambda_a / L_c)^2]\cos[\pi / (n + \delta)]}$$

$$\tag{3.2.54}$$

The normalized intensity difference between the central fringe in the central fringe packet and that in the first side fringe packet is then

$$\Delta I_{10n} = (I_{00} - I_{10})/ I_{00}$$

$$= 1 - I_{10n} \qquad (3.2.55)$$

and the corresponding minimum signal-to-noise ratio required by the system is then

$$SNR_{min} = 1/\Delta I_{10n} = 1/(1 - I_{10n}) \qquad (3.2.56)$$

or $\qquad SNR_{min} (dB) = -20\lg(1 - I_{10n}) \qquad (3.2.57)$

For the same reason as discussed previously, I_{10n} is also a function of $\Delta\lambda$. From equation (3.2.17) and (3.2.42), it can be seen that $\lambda_m/\lambda_a = 1 + 2\lambda_1/\Delta\lambda = n + \delta$, which leads to $\Delta\lambda = 2\lambda_1 /(n-1+\delta)$. If the wavelength difference, $\Delta\lambda$, can be divided into a series of sections $[2\lambda_1/n, 2\lambda_1/(n-1)]$, then $I_{10n}(\Delta\lambda)$ is a monotonic increasing function for the end points: $2\lambda_1/n, 2\lambda_1/(n-1), \dots$, and within a particular section, i.e. when

$$\Delta\lambda \in [2\lambda_1/n_0, 2\lambda_1/(n_0-1)]$$

where n_0 is a given integer, $I_{10n}(\Delta\lambda)$ appears as a convex curve [Appendix A].

Since the section length, $2\lambda_1/(n-1) - 2\lambda_1/n = 2\lambda_1/n(n-1)$ is small as n is usually large, the curve, $I_{10n}(\Delta\lambda)$, may be considered to intersect with $I_{01n}(\Delta\lambda)$ at only one point, at this point, where $\Delta\lambda = \Delta\lambda_{opt}$, and

$$I_{01n}(\Delta\lambda_{opt}) = I_{10n}(\Delta\lambda_{opt}) \qquad (3.2.58)$$

Moreover, when $\Delta\lambda < \Delta\lambda_{opt}$, so $I_{01n} > I_{10n}$, the SNR_{min} is determined by I_{01n}, thus having a relatively large value. If $\Delta\lambda > \Delta\lambda_{opt}$, then $I_{01n} < I_{10n}$, but the SNR_{min} is now defined by I_{01n}, and also possesses a high value. Only at $\Delta\lambda = \Delta\lambda_{opt}$, can the SNR_{min} reach its lowest possible value, and hence this point can be termed the **optimum point**, and the corresponding wavelength difference, $\Delta\lambda_{opt}$, can be defined as the **optimum wavelength difference.**

This feature, in turn, provides a guide in selecting the appropriate wavelength combinations for a two wavelength source in a white light system. For any given laser diode of wavelength λ_1, there exists an optimum wavelength difference, $\Delta\lambda_{opt}$, when the wavelength of the second laser diode can be chosen to be

$$\lambda_2 = \lambda_1 + \Delta\lambda_{opt} \tag{3.2.59}$$

where the SNR_{min} reaches its lowest possible value, and thus the wavelength combination of λ_1 and λ_2 constitutes an **optimum wavelength combination**.

For a given wavelength, λ_1, in order to obtain $\Delta\lambda_{opt}$, the equation (3.2.58) must be satisfied. Because of the nonlinear nature of the equation, an analytical solution is usually not available. However, a numerical solution can readily be obtained by the use of a computer program, as will be discussed in Section 3.3.

It should be noted that the optimum wavelength difference, $\Delta\lambda_{opt}$, only provides a reference value for selecting the appropriate wavelength combination, and a satisfactory but not necessarily optimum SNR_{min} value may be obtained when the wavelength difference, $\Delta\lambda$, is near this reference value. The actual selection should take into account the commercial availability of the laser diodes and make a selection on that basis for ease of availability of components and low cost.

3.2.4 Equivalent Coherence Length

For a single light source white light interferometric system, the measurement precision is determined by the coherence length of light sources used, and in the case of a two wavelength system, the precision depends on the central fringe packet width or the equivalent coherence length. Equation (3.2.7) may be rewritten, where the visibility curve is given by

$$V(x) = \exp[-(2x/L_c)^2]\cos(2\pi x/\lambda_m)$$

when $x = \pm \lambda_m/4$, $V(x) = 0$. The central fringe packet width is only $\lambda_m/2$, which is greatly reduced compared with the use of the original laser diode with its coherence length. The corresponding **equivalent coherence length**, L_{ce}, of the two wavelength source, as shown in Fig.3.2, can then be defined as the full width of the central fringe packet when the visibility has fallen to $1/e$ of its peak value, which is given by $2x_0$, where x_0 satisfies the condition

$$\exp[-(2x_0/L_c)^2]\cos(2\pi x_0/\lambda_m) = 1/e \qquad\qquad (3.2.60)$$

Similarly, the value of $L_{ce} = 2x_0$ can also be obtained from the results of the computer simulations, as will be described in the next Section.

3.3 Computer Simulations of two Wavelength Combination Sources

The computer simulations of two wavelength combination sources can be used to illustrate the principle of the theoretical analysis discussed earlier in graphical form and furthermore, it is a valuable aid to explore the main characteristics of two wavelength combination sources and to their optimization.

The characteristics of interference fringe patterns for different wavelength combinations of a two wavelength source can be studied by changing the wavelength difference between the two laser diode sources, and a series of simulation results are shown in Fig.3.3, where a given laser diode wavelength is $\lambda_1 = 635\text{nm}$ and the second laser diode wavelengths λ_2 are 688nm, 797nm and 830nm respectively or in other words, the corresponding wavelength difference between the two laser diodes, $\Delta\lambda = \lambda_2 - \lambda_1$ are 53nm, 162nm and 195nm respectively. All the laser diodes are assumed to exhibit the same coherence length of 16µm, when operated below the threshold current.

It becomes clear from these fringe patterns that as the wavelength difference, $\Delta\lambda = \lambda_2 - \lambda_1$, increases, the normalized first side fringe intensity in the central fringe packet, I_{01n}, will decrease, but the normalized central fringe intensity in the first side packet, I_{10n}, will increase. Hence, there exists a value of $\Delta\lambda_{opt}$, discussed earlier, such that when the wavelength of the second light source $\lambda_2 = \lambda_1 + \Delta\lambda_{opt}$, then $I_{01n} = I_{10n}$. In such a situation, the SNR_{min} has the lowest possible value, and the wavelength combination corresponds to an optimum wavelength combination.

The process of finding such an optimum wavelength combination is illustrated in Fig.3.4, where the two laser diodes selected are assumed to have the same coherence length of 60μm, (a reasonable assumption for a commercial system) and the given initial laser diode wavelength is 630nm as these devices are widely available from a range of manufacturers. A simple computer program was designed to locate the positions and calculate the normalized peak-to-peak values of the first side fringe in the central fringe packet, I_{01n}, and the central fringe in the first side fringe packet, I_{10n}, which may be found in Appendix B.

With the variation of wavelength difference, $\Delta\lambda$, both the values of I_{01n} and I_{10n} are altered accordingly. I_{01n} is a strict monotonically decreasing function of wavelength difference, $\Delta\lambda$, whereas I_{10n} represents an increasing function. Consequently, the two curves can intersect at one point, that being where $\Delta\lambda = \Delta\lambda_{opt} = 77$nm. At this point, as shown in Fig.3.5, the SNR_{min} reaches its lowest possible value, thus an optimum wavelength combination may be obtained over this wavelength region.

These two figures, Fig.3.4 and Fig.3.5, are representative of the trends experienced with a range of diodes and the same analysis is applicable for any given initial wavelength and coherence length of the laser diodes used.

Assuming that the two sources have the same coherence length, by the use of the same analysis procedure, it can be seen that the value of the optimum wavelength difference, $\Delta\lambda_{opt}$, varies with the given wavelength, λ_1, but a linear relationship may be maintained as indicated in Fig.3.6. Hence the optimum wavelength combination for any given laser diode may be easily selected by the use of this figure. As an example, a multimode laser diode can typically have a central wavelength of 635nm and a coherence length of 16μm, and thus it can be determined from the figure that the corresponding optimum wavelength difference is about 162nm and so the most appropriate second laser diode would have a wavelength of 797nm, i.e. a laser diode selected in the ~800nm wavelength region could be ideal. The results of the simulation also show that the larger values of coherence length correspond to the smaller values of $\Delta\lambda_{opt}$, whereas a smaller coherence length implies a larger value of $\Delta\lambda_{opt}$.
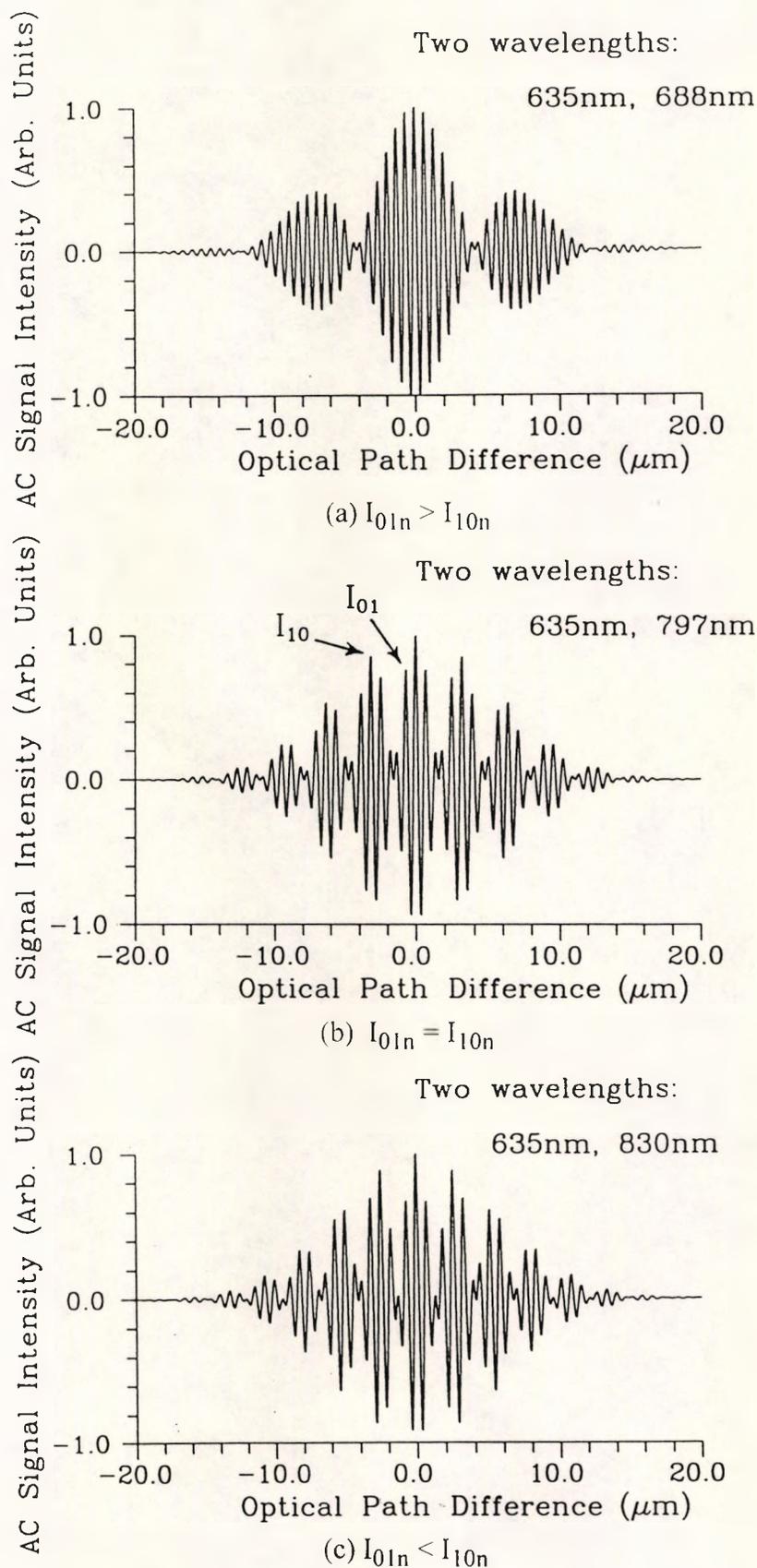
Fig.3.3 Computer Simulated Interference Fringe Patterns for a two Wavelength

Combination Source with the same Coherence Length $L_c = 16\mu m$
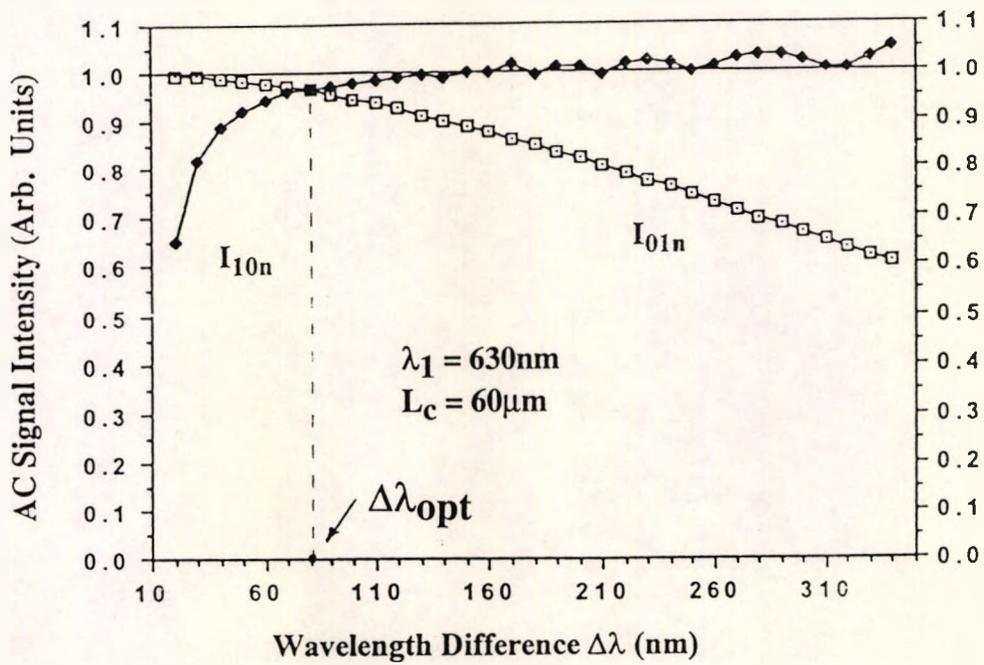
Fig. 3.4 The Variation of Normalized Fringe Intensity I_{01n} and I_{10n} with Wavelength Difference
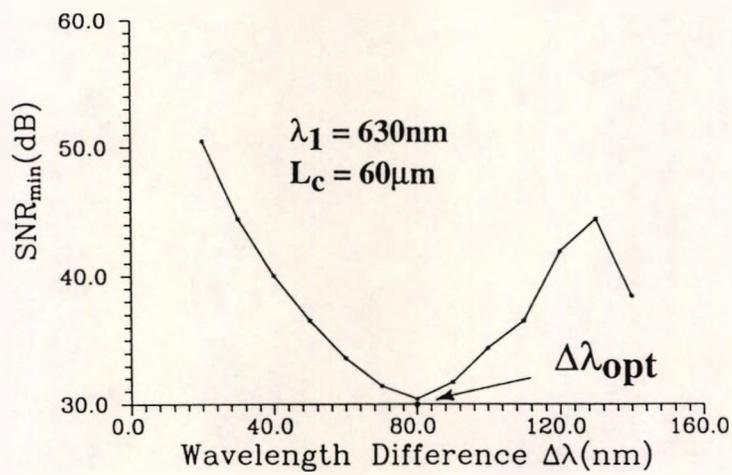
Fig. 3.5 The Variation of SNR_{min} with Wavelength Difference
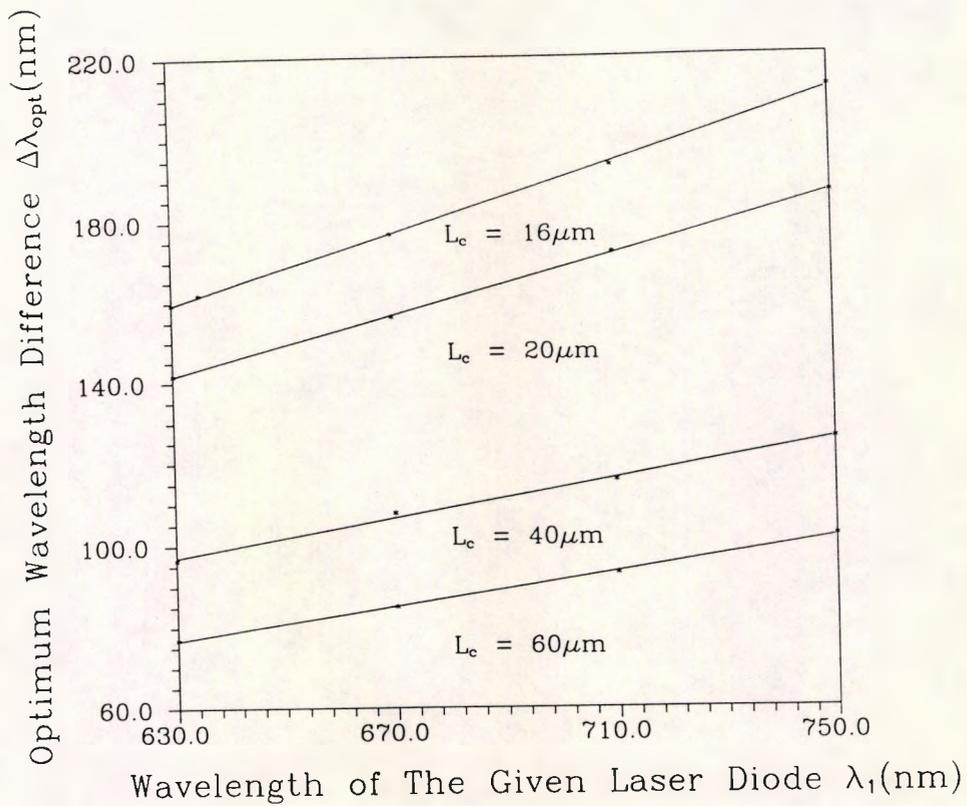
Fig. 3.6 The Optimum Wavelength Difference for a Given Wavelength
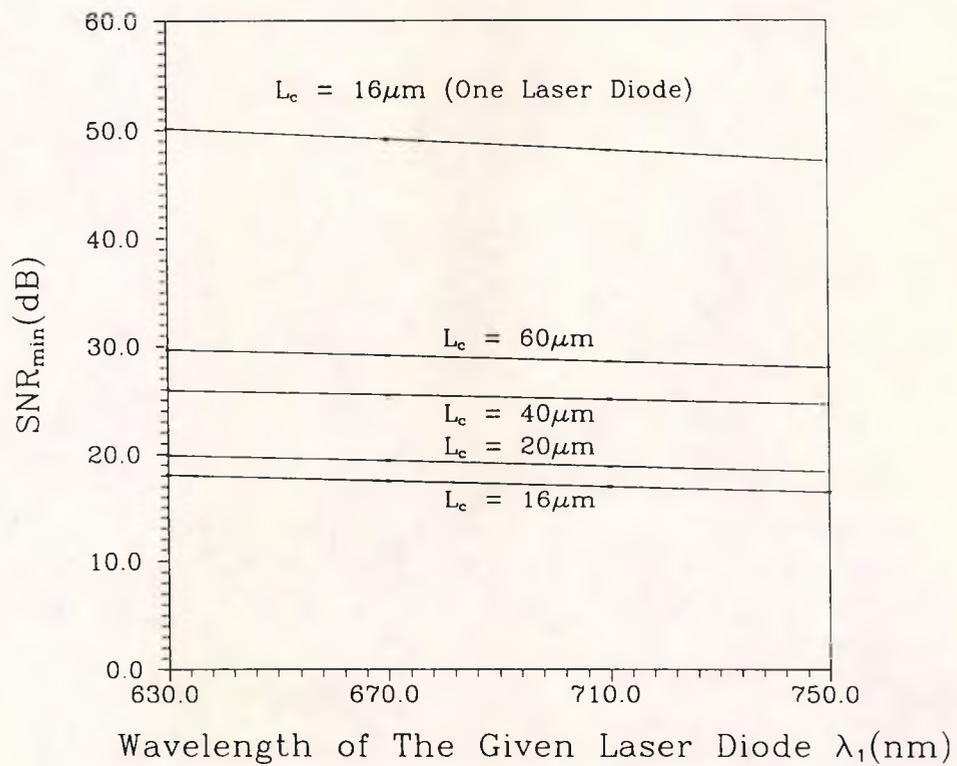
Fig. 3.7 The SNR$_{min}$ at Optimum Wavelength Combinations
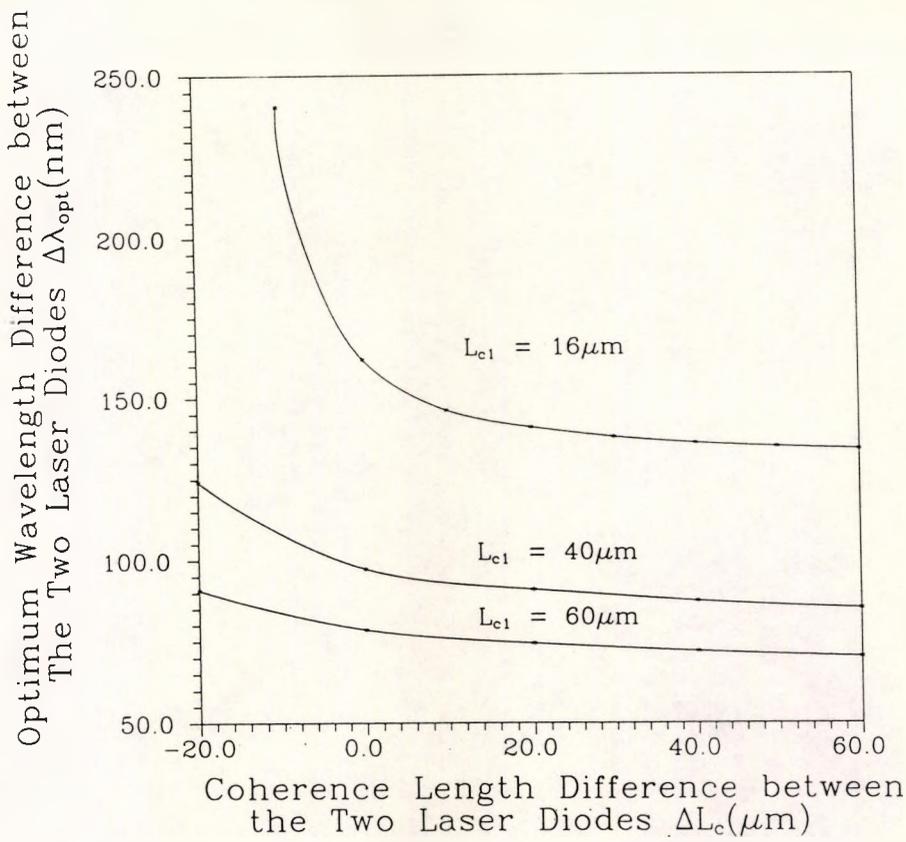
Fig.3.8 The Optimum Wavelength Difference for two Laser Diodes with

Different Coherence Lengths $\Delta L_c = L_{c2} - L_{c1}$ ($\lambda_1 = 635nm$)
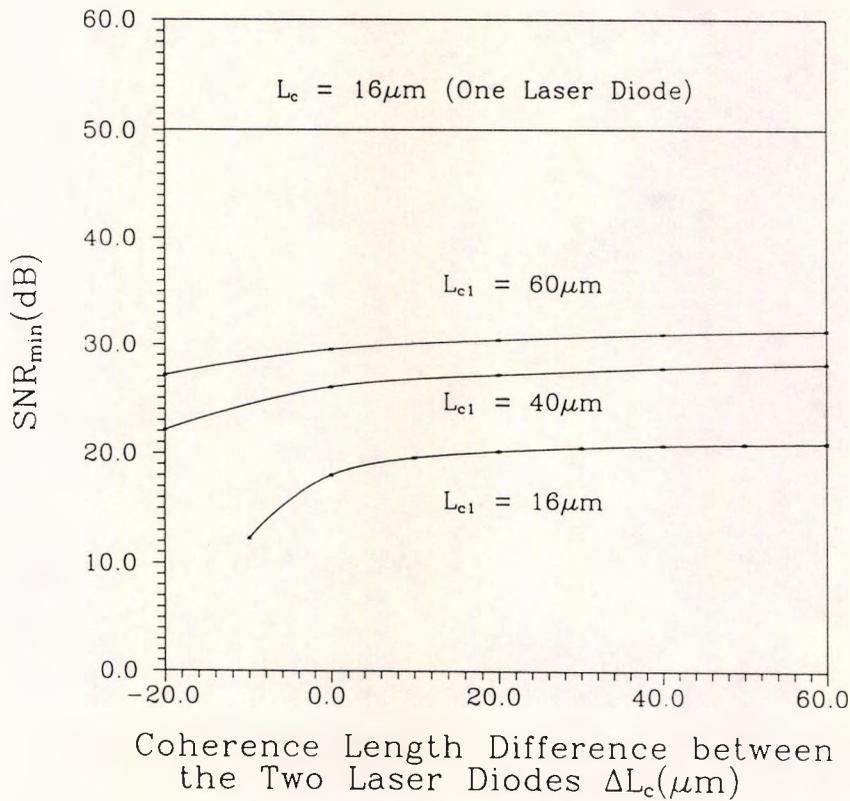
Fig.3.9 The SNR_{min} for two Laser Diodes with Different Coherence

Lengths $\Delta L_c = L_{c2} - L_{c1}$ ($\lambda_1 = 635nm$)

For two laser diodes operated at the optimum wavelength combination, the SNR_{min}, as shown in Fig.3.7, is almost a linear function of λ_1, and is significantly reduced when compared with the use of a single laser diode source. The SNR_{min} also depends on the coherence length, and a larger SNR_{min} reduction can be expected when smaller coherence length sources are employed. For instance, if $\lambda_1 = 635nm$ and $L_c = 16\mu m$, then a $SNR_{min} = 18dB$ can be obtained, thus increasing the system performance. In addition, an interesting result may also be noted from the graph in that the reduction of SNR_{min} is about the same for different values of given wavelength, λ_1, this enabling a wide selection for the initial laser diode.

In the above examples, the two laser diodes of optimum wavelength combination are assumed to possess the same coherence length. If this is not the case, then the **coherence length difference** between the two sources, $\Delta L_c = L_{c2} - L_{c1}$, will have a significant effect on both the optimum wavelength difference and the value of SNR_{min}.

From Fig.3.8 and Fig.3.9, where the wavelength of a given laser diode is still 635nm, it is clear that SNR_{min}, at the optimum wavelength combination can be altered, depending on the values of the coherence length difference between the two laser diodes, and an increase in ΔL_c will result in a decrease in $\Delta \lambda_{opt}$ but an increase in SNR_{min}.

Fig.3.10 reveals that with the increase of wavelength difference, the equivalent coherence length of the system is decreased, such a decrease is sharp for a wavelength difference region between 0 to 20nm, and becomes considerably less so when the wavelength difference is larger than 100nm. In a two wavelength system, a small equivalent coherence length means a high measurement precision may be achieved, provided that the central fringe packet and thus the central fringe can be readily identified. When the wavelength difference is relatively large, only a very small reduction of the equivalent coherence length can be obtained, whereas the central fringe in the first side fringe packet is significantly increased (Fig.3.4) which increases the central fringe identification difficulty, and thus it is essential for a two wavelength system to operate with the optimum wavelength combination.
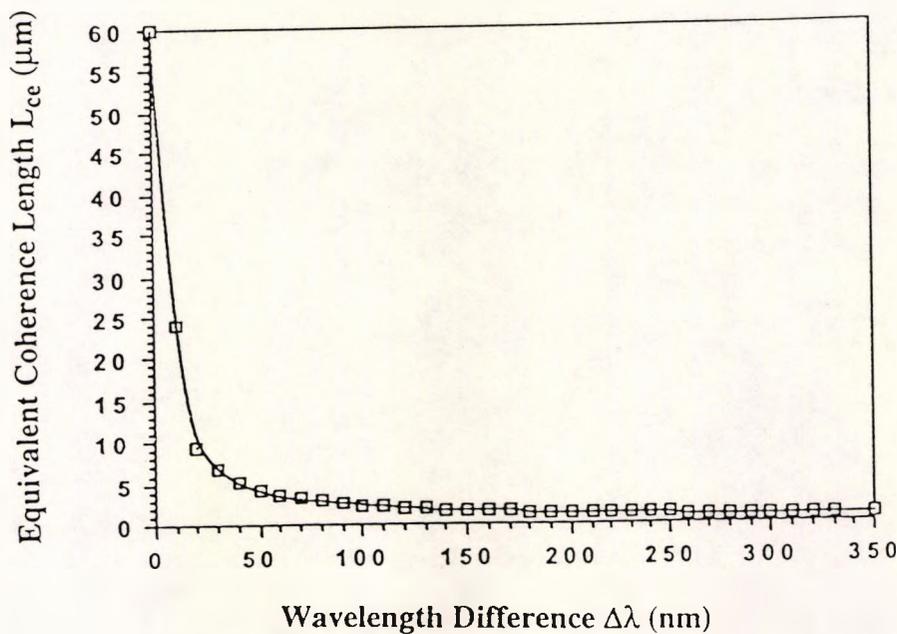
Fig.3.10 The Variation of Equivalent Coherence Length, L_{ce}, with Wavelength Difference

3.4 Experimental Results of two Wavelength Combination Sources

In order to verify the principle of operation established in the theoretical analysis given earlier and to confirm the results of the computer simulation, a series of experiments has been carried out in a white light interferometric system, illuminated by a two wavelength combination source.

3.4.1 Experimental Arrangement for the two Wavelength Combination Sources

The experimental arrangement used to investigate the characteristics of the two wavelength combination sources in a white light interferometric system is shown in Fig.3.11, which represents a simple Michelson interferometer arrangement.

Beam Splitter

M1

Micrometer

MLD 1

MLD 2

M2

PD

OC

DSA

PC
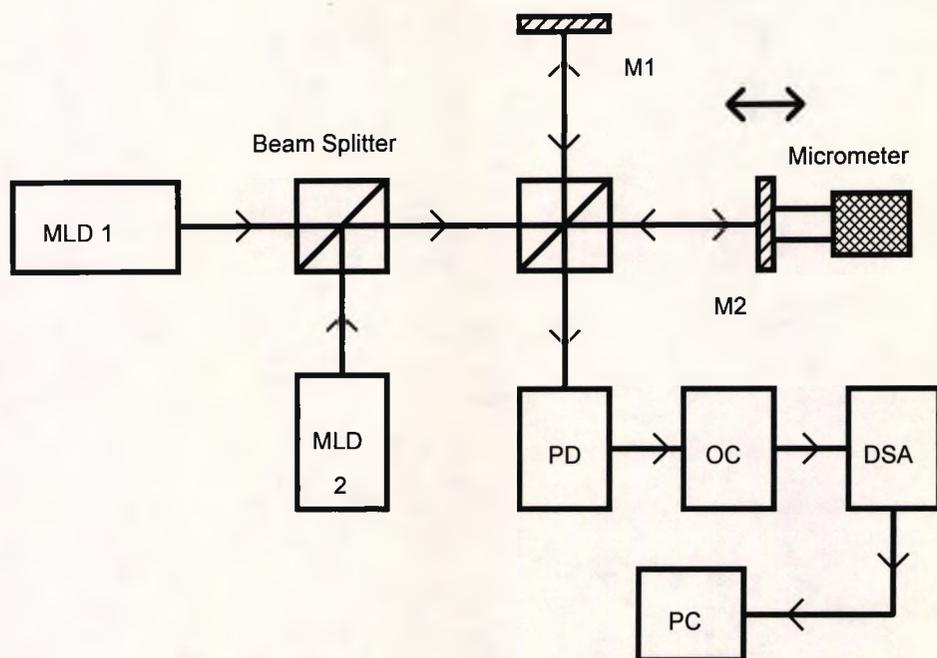
MLD : Multimode Laser Diode;   M : Mirror;

PD : Photodetector;   OC : Oscilloscope;

DSA : Digital Storage Adaptor;   PC : Personal Computer

Fig.3.11 Experimental Arrangement

The outputs from the two multimode laser diodes were combined through a beam splitter to form a single light beam before entering the interferometer. The beam was then divided by another beam splitter into two and reflected by two mirrors, M_1 and M_2 respectively. Mirror M_1 was a reference mirror, and mirror M_2 was mounted on a micrometer to allow a continuous adjustment of the OPD in the interferometer. In order to generate such phase modulation signals that can be observed on an oscilloscope, mirror M_2 was also driven by a loudspeaker at the micrometer. The reflected beams from the two mirrors were combined again and detected by a photodetector connected to an oscilloscope to observe its output. The interference fringe patterns were recorded on a personal computer which was connected to the oscilloscope through a digital storage adaptor (Thurlby DSA524).

The laser diodes used were operated just below their threshold to achieve a short coherence length output as this allows the overall profile to be observed more easily on the oscilloscope.

3.4.2 Experimental Results of the two Wavelength Combination Sources

A set of experiments was performed by the use of the arrangement shown in Fig.3.11. All the laser diodes employed in each experiment possessed a similar coherence length of about $16\mu m$, and the given laser diodes were also the same, at a wavelength of 635nm, but in this case different central wavelengths were selected for the second laser diodes, these being 655nm, 688nm and 830nm respectively. The recorded interference fringe patterns are shown in Fig.3.12, which shows a similarity to those with similar wavelengths and coherence lengths in Fig.3.3, thus verifying the computer simulation results in that when the wavelength difference between the two laser diodes is increased, the normalized intensity of the first side fringe in the central fringe packet, I_{01n}, decreases monotonically, while the central fringe intensity in the first side fringe packet, I_{10n}, is seen to increase. Obviously, at a specific value of wavelength difference, the equation $I_{01n} = I_{10n}$ can be satisfied. The values obtained for I_{01n} and I_{10n} are demonstrated in Fig.3.13, which show agreement with the previous computer simulation results in Fig.3.4, thus confirming the theoretical prediction in relation to the optimum wavelength combination for the two multimode laser diode sources.

In the experimental situation, the optimum wavelength difference, $\Delta\lambda_{opt}$, is determined to be about 175nm and the corresponding SNR_{min}, is about 17.1 dB. When compared with the theoretical values previously obtained, of $\Delta\lambda_{opt} = 162nm$ and $SNR_{min} = 18.0dB$, these results can still be considered as satisfactory confirmation within experimental error, although the small discrepancy between the two sets may have been caused by the fact that only three different laser diodes were employed as the second laser diodes, to generate the data, due to limited availability of such sources.
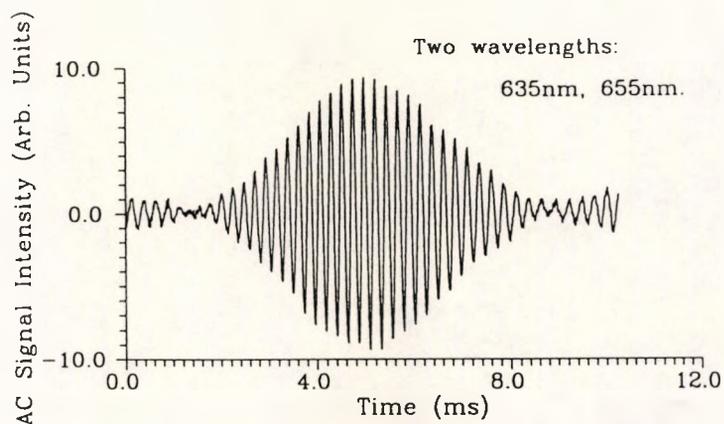
(a) $\lambda_1 = 635nm$, $\lambda_2 = 655nm$, $L_{c1} = 16\mu m$, $L_{c2} = 16\mu m$;
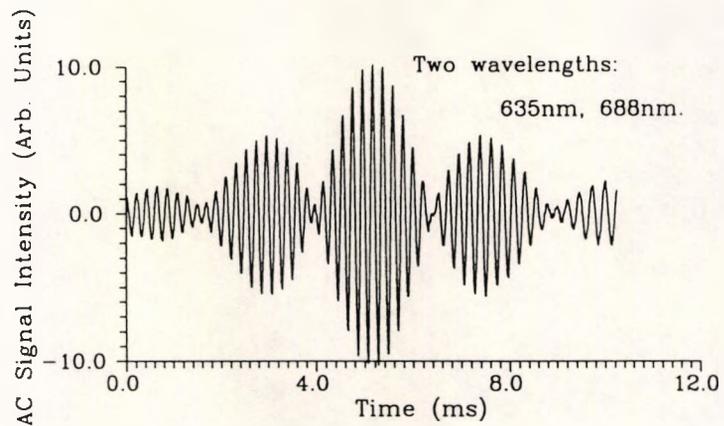
(b) $\lambda_1 = 635nm$, $\lambda_2 = 688nm$, $L_{c1} = 16\mu m$, $L_{c2} = 15\mu m$;
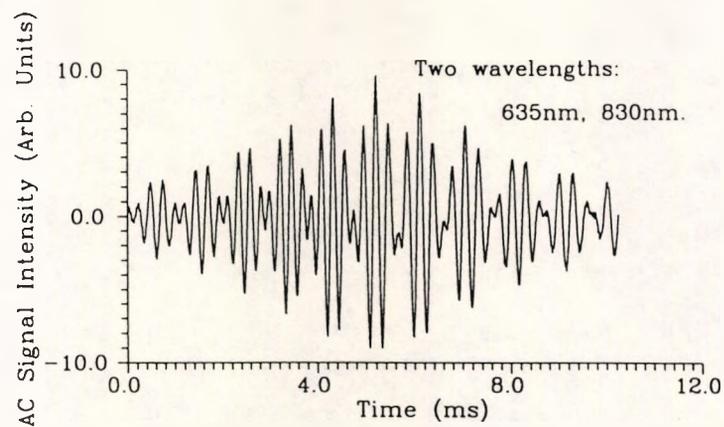
(c) $\lambda_1 = 635nm$, $\lambda_2 = 830nm$, $L_{c1} = 16\mu m$, $L_{c2} = 15\mu m$

Fig.3.12 Experimental Interference Fringe Patterns of two

Wavelength Combination Sources

79
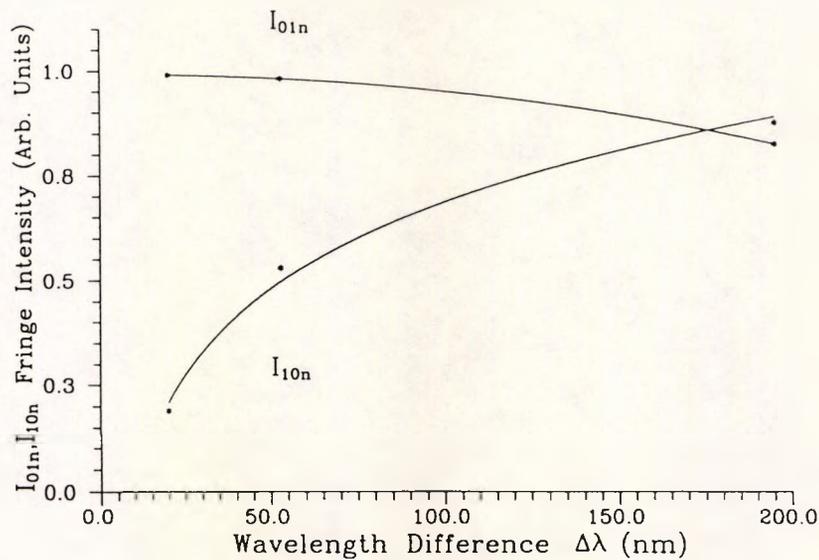
Fig.3.13 Experimental Results of I_{01n} and I_{10n} for Different

Wavelength Combinations ($\lambda_1 = 635nm$)

Another set of experiments was carried out to support further the determination of the optimum wavelength combination. The given laser diode was the same as that used before, i.e. $\lambda_1 = 635nm$, and $L_{c1} = 16\mu m$. Three laser diodes that played the role as the second source were chosen to have different coherence lengths, the values of their central wavelengths and coherence lengths being 670nm and 20μm; 750nm and 40μm; and 786nm and 35μm respectively. The corresponding interference fringe patterns are shown in Fig.3.14. In this case, the value of the optimum wavelength difference, $\Delta\lambda_{opt}$, is between 115nm and 151nm, less than what was obtained in the first set of experiments. However, this fact has already been explained by the simulation shown in Fig.3.8, where the increase of the coherence length difference between the two laser diodes, ΔL_c, results in the decrease of the optimum wavelength difference, $\Delta\lambda_{opt}$, as was accurately predicted.
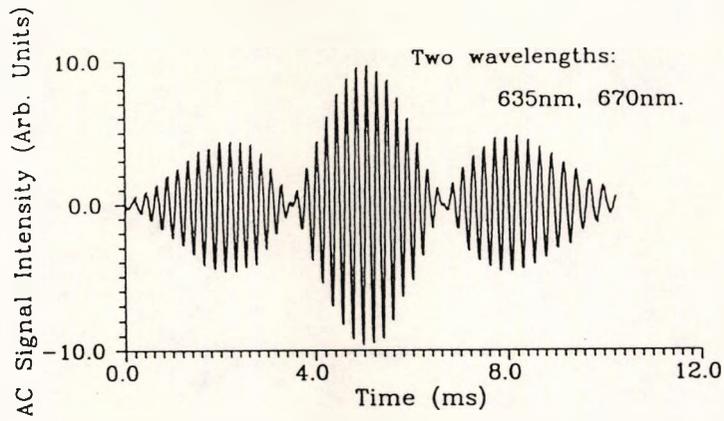
(a) $\lambda_1 = 635\text{nm}$, $\lambda_2 = 670\text{nm}$, $L_{c1} = 16\mu\text{m}$, $L_{c2} = 20\mu\text{m}$;
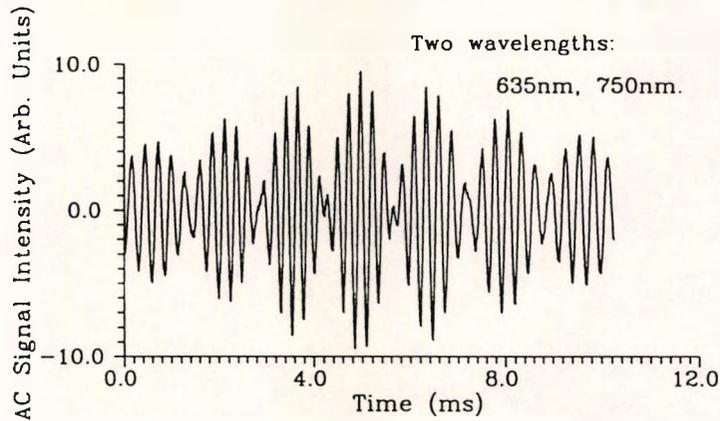
(b) $\lambda_1 = 635\text{nm}$, $\lambda_2 = 750\text{nm}$, $L_{c1} = 16\mu\text{m}$, $L_{c2} = 40\mu\text{m}$;
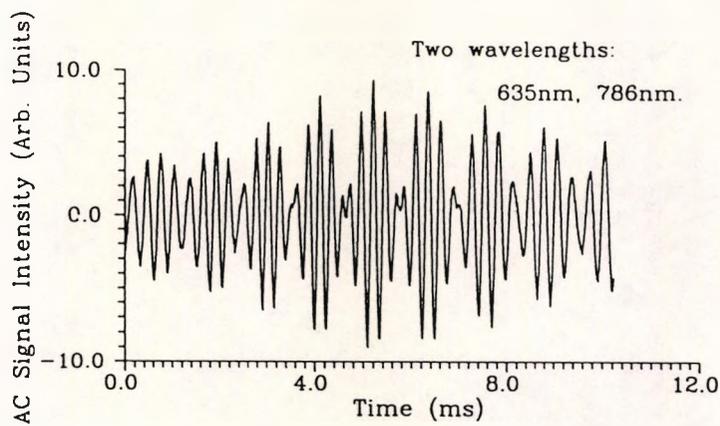
(c) $\lambda_1 = 635\text{nm}$, $\lambda_2 = 786\text{nm}$, $L_{c1} = 16\mu\text{m}$, $L_{c2} = 35\mu\text{m}$

Fig.3.14 Experimental Interference Fringe Patterns of two

Wavelength Combination Sources

Moreover, in both sets of the experiments, it is evident from the interference fringe patterns that the equivalent coherence length of the central fringe packet can be reduced as long as the wavelength difference is increased, and this will greatly enhance the measurement resolution, as discussed earlier.

3.5 Discussion

Compared with a single wavelength light source, the use of a two wavelength combination source can facilitate the central fringe identification, which is of crucial importance in performing high precision measurement in a white light interferometric system. By varying the wavelength difference between the two laser diode sources, the variation of the interference fringe patterns, in a regular and predicted manner, has been revealed. For efficient operation, a method of choosing the optimum wavelength combination of the two laser diode sources has been developed theoretically, and verified experimentally. It has been found that when operated at the optimum wavelength combinations, the minimum signal-to-noise ratio required by the system to identify the central fringe position can be greatly improved when compared to the case of a small or a large wavelength difference. The equivalent coherence length of the central fringe packet can also be decreased as a result of the increase of the wavelength difference, which enhances the measurement precision. The optimum wavelength combination is determined by λ_1, $\Delta\lambda$ and L_c and the variation of which may change the values of SNR_{min} and L_{ce}. Although the cost and slight alignment difficulty may be increased as more optical components are needed than when using a single wavelength light source, this technique shows its importance for optical fibre sensor uses.

As can be seen from this Chapter, the increase of the central fringe intensity in the first side fringe packet with the wavelength difference imposes a limit on both the minimum required signal-to-noise ratio and the equivalent coherence length of a two

wavelength system. To overcome this difficulty and improve further the system performance, a three wavelength or multiwavelength combination source technique has been developed, which becomes the topic of the next Chapter.

References

1. A. S. Gerges, T. P. Newson and D. A. Jackson, "Coherence Tuned Fiber Optic Sensing System, with Self-Initialization, Based on a Multimode Laser Diode", Applied Optics, Vol.29, No.30, pp.4473-4480, 20 October, 1990

2. P. Sandoz and G. Tribillon, "Profilometry by Zero-Order Interference Fringe Identification", Journal of Modern Optics, Vol.40, No.9, pp.1691-1700, 1993

3. W. J. Bock, W. Urbanczyk and M. B. Zaremba, "Electronically Scanned White-Light Interferometric Strain Sensor Employing Highly Birefringent Fibers", Optics Communications, Vol.101, No.3,4, pp.157-162, 15 August 1993

4. P. Hariharau and M. Roy, "White-Light Phase-Stepping Interferometry for Surface Profiling", Journal of Modern Optics, Vol.41, No.11, pp.2197-2201, 1994

5. R. Dändliker, E. Zimmermann and G. Frosio, "Electronically Scanned White-Light Interferometry: a Novel-Resistant Signal Processing", Optics Letters, Vol.17, No.9, pp.679-681, May 1, 1991

6. S. Chen, A. W. Palmer, K. T. V. Grattan and B. T. Meggitt, "Digital Signal-Processing Techniques for Electronically Scanned Optical-Fiber White-Light Interferometry", Applied Optics, Vol.31, No.28, pp.6003-6010, 1 October 1992

7. C. Polhemus, "Two Wavelength Interferometry", Applied Optics, Vol.12, No.9, pp.2071-2074, September 1973

8. Y. Y. Cheng and J. C. Wyant, "Two Wavelength Phase Shifting Interferometry", Applied Optics, Vol.23, No.24, pp.4539-4543, 15 December 1984

9. A. D. Kersey and A. Dandridge, "Dual-Wavelength Approach to Interferometric Sensing", Proceedings of SPIE., Vol.798, pp.176-181, 1987

10. B. K. Ward and K. Seta, "Quasimonochromatic White Light Fringe Interferometer", Applied Optics, Vol.30, No.1, pp.66-71, 1 January 1991

11. S. Chen, K. T. V. Grattan, B. T. Meggitt and A. W. Palmer, "Instantaneous Fringe-Order Identification Using Dual Broad-Band Sources with Widely Spaced Wavelengths", Electronics Letters, Vol.29, No.4, pp.334-335, 18th February 1993

12. Y. J. Rao, Y. N. Ning and D. A. Jackson, "Synthesized Source for White-Light Sensing Systems", Optics Letters, Vol.18, No.6, pp.462-464, March 15, 1993

13. D. N. Wang, Y. N. Ning, K. T. V. Grattan, A. W. Palmer and K. Weir, "Characteristics of Synthesized Light Sources for White-Light Interferometric System", Optics Letters, Vol.18, No.22, pp.1884-1886, November 15, 1993

14. D. N. Wang, Y. N. Ning, K. T. V. Grattan, A. W. Palmer and K. Weir, "The Optimized Wavelength Combinations of Two Broadband Sources for White Light Interferometry", IEEE/OSA Journal of Lightwave Technology, Vol.12, No.5, pp.909-916, May 1994

15. M. Born and E. Wolf, "Principle of Optics", Sixth Edition, p.256, Pergamon Press, 1983

Chapter 4

Multiwavelength Combination Sources

In this Chapter, a multiwavelength combination source technique has been developed, which can improve further the ease of central fringe identification when compared with the two wavelength technique and thus increasing the measurement precision in a white light interferometric system. The optimization of the multiwavelength combination source can be obtained by the use of the results of computer simulations. The interference fringe pattern from such a multiwavelength combination source corresponding to the three commercially available laser diodes is first computer simulated and then experimentally confirmed. The main theoretically and experimentally obtained SNR_{min} values for a single wavelength source, with different combinations of two wavelength sources and multiwavelength sources are also compared, showing a clear and progressive improvement in the ease of the central fringe identification.

4.1 Introduction

As has been discussed, in a white light interferometric system, the central fringe position in the output fringe pattern possesses crucial importance as such a position (i.e. zero OPD position) provides a reliable reference for a high precision measurement [1-2].

As considered in Chapter 3, for a relatively long coherence length light source, such as a multimode laser diode, the precision in determining the central fringe position may

be reduced, but by the use of a two wavelength combination source technique [3-5], the situation can be significantly improved, especially when the two sources have an "optimum" wavelength combination [6-7]. However, the identification problem may still remain in some cases of extremely noisy signals, and further improvements are therefore necessary for a high performance of system operation.

One of the possible techniques that can be explored is that of multiwavelength interferometry [8-9]. A multiwavelength interferometric method has been used in [8] to enhance the capability of dual wavelength interferometry in which, as discussed in Chapter 1, the unambiguous range is increased by the use of equivalent wavelength, λ_{eq}, and when λ_{eq} is large, the fringe visibility curve becomes flat, which makes it harder to determine the information of λ_{eq}, especially when a significant level of amplitude noise exists in the system. In the multiwavelength approach, a third wavelength was introduced, and by the combination of two wavelengths from the three different wavelength sources, a largest equivalent wavelength, λ_{eql}, and a shortest equivalent wavelength, λ_{eqs}, can be produced. Then, by using the phase information of λ_{eql} to correct the 2π ambiguities in the phase data of λ_{eqs}, the corrected phase information of λ_{eqs} is again used to correct the 2π ambiguities experienced in a single wavelength measurement and so the unambiguous range can be increased without the difficulty mentioned above. However, this method is still a conventional interferometric technique as the long coherence length light sources are used, thus suffering the disadvantage that the measurement result is sensitive to the source wavelength stability, as also discussed in Chapter 1.

In the work of Flavin et al [9], a multiwavelength white light interferometric method was used. Light beams from three LEDs of central wavelengths 778nm, 821nm and 856nm, each with a spectral width of ~40nm, were combined by a diffraction grating to form a combination source of central wavelength of 810nm with a spectral width of 100nm, and then the light was launched into a single mode fibre. The combination of LEDs gives a continuous spectrum which was especially required by the work in [9]:

however, as discussed earlier, LEDs have poor coupling efficiency into optical fibres, which represents a drawback for practical optical fibre sensor applications.

In this Chapter, the technique of using several laser diode sources to form a multiwavelength combination source and with it a corresponding method of selecting the optimum wavelength combinations is presented [10-11]. A comparison of single wavelength sources, two wavelength combination sources and three wavelength combination sources has also been made to demonstrate clearly the progressive improvement in the central fringe identification in using these techniques.

As employed before, theoretical analysis, computer simulations and experimental verifications constitute the procedures of this technical development.

4.2 Theoretical Analysis of Multiwavelength Combination Sources

As discussed in Section 3.2, if the light beams from different wavelength sources are mutually incoherent, the resultant output signal intensity is simply the sum of the output signal intensities generated by each light source individually. It also can be understood that the extent of central fringe identification difficulty is actually determined by the visibility profile of the output interference fringe pattern, where a larger visibility difference between the central fringe and its side fringes makes for an easier identification. In a two wavelength combination source situation, the visibility function is essentially the absolute value of the product of a Gaussian function and a cosine function, hence the improvement in the central fringe identification becomes evident when comparing the visibility profile of a single wavelength light source and that using two wavelengths. An example is shown in Fig.4.1, where a single laser diode source of wavelength $\lambda = 635$nm and a two wavelength combination source of wavelength $\lambda_1 =$

635nm and λ_2 = 830nm are assumed, and the coherence lengths are chosen to be the same, at L_c = 16μm.

Although, as indicated by Fig.4.1, a significant reduction in the visibility difference between the central fringe and its side fringe can be realized by the use of a two wavelength combination source, a limitation arises as the visibility peak of the first side packet becomes higher with the increase of the wavelength difference between the two light sources, as discussed in Chapter 3. A logical step to remove this limit is to explore the use of three wavelength or multiwavelength combination sources.

In a multiwavelength combination source, the corresponding normalized output ac signal intensity from an interferometer illuminated by three multimode laser diode sources can be expressed as

$$I_{ac}(x) = (1/3)\{\exp[-(2x/L_{c1})^2]\cos(2\pi x/\lambda_1) + \exp[-(2x/L_{c2})^2]\cos(2\pi x/\lambda_2)$$

$$+ \exp[-(2x/L_{c3})^2]\cos(2\pi x/\lambda_3)\}$$

(4.2.1)

where λ_1, λ_2 and λ_3 are the central wavelengths of the three laser diodes respectively, and L_{c1}, L_{c2} and L_{c3} are their corresponding coherence lengths.

Assuming that all the three laser diodes have the same coherence length, i.e. L_{c1} = L_{c2} = L_{c3} = L_c, and writing $\lambda_1 = \lambda$, $\lambda_2 = a\lambda$ and $\lambda_3 = b\lambda$, where a and b are real numbers and can be termed the **wavelength coefficients**, equation (4.2.1) becomes:

$$I_{ac}(x) = (1/3)\exp[-(2x/L_c)^2][\cos(2\pi x/\lambda) + \cos(2\pi x/a\lambda) + \cos(2\pi x/b\lambda)]$$

(4.2.2)

In a multiwavelength combination source operation, as indicated in equation (4.2.2), an analytical formula for the fringe visibility function is generally not available. However, the situation can still be modelled by means of the computer simulations and the optimum wavelength combinations for such a source can also be obtained by a simple analysis.

The minimum signal-to-noise ratio required by the system to identify the central fringe position, SNR_{min}, as defined in Section 3.2, may also be used in the process of this analysis in order to compare the main results quantitatively.
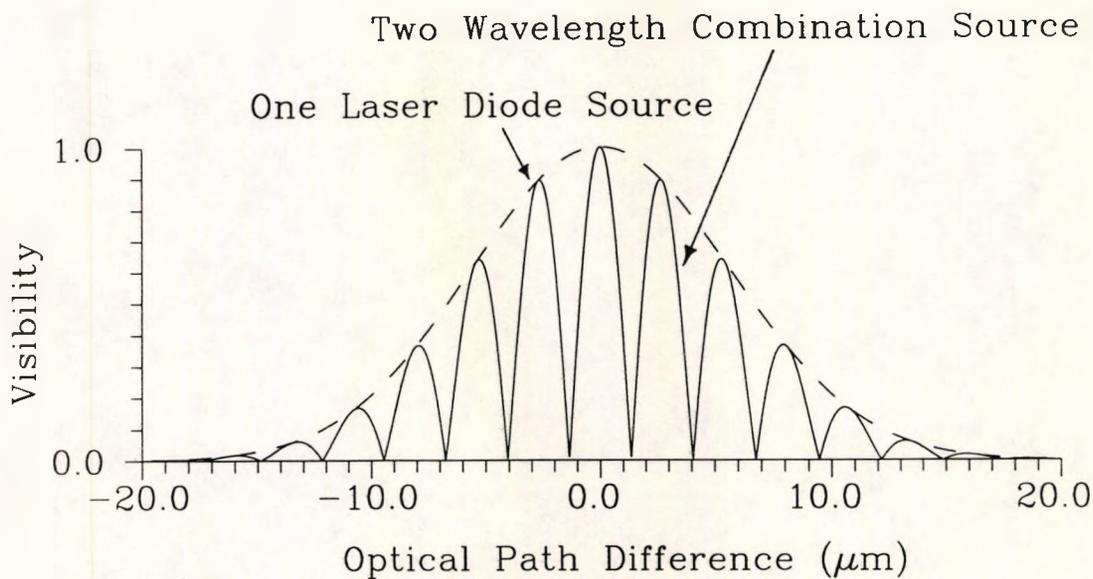
Fig.4.1 Visibility Profiles of a Typical One Laser Diode Source

and a two Wavelength Combination Source

(One Laser Diode Source: $\lambda = 635nm$, $L_c = 16\mu m$;

Two Wavelength Combination Source: $\lambda_1 = 635nm$, $\lambda_2 = 830nm$, $L_c = 16\mu m$;)

4.3 Computer Simulations of Multiwavelength Combination Sources

Computer simulation is an useful tool to analyze the characteristics of interference fringe patterns of a multiwavelength combination source and to determine the corresponding optimum wavelength combination. In the computer simulations undertaken during the course of this work, the theoretical interference fringe patterns of

90

a single wavelength laser diode source, the two wavelength combination sources and the multiwavelength combination sources are generated and compared, the largest side fringe intensities (peak-to-peak value) in the output fringe patterns for different multiwavelength combination sources are calculated, and as a result, the optimum wavelength combinations can be selected.

4.3.1 A Comparison of Different Wavelength Combination Sources

A series of computer simulations has been carried out to generate the corresponding interference fringe patterns for different wavelength combination sources and the results are shown in Fig.4.2.

In these simulations, the light sources considered are typical of commercially available laser diodes. Fig.4.2(a) represents an interference fringe pattern corresponding to a single wavelength multimode laser diode source, with $\lambda = 635nm$ and $L_c = 16\mu m$. It reveals that even in this ideal situation, i.e. a system free of intensity noise and using a light source with a relatively short coherence length, the central fringe identification is still not straightforward, due to the flat shape of the Gaussian visibility profile near the zero OPD position. To describe the situation quantitatively, the minimum signal-to-noise ratio required by the system to identify the central fringe, SNR_{min}, according to equation (3.2.39), is about 50.1dB in this case.

By the use of two wavelength combination sources, the results obtained can be clearly improved over a single wavelength source as shown in Fig.4.2(b) and (c), the fringe patterns of which are actually the same with those in Fig.3.3. i.e. in both cases the coherence lengths and the wavelengths of the given laser diodes are chosen the same corresponding values, $L_c = 16\mu m$ and $\lambda = 635nm$ respectively, but the wavelength of the second laser diode source in each case is different, being 688nm and 830nm respectively. The fringe patterns are redrawn here in order to be able to make an easy comparison between them.
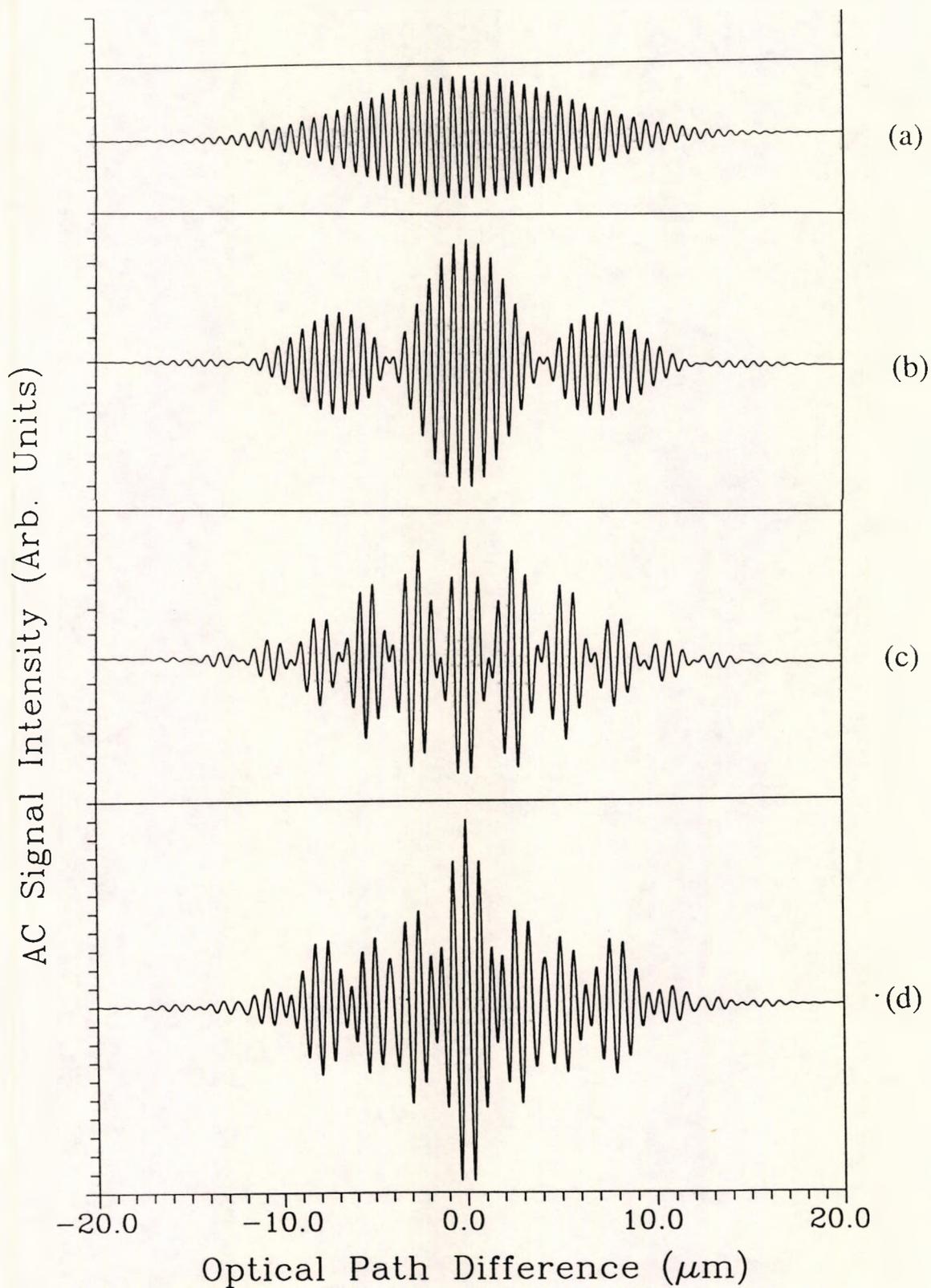
Fig.4.2 Computer Simulated Interference Fringe Patterns

(a) Single Wavelength: $\lambda = 635$nm, $L_c = 16\mu$m;

(b) Two Wavelengths: $\lambda_1 = 635$nm, $\lambda_2 = 688$nm, $L_c = 16\mu$m;

(c) Two Wavelengths: $\lambda_1 = 635$nm, $\lambda_2 = 830$nm, $L_c = 16\mu$m;

(d) Three Wavelengths: $\lambda_1 = 635$nm, $\lambda_2 = 688$nm, $\lambda_3 = 830$nm, $L_c = 16\mu$m

It is obvious that, when compared with Fig.4.2(a), the central fringe identification becomes easier in Fig.4.2(b), and is especially so in Fig.4.2(c), where the wavelength difference between the two laser diodes has a relatively large value. The obtained SNR_{min} values in this case, according to equation (3.2.39), are 34.4dB and 21.2dB respectively, thus showing a big reduction compared with the value obtained for a single laser diode source, 50.1dB.

A further significant improvement can be made by using these three laser diodes together to generate a three wavelength combination source. The interference fringe pattern obtained in such a source is demonstrated in Fig.4.2(d) where $\lambda_1 = 635nm$, $\lambda_2 = 688nm$ and $\lambda_3 = 830nm$, and the coherence lengths assumed are the same, at 16μm, for all the three laser diodes. In this case, the SNR_{min} value obtained is 18.5dB, representing an increasing central fringe dominance when compared to a two wavelength combination source.

Hence, a clear and progressive improvement can be observed from Fig.4.2(a) to (d) in the ease of central fringe identification. In terms of SNR_{min} value, the progression is: 50.1dB in Fig.4.2(a), 34.4dB and 21.2dB in Fig.4.2(b) and (c) respectively, and 18.5dB in Fig.4.2(d).

The above represents a situation typical of using commercially available laser diodes and their characteristics. If, supposing that laser diodes of any wavelength could be chosen without restriction, then it may be possible to select the optimum wavelength combination to increase further the system performance. An example is shown in Fig.4.3(a), which is similar to Fig.3.3 (and is reproduced here to facilitate a comparison with the optimized multiwavelength combination source). The two wavelengths of the laser diodes used in Fig.4.3(a) are chosen to be 635nm and 797nm respectively, and the coherence length, $L_c = 16\mu$m, is the same for both laser diodes. In this optimum wavelength combination, the SNR_{min} value obtained is only 18.0dB, the lowest possible value for the given wavelength of 635nm and coherence length of 16μm of the two wavelength combination source.
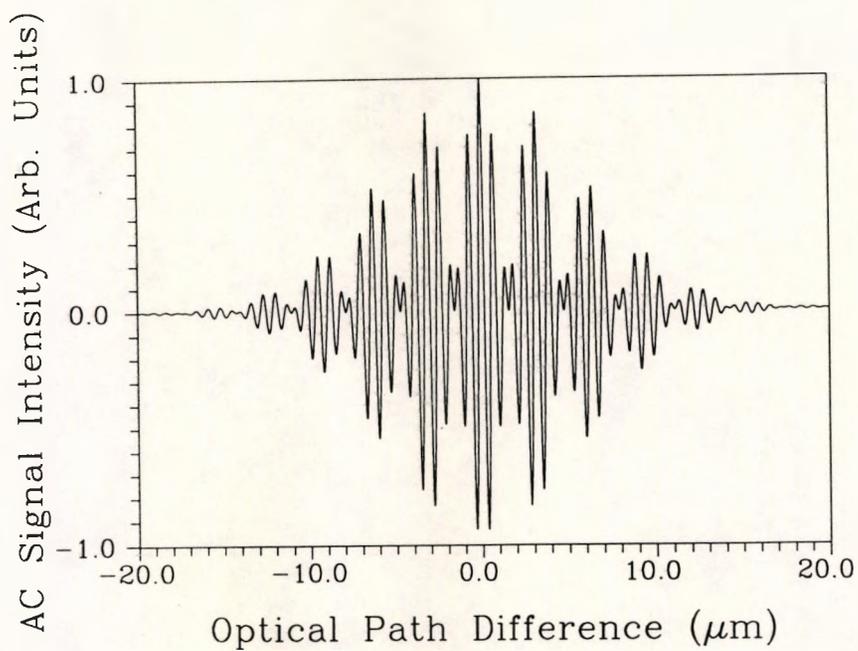
(a) $\lambda_1 = 635\text{nm}$, $\lambda_2 = 797\text{nm}$, $L_c = 16\mu\text{m}$
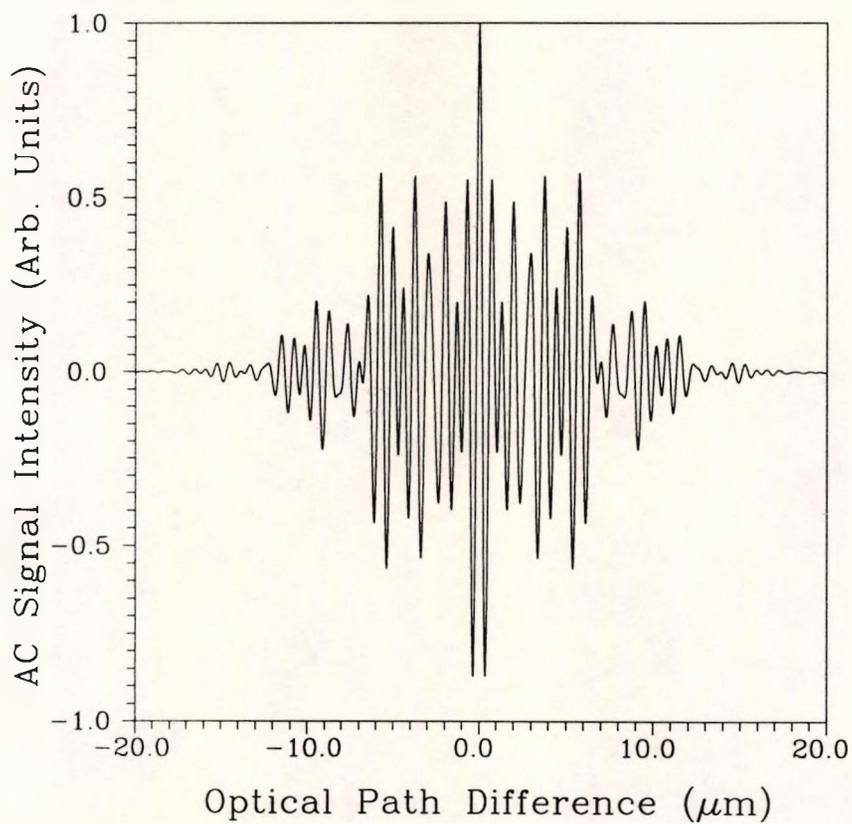
(b) $\lambda_1 = 635\text{nm}$, $\lambda_2 = 724\text{nm}$, $\lambda_3 = 959\text{nm}$, $L_c = 16\mu\text{m}$

Fig.4.3 Computer Simulated Interference Fringe Patterns of the Optimized

Multiwavelength Combination Source

The corresponding interference fringe pattern of an optimized three wavelength combination source is shown in Fig.4.3(b), where the three laser diodes have central wavelengths of 635nm, 724nm and 959nm, i.e. the wavelength coefficients a and b are 1.14, 1.51 respectively, and the coherence lengths are assumed still to be 16μm for all these three laser diodes. In this case, the value of SNR_{min} reveals a sharp decrease, becoming 12.9dB only, showing an extraordinary improvement in the central fringe identification technique and making the detection process extremely straightforward.

In addition, it can be seen from this fringe pattern that only one fringe, the central fringe, is now absolutely dominant. This represents the high measurement precision that can be achieved and thus there is a real advantage to be had in applying such a source in a white light interferometric sensor system.

Therefore, by comparing the fringe patterns from Fig.4.2 and Fig.4.3, it is evident that the central fringe identification, as a serious problem in a single wavelength laser diode source operation, can be significantly improved by the use of a two wavelength combination source and finally it becomes much more straightforward in a multiwavelength system. The most efficient system operation can be achieved when the optimum wavelength combination is selected, especially in the case of the three wavelength combination source, where the central fringe becomes dominant to an even greater extent.

4.3.2 The Optimization of a Multiwavelength Combination Source

It is clear from the above that the multiwavelength combination source has to be optimized in order to yield the most efficient system operation in white light interferometry.

In the case of two wavelength combination sources, as discussed in Chapter 3, the normalized largest side fringe intensity (peak-to-peak value) is either I_{01n}, the normalized first side fringe intensity in the central fringe packet, or I_{10n}, the normalized central fringe intensity in the first side fringe packet, as shown in Fig.3.3. By following

the variation of I_{01n} and I_{10n} with the wavelength difference between the two laser diodes until the condition: $I_{01n} = I_{01n}$ can be satisfied, the corresponding wavelength difference can then be selected as representing the optimum wavelength difference and hence an optimum wavelength combination can be obtained for any given laser diode.

However, the situation becomes more complicated for a multiwavelength combination source as any side fringe intensity may become the largest overall, and an underlying pattern may be difficult to find. In order to determine the optimum wavelength combination for such a source, a FORTRAN computer program is used, to perform the corresponding calculations, as discussed below.

Assuming that the three laser diodes possess the same coherence length, L_c, and $1 < a < b$, where a and b are wavelength coefficients, then for a given laser diode of wavelength λ, different values of a and b can be calculated until a set of optimized values, a_{opt} and b_{opt} can be found. With the wavelength combinations of λ, $a_{opt}\lambda$ and $b_{opt}\lambda$, the maximum side fringe intensity (peak-to-peak value) has the lowest possible value, as does SNR_{min}. Hence, this wavelength combination is selected as the **optimum wavelength combination** and the corresponding coefficients a_{opt} and b_{opt} are called the **optimum wavelength coefficients.** More detail on the computer program may be found in Appendix B.

By developing and running a computer program to make such calculations, a number of the optimum wavelength coefficients obtained, corresponding to different given initial wavelengths, λ, and coherence lengths, L_c, are shown in Fig.4.4. In Fig.4.4(a), where $L_c = 16\mu m$, the optimum wavelength coefficient a_{opt} remains constant in the wavelength range from 630nm to 850nm whereas b_{opt} shows a rather smooth variation. If L_c is increased to $20\mu m$, an abrupt change in a_{opt} and b_{opt} can be seen in Fig.4.4(b), when the wavelength of the given laser diode changes from 770nm to 780nm. A further increase of L_c to $40\mu m$ also results in an abrupt change of a_{opt} while b_{opt} has a smooth variation, as shown in Fig.4.4(c).
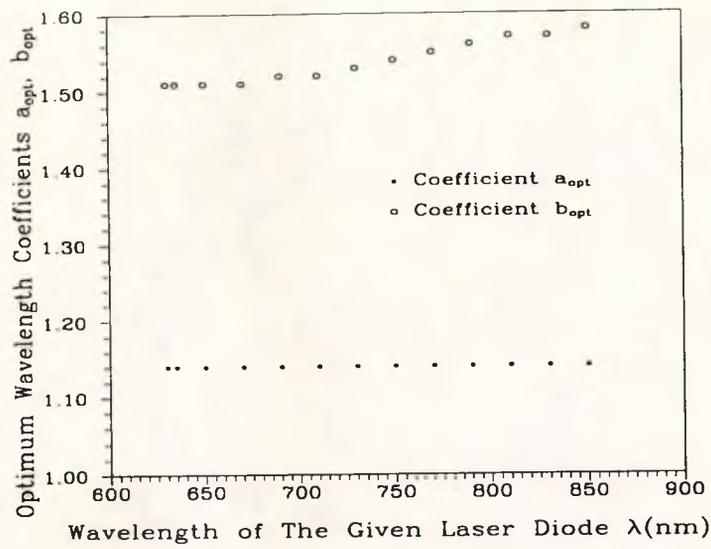
(a) $L_C = 16\mu m$
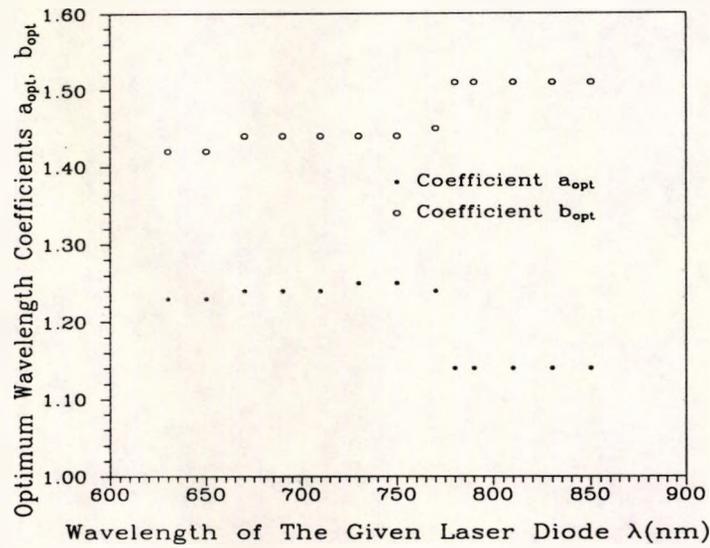
(b) $L_c = 20\mu m$
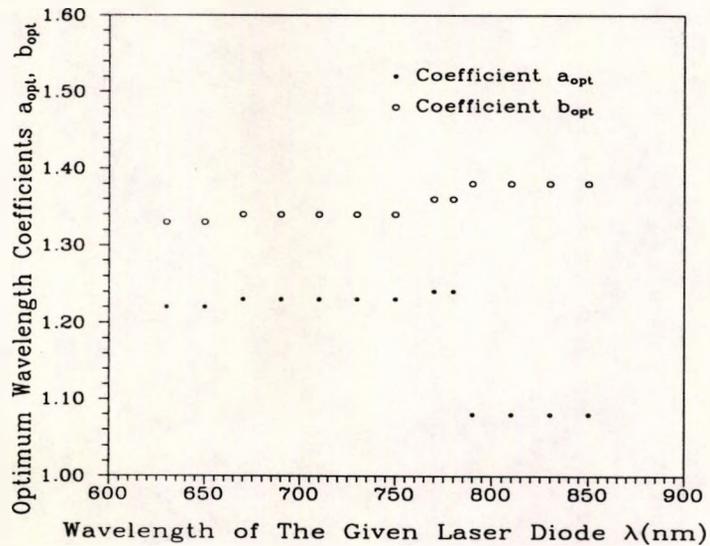
(c) $L_C = 40\mu m$

Fig.4.4 The Optimum Wavelength Coefficients for a Multiwavelength Combination

Source with Given Laser Diode Wavelength λ

The reason for such an abrupt change in the optimum wavelength coefficients may be explained by the fact that the largest side fringe is now shifted from one position to another. An example is illustrated in Fig.4.5. In Fig.4.5(a), the given wavelength is 770nm and the coherence length is 20μm, with the corresponding optimum wavelength coefficients a_{opt} = 1.24 and b_{opt} = 1.45. If the given wavelength now changes to λ = 780nm, while the coherence length is still the same, then as shown in Fig.4.5(b), there is a shift in the largest side fringe and consequently, the optimum wavelength coefficients become 1.14 and 1.51 respectively. Fig.4.5 can then be used to explain the situation in Fig.4.4(b), i.e. the abrupt change in the optimum wavelength coefficients is caused by a shift experienced in the largest side fringe in the interference fringe pattern of a multiwavelength combination source.

It should be noted that these optimum wavelength coefficients only provide a guide to the selection of the most appropriate laser diodes. For a given laser diode of wavelength 635nm and coherence length of 16μm, the wavelength coefficient distribution area, which correspondents to the different SNR_{min} values, is shown in Fig.4.6(a). At the lowest SNR_{min} value of 12.9dB, only one point or in other words, one pair of wavelength coefficient values satisfies the condition and they represent the optimum wavelength coefficients, a_{opt} = 1.18 and b_{opt} = 1.52. When the SNR_{min} value is increased step by step, the distribution area of corresponding wavelength coefficients is enlarged progressively. If the value of SNR_{min} is set to be 13.1dB, two points, a = 1.18, b = 1.52, and a = 1.18, b = 1.50 can be selected, at which the requirement of $SNR_{min} \leq$ 13.1dB is fulfiled. When the SNR_{min} = 13.2dB, then seven points can be chosen to satisfy such a condition. If, for a particular white light interferometric system, the SNR_{min} is set to a value $\leq$ 15.0dB in order to achieve an accurate measurement, then as a considerable number of pairs of wavelength coefficients can fulfil this SNR_{min} requirement, which forms a distribution area of the values of a and b as shown in Fig.4.6(b), the appropriate laser diodes can be selected by an analysis of this distribution diagram and with it their corresponding commercial availability, to obtain as close a match as possible to the wavelengths required for the required SNR_{min} value.
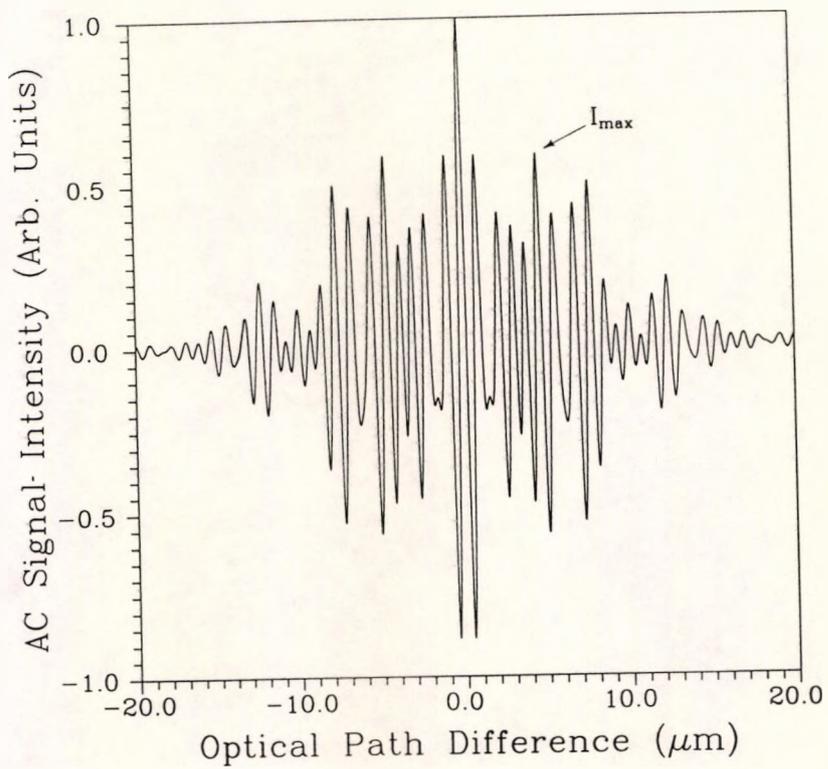
(a) $\lambda = 770$nm, $L_c = 20\mu$m. $a_{opt} = 1.24$, $b_{opt} = 1.45$
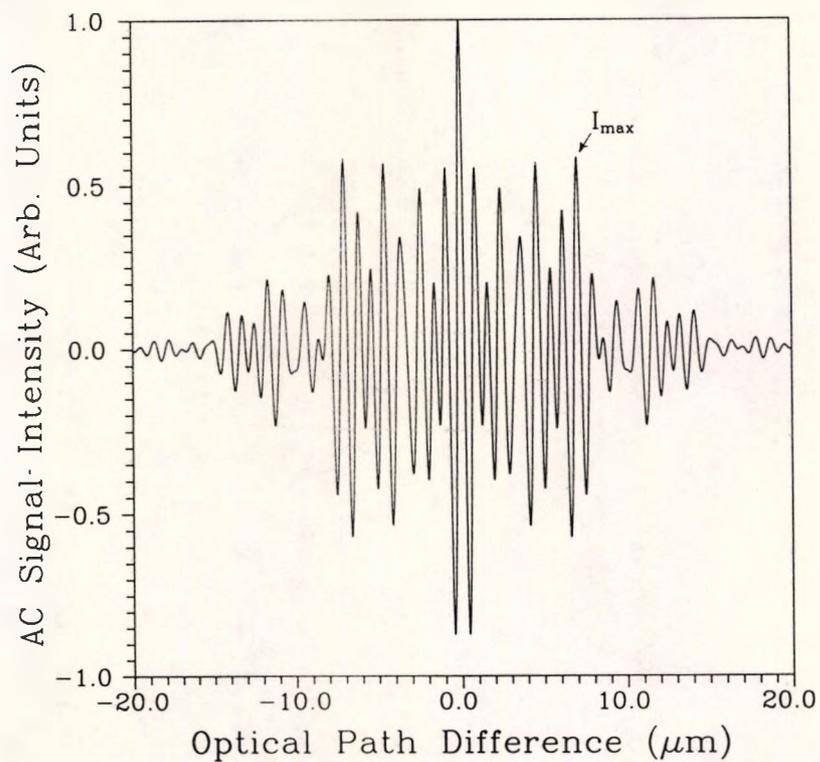
(b) $\lambda = 780$nm, $L_c = 20\mu$m, $a_{opt} = 1.14$, $b_{opt} = 1.51$

Fig.4.5 Computer Simulated Interference Fringe Patterns for two Sources with

Different Optimum Wavelength Coefficients
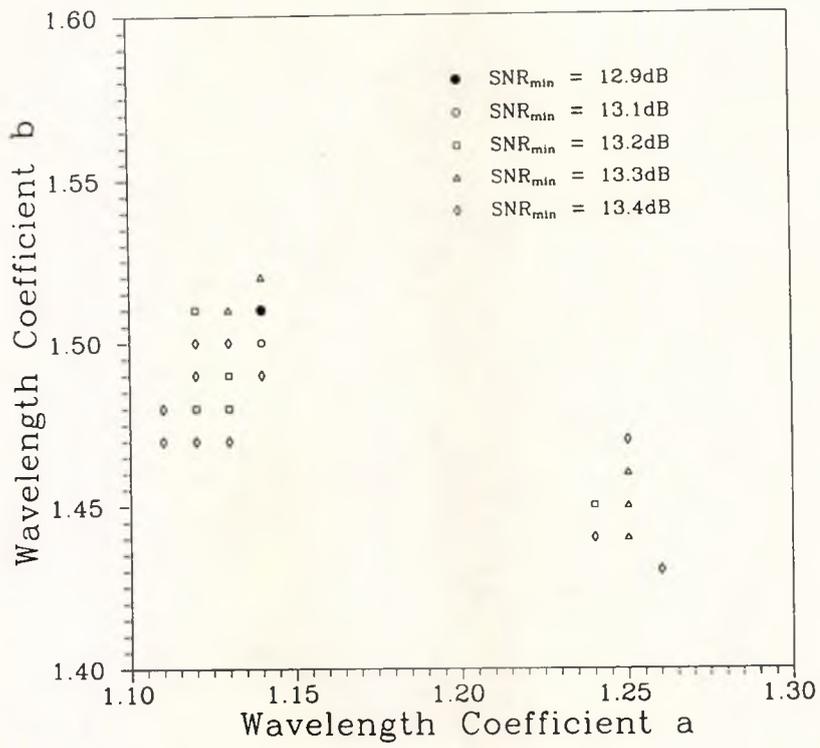
(a)
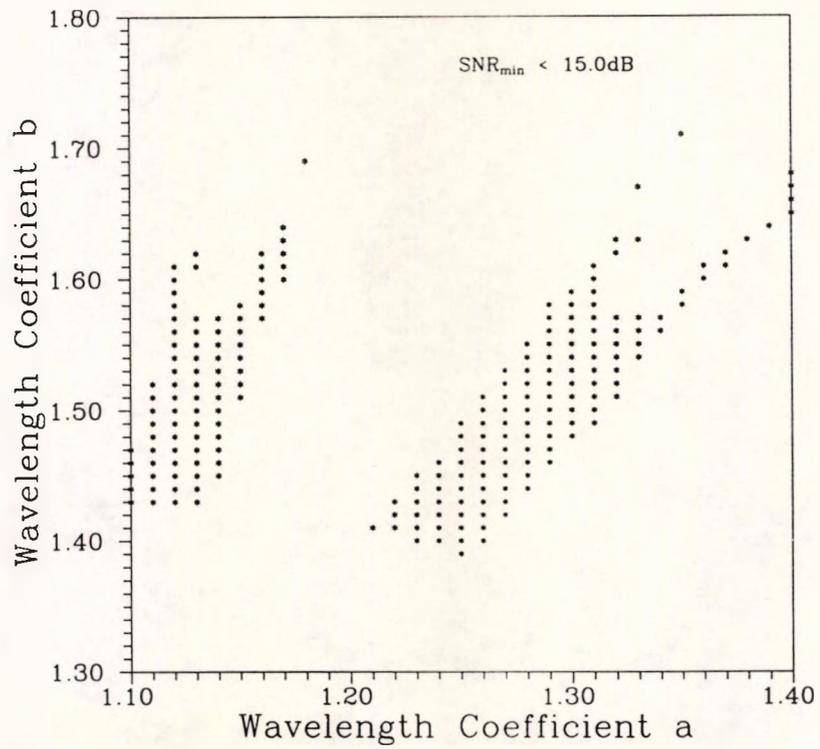
(b)

Fig.4.6 Wavelength Coefficients Distribution for a Typical Laser Diode

$(\lambda = 635nm, L_C = 16\mu m)$

For an optimized multiwavelength combination source, assuming that the three laser diodes considered possess the same coherence length, L_c, there exists a linear relationship between the wavelength of the given laser diode and the SNR_{min} value as illustrated in Fig.4.7. When the given wavelength, λ, is increased, the SNR_{min} value will decrease accordingly. The SNR_{min} value of a multiwavelength system is also determined by the coherence length of the laser diode source and can be reduced by using three laser diodes of shorter coherence lengths. For different values of the given wavelength, λ, this rate of reduction is essentially constant according to the results of the computer simulations.
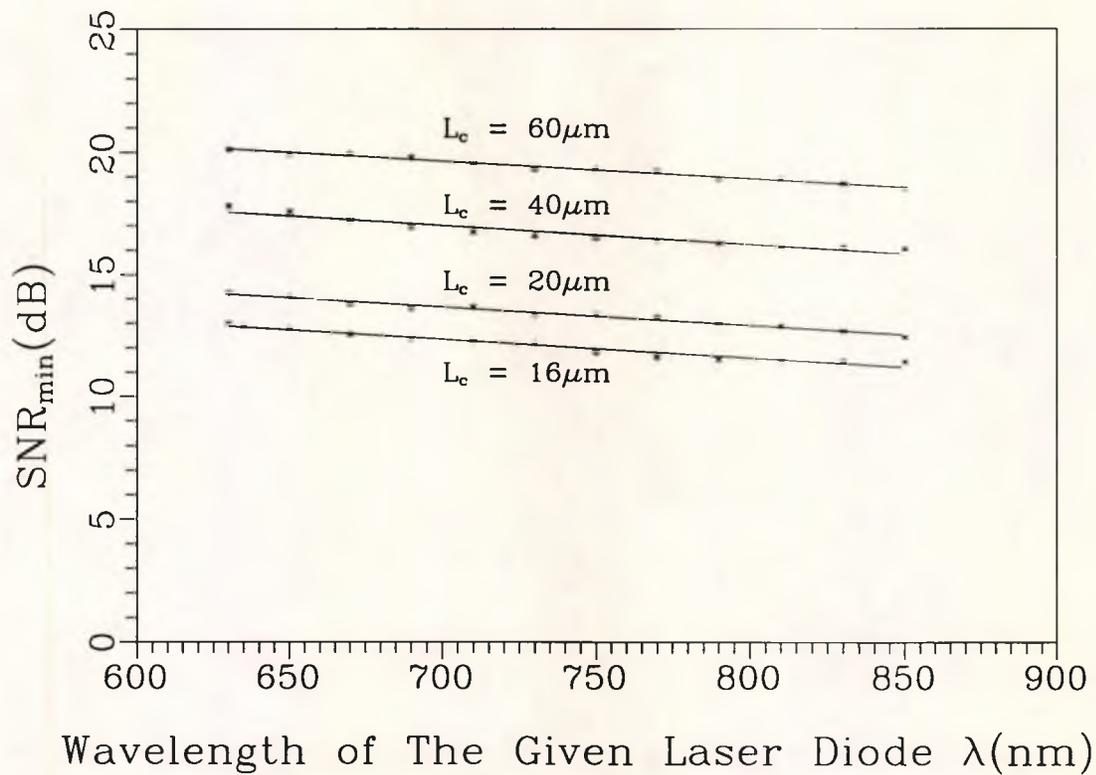
Fig.4.7 The SNR_{min} for the three Wavelength Combination Source with Optimum Wavelength Combination
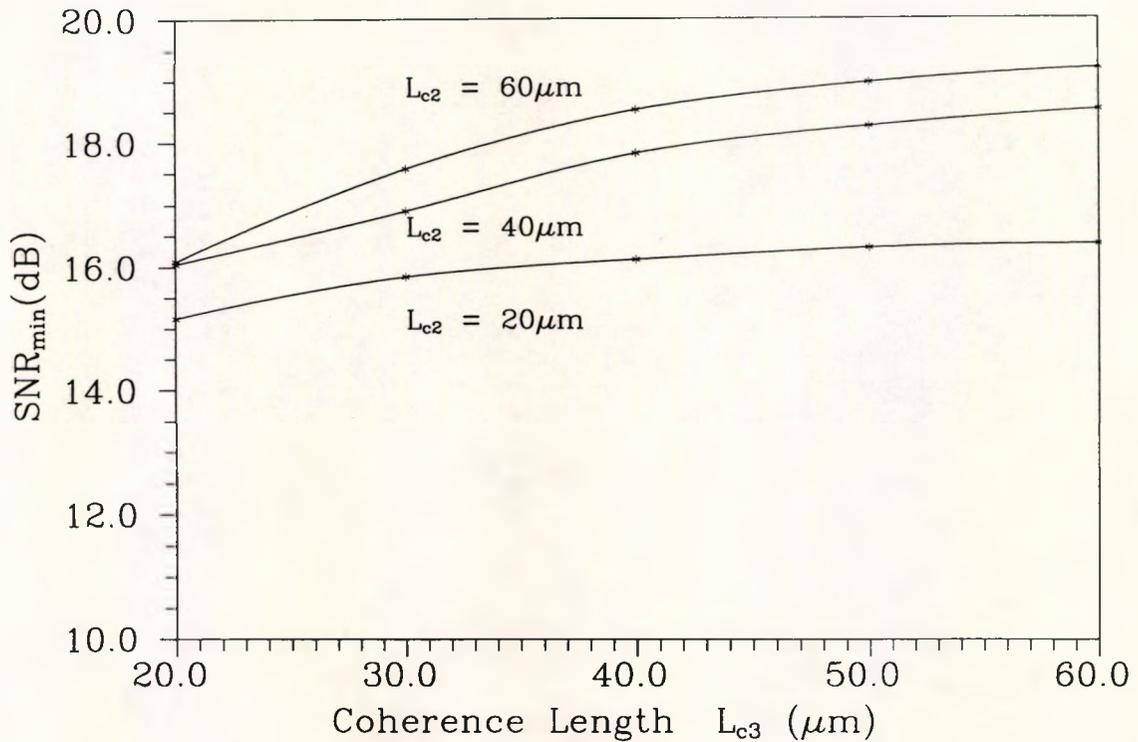
Fig.4.8 The SNR_{min} for the three wavelength Combination Sources with Different

Coherence Lengths (λ_1 = 635nm, L_{c1} = 40µm)

If, however, the three laser diodes have different coherence lengths, then for a given laser diode of wavelength λ_1 and coherence length L_{c1}, the SNR_{min} values at the optimum wavelength combination will become larger when the coherence lengths, L_{c2}, L_{c3}, or both are increased. For instance, if the given laser diode wavelength λ = 635nm and coherence length L_{c1} = 40µm, then the variation of SNR_{min} with the coherence lengths L_{c2} and L_{c3} is depicted in Fig.4.8, which represents a general trend that can be useful in the selection of the most appropriate laser diodes under a range of different conditions.

From both the work considered in Chapter 3 and the discussion here, it can be seen that the computer simulations are able to play an important role in the analysis of the characteristics of multiwavelength combination sources and in the determination of optimum wavelength combinations, but the success of this technique still needs the experimental verification provided in the next Section.

4.4 Experimental Results of a Multiwavelength Combination Source

In the experiments described, a number of commercially available laser diodes were used as the light sources to illuminate an interferometer in order to obtain the interference fringe pattern to compare with the computer simulation results, and thus to verify the value of multiwavelength combination source technique as an efficient aid for central fringe identification in white light interferometry.

4.4.1 Experimental Arrangement

The optical configuration employed to investigate the characteristics of a multiwavelength combination source is depicted in Fig.4.9, which represents a basic Michelson interferometer arrangement, as used in Chapter 3. However, a three wavelength source was used as discussed below.

The output beams from three typical commercially available laser diodes were first combined by the use of two beam splitters to generate a single light beam which was then input to the interferometer. The input beam was divided in two, reflected by the two mirrors respectively without giving any OPD and finally, the interference between the two output beams was detected by a photodetector. The OPD between the two mirrors in the interferometer was balanced by controlling the position of one of the mirrors, M_2, which was attached to a micrometer. Mirror M_1 was used as the reference mirror in order to obtain a reference beam with known optical path length in the interferometer. The interference pattern was generated by modulating the OPD via an electromechanical modulation of the position of one of the mirrors, M_2, and the output was observed on an oscilloscope connected to the photodetector. The three laser diodes were all operated below their threshold in order to ensure the multimode nature of the output light beam and hence the fringe patterns could be observed more easily on the oscilloscope.
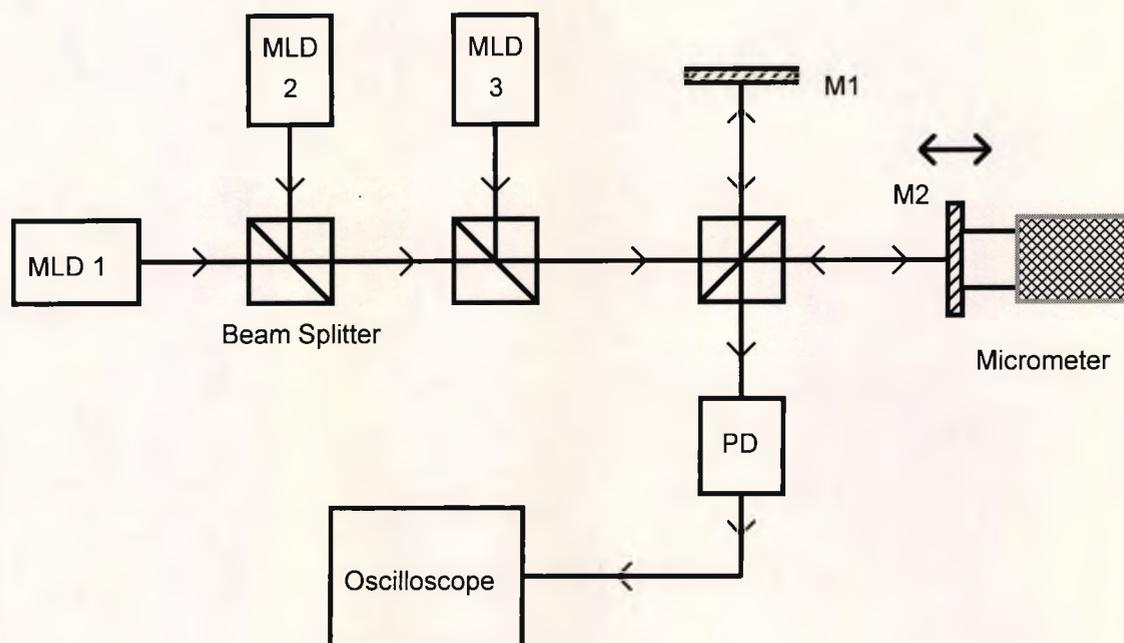
MLD : Multimode Laser Diode;   M : Mirror;   PD : Photodetector

Fig.4.9 Experimental Arrangement

4.4.2 Experimental Results of a Multiwavelength Combination Source

A set of experiments was carried out by utilizing different combinations of three commonly available laser diodes, similar in characteristics to those modelled in the computer simulations, i.e. $\lambda_1 = 635$nm, $L_{c1} = 16\mu$m, $\lambda_2 = 688$nm with $L_{c2} = 15\mu$m, $\lambda_3 = 830$nm and $L_{c3} = 15\mu$m. The interference fringe patterns obtained in the experiment are shown in Fig.4.10, corresponding to the situation of using one multimode laser diode source (Fig.4.10(a)), a two wavelength combination source (Fig.4.10(b) and (c)) and a three wavelength combination source (Fig.4.10(d)).
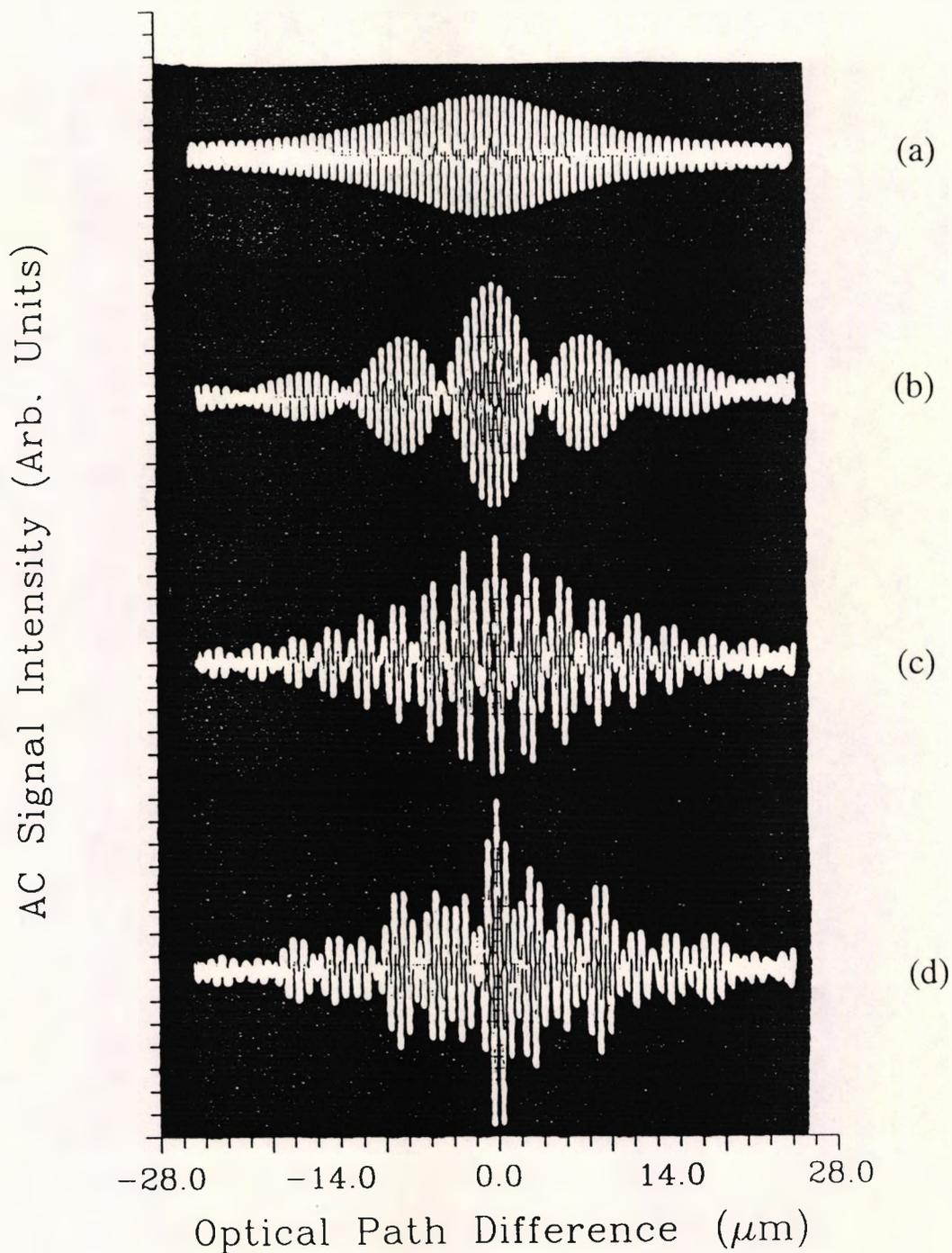
Fig.4.10 Experimentally Obtained Interference Fringe Patterns

(a) Single Wavelength: $\lambda = 635$nm, $L_c = 16\mu$m;

(b) Two Wavelengths: $\lambda_1 = 635$nm, $\lambda_2 = 688$nm, $L_{c1} = 16\mu$m, $L_{c2} = 15\mu$m;

(c) Two Wavelengths: $\lambda_1 = 635$nm, $\lambda_2 = 830$nm, $L_{c1} = 16\mu$m, $L_{c2} = 15\mu$m;

(d) Three Wavelengths: $\lambda_1 = 635$nm, $\lambda_2 = 688$nm, $\lambda_3 = 830$nm, $L_{c1} = 16\mu$m,

$L_{c2} = 15\mu$m, $L_{c3} = 15\mu$m

From these figures, it can be seen that, in the experimental situation, the task of central fringe identification is eased by using a two wavelength combination source with a suitable wavelength difference, and is even further and greatly simplified by employing a three wavelength combination source. The central fringe becomes so dominant that the measurement precision can be extremely high, as predicted from the theoretical simulations when compared with a single wavelength source white light interferometric system.

The experimentally obtained SNR_{min} values were 48.3dB for a single wavelength source, 31.4dB and 23.8dB for the two wavelength combination sources respectively, and finally 18.1dB for a three wavelength operation. These results are in good agreement with those obtained from the computer simulations under similar conditions.

There are clear similarities between the interference fringe patterns shown in Fig.4.10 and Fig.4.2, although some asymmetry appears in the experimental situation. This may be caused by the slight misalignment of the beam splitter and the mirrors in the interferometer. Nevertheless, the experimental results have strongly confirmed the theoretical prediction of reducing SNR_{min} and hence the value of using multiwavelength combination sources to enhance the central fringe identification.

4.5 Discussion

A summary and comparison of the main theoretically and experimentally obtained SNR_{min} values for a single wavelength source, two wavelength combination sources and multiwavelength combination sources are shown in Table 4.1.

As is indicated, both from the theory developed and simulated and experiments carried out, a clear and progressive improvement has been made in central fringe identification by using a two wavelength combination source and further a

multiwavelength combination source in a white light interferometric system. The optimum wavelength combinations for such a source can be obtained with the help of the analysis described and the corresponding computer program developed and implemented. With the optimum wavelength combination, the SNR_{min} can be greatly reduced, especially in the case of a multiwavelength combination source, where only one fringe, the central fringe, becomes particularly dominant.

Table 4.1 A Summary and Comparison of Results

Light Source λ(nm)	$L_c(\mu m)$	SNR_{min} (dB) (Theory)	$L_c(\mu m)$	SNR_{min} (dB) (Experiment)
635	16	50.1	16	48.3±1.0
635 + 688	16, 16	34.4	16, 15	31.4±1.0
635 + 830	16, 16	21.2	16, 15	23.8±1.0
635+688 +830	16, 16, 16	18.5	16, 15, 15	18.1±1.0
635 + 797	16	*18.0		
635+724+959	16	*12.9		

* With Optimum Wavelength Combination

In order to focus on the principle of multiwavelength combination source operation, only a simple Michelson interferometer arrangement has been used in the investigation. However, the technique developed is also suitable for use in a typical remote sensing white light interferometric system where two interferometers are connected in tandem and the OPD of the sensing interferometers is larger than the coherence length of each laser diode in the multiwavelength combination source. In this case, if the OPD introduced by the sensing interferometer is balanced by the receiving interferometer

within the coherence lengths of each laser diode source, the corresponding interference fringe pattern can be observed and a subfringe measurement precision can be readily obtained by the use of the dominant central fringe in the fringe pattern.

The work described in this Chapter shows that the use of a multiwavelength combination source as an instant fringe detection technique without further signal processing is simple and effective and can be used for a high precision white light interferometric sensor system. Moreover, because of the highly increased output power of the system and the extremely dominant central fringe in the interference fringe pattern, potential applications of this technique in coherence multiplexed interferometric sensor systems [12-16] can also be expected. Since coherence multiplexing is achieved by the use of a broadband light source with a coherence length less than the OPD introduced by the sensing interferometer, and for each sensing interferometer in the system, the OPD information can be retrieved by the corresponding receiving interferometer with the matched OPD, it is obvious that for the largest OPD that can be achieved by the interferometers in the system, a shorter coherence length light source means a larger number of interferometric sensors that potentially can be multiplexed, thus increasing the system efficiency.

The price paid for this multiwavelength combination source technique is the increased cost and complexity of the system, as more components are involved. The system alignment also becomes more difficult and time consuming and a slight misalignment may result in some asymmetry of the interference fringe pattern obtained by the system.

The alignment difficulty for a multiwavelength combination source may be avoided by the use of a fibre fluorescent source [17-18] which exhibits several broadband fluorescent peaks in its spectrum and hence can be used alone as a two wavelength or a multiwavelength combination source, as will be described in Chapter 5.

References

1. P. Sandoz and G. Tribillon, "Profilometry by Zero-Order Interference Fringe Identification", Journal of Modern Optics, Vol.40, No.9, pp.1691-1700, 1993

2. W. J. Bock, W. Urbanczyk and M. B. Zaremba, "Electronically Scanned White-Light Interferometric Strain Sensor Employing Highly Birefringent Fibers", Optics Communications, Vol.101, No.3,4, pp.157-162, 15 August 1993

3. B. K. Ward and K. Seta, "Quasimonochromatic White Light Fringe Interferometer", Applied Optics, Vol.30, No.1, pp.66-71, 1 January 1991

4. S. Chen, K. T. V. Grattan, B. T. Meggitt and A. W. Palmer, "Instantaneous Fringe-Order Identification Using Dual Broad-Band Sources with Widely Spaced Wavelengths", Electronics Letters, Vol.29, No.4, pp.334-335, February 18, 1993

5. Y. J. Rao, Y. N. Ning and D. A. Jackson, "Synthesized Source for White-Light Sensing Systems", Optics Letters, Vol.18, No.6, pp.462-464, March 15, 1993

6. D. N. Wang, Y. N. Ning, K. T. V. Grattan, A. W. Palmer and K. Weir, "Characteristics of Synthesized Light Sources for White Light Interferometric Systems", Optics Letters, Vol.18, No.22, pp.1884-1886, November 15, 1993

7. D. N. Wang, Y. N. Ning, K. T. V. Grattan, A. W. Palmer and K. Weir, "The Optimized Wavelength Combinations of two Broadband Sources for White Light Interferometry", IEEE/OSA Journal of Lightwave Technology, Vol.12, No.5, pp.909-916, May 1994

8. Y. Y. Cheng and J. C. Wyant, "Multiple-Wavelength Phase-Shifting Interferometry", Applied Optics, Vol.24, No.6, pp.804-807, 15 March 1985

9. D. A. Flavin, R. McBride and J. D. C. Jones, "Temperature-Insensitive Interferometric Measurement of Strain Using Grating-Coupled LED Sources", Proceedings of the 10th International Optical Fibre Sensors Conference", pp.195-198, Glasgow, U.K., October 1994

10. D. N. Wang, Y. N. Ning, K. T. V. Grattan, A. W. Palmer and K. Weir, "Three-Wavelength Combination Source for White-Light interferometry", IEEE Photonics Technology Letters, Vol.5, No.11, pp.1350-1352, November 1993

11. D. N. Wang, Y. N. Ning, K. T. V. Grattan, A. W. Palmer and K. Weir, "Optimized Multiwavelength Combination Sources for Interferometric Use", Applied Optics, Vol.33, No.31, pp.7326-7333, 1 November 1994

12. S. A. Al-Chlabi, B. Culshaw and D. E. N. Davies, "Partially Coherent Sources in Interferometric Sensors", Proceedings of the First Internatinal Optical Fibre Sensors Conference, pp.132-135, London, U.K., April 1983

13. J. L. Brooks, R. H. Wentworth, R. C. Youngquist, M. Tur. B. Y. Kim and H. J. Shaw, "Coherence Multiplexing of Fiber-Optic Interferometric Sensors", IEEE/OSA Journal of Lightwave Technology, Vol.LT-3, No.5, pp.1062-1072, October 1985

14. A. D. Kersey, "Distributed and Multiplexed Fiber Optic Sensors", in "Fiber Optic Sensors: An Introduction for Engineers and Scientists", Edited by E. Udd, pp.325-368, John Wiley & Sons, Inc., 1991

15. J. L. Santos and D. A. Jackson, "Coherence Sensing of Time-Addressed Optical-Fiber Sensors Illuminated by a Multimode Laser Diode", Applied Optics, Vol.30, No.24, pp.5068-5076, 1 December 1991

16. T. Y. Liu, J. Cory and D. A. Jackson, "Partially Multiplexing Sensor Network Exploiting Low Coherence Interferometry", Applied Optics, Vol.32, No.7, pp.1100-1103, 1 March 1993

17. B. J. Ainslie, S. P. Craig and S. T. Davey, "The Absorption and Fluorescence Spectra of Rare Earth Ions in Silica-Based Monomode Fiber", IEEE/OSA Journal of Lightwave Technology, Vol.6, No.2, pp.287-292, February 1988

18. M. C. Farries, P. R. Morkel and J. E. Townsend, "Samarium-Doped Glass Laser Operating at 651nm", Electronics Letters, Vol.24, No.11, pp.709-710, 26th May 1988

Chapter 5

A Fibre Fluorescent Source

This Chapter demonstrates that, by the use of a Sm^{3+}-doped fibre (in this case pumped by an Ar-ion laser), a low coherence, visible light source can be generated, equivalent to a two wavelength or potentially, a multiwavelength combination source, for white light interferometric use. This fibre fluorescent light source is compatible with other fibre components in the optical sensor system, has good coupling efficiency into single mode fibres and high spatial coherence, thus showing significant potential for application as a source in white light interferometric sensor systems.

5.1 Introduction

As discussed in Chapter 3 and 4, a two wavelength or a multiwavelength combination source can be used in a white light interferometric system to enhance the capability of central fringe identification and hence the performance of high precision and absolute measurements. However, the price paid is the increased system complexity and alignment difficulty resulting. Other techniques have been investigated to tackle this problem, such as the use of a single broadband light source to generate two wavelengths [1-2].

The broadband light source employed in the work of Webb *et al* [1] was an LED with a peak wavelength of 815nm and bandwidth of 50nm. The two wavelengths were

produced at the output end of the white light interferometric system. The output beam of the receiving interferometer was divided by a beam splitter. One beam was directly received by a photodetector, while the other was passed through an interference filter centred on the wavelength of 803nm with a passband of 10nm, and then received by another photodetector. As a result, the outputs of the system were seen to correspond to the two sources at 815nm and 803nm respectively. However, this system still exhibited considerable degree of complexity as two detectors and phase detection electronics device were used. A similar technique was also reported by Gusmeroli *et al* [2], where two interference filters were used in the receiving interferometer, to extract two wavelengths from a superluminescent source, at 840nm and 860nm respectively, both with a bandwidth of 5nm, before being received by two photodetectors respectively. The phase delay between the two detected signals was measured by a phasemeter.

As shown in Chapter 3, in order to realize an optimum wavelength combination, a relatively large wavelength difference between the two light sources may be required. However, in both of the experiments reported, there was only a small difference between the two wavelengths obtained, i.e. 12nm and 20nm respectively, restricted by the bandwidths of the LED and the superluminescent diode source employed.

An alternative way to generate a two wavelength or a multiwavelength combination source is to utilize the recently developed rare-earth-doped fibres as several fluorescent peaks may be existed in their emission spectra [3].

Rare-earth-doped fibres have been a very active research area in recent years [4-20], as they provide a simple, compact and efficient light source or optical amplifier for both optical communications and optical fibre sensor applications. When pumped by a suitable laser source of an appropriate intensity, the rare-earth-doped fibre can generate a broadband fluorescence spectrum and hence function as a low temporal-coherence light source, which is desirable for some optical sensor applications such as the fibre-optic gyroscope [6] [8-9] and in white light interferometry. Up until now, the efforts being made are dominated by Er^{3+}-doped and Nd^{3+}-doped fibres, from which a high

output power, broadband light source can be created, with an operating wavelength usually in the infrared region [6] [8-9] [15]. However, in some white light interferometric systems, a shorter wavelength, visible light source may be preferred as more accurate measurements can be achieved and the operation is easier and the use of visible light helps limit accident eye exposure. One of the several suitable candidates for such an application is Sm^{3+}-doped fibres [3] [7]. Moreover, as several fluorescent spectral peaks exist in its output spectrum, a two wavelength or even a multiwavelength combination source can be readily realized.

In this Chapter, an Ar-ion laser pumped Sm^{3+}-doped fibre is presented as a low coherence light source. It has a visible light output and particularly, provides a convenient and flexible means to create a two wavelength and potentially, a multiwavelength combination source which may be used in white light interferometry.

5.2 Sm^{3+}-Doped Fibres

5.2.1 Energy Level of the Rare-Earth Elements

The electronic energy level diagram associated with the Sm^{3+} ion is shown in Fig.5.1 (together with several other rare-earth-ions) [21], from which the possible electron energy transitions between different levels can be determined. In the process of fluorescence, electrons in the ground state absorb the energy of incident photons and are raised to a higher energy state. Since the higher state usually has a very short lifetime, the electrons then relax to a lower energy level. Initially, the electrons drop down to the metastable level, exhibiting non-radiative decay and then drop down again exhibiting radiative decays, emitting photons of a longer wavelength.
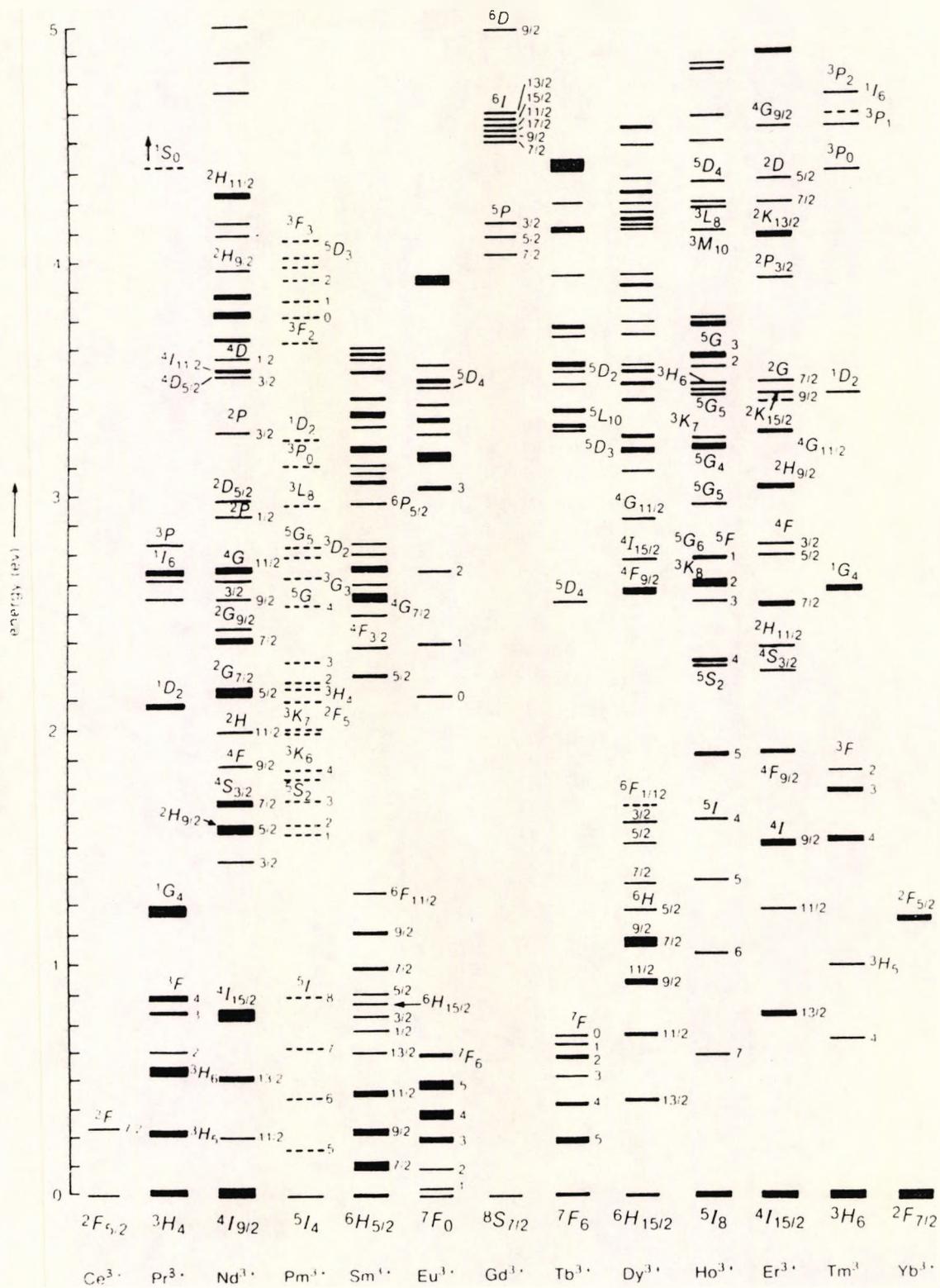
Fig.5.1 Energy Level Diagram of Triply Ionised Lanthanide Ions with Potential for

Fibre Optic Lasers / Fluorescent Sources [21]

In order to obtain the required fluorescence characteristics, an appropriate pump wavelength has to be used as the electrons in the ground level must absorb energy over the correct frequency band to be transferred to a specific higher energy state, hence the suitable pump wavelengths should correspond to an appropriate absorption band.

5.2.2 Absorption and Fluorescence Spectrum of Samarium

The typical absorption spectrum for Sm^{3+} in the host glass of $GeO_2 + P_2O_5 + SiO_2$ is shown in Fig.5.2 [3]. It can be seen from this figure that there is an absorption band near the 525nm region which corresponds to a transition from the ground state $^6H_{5/2}$ to the energy level $^4F_{3/2}$.

Wavelength (nm)
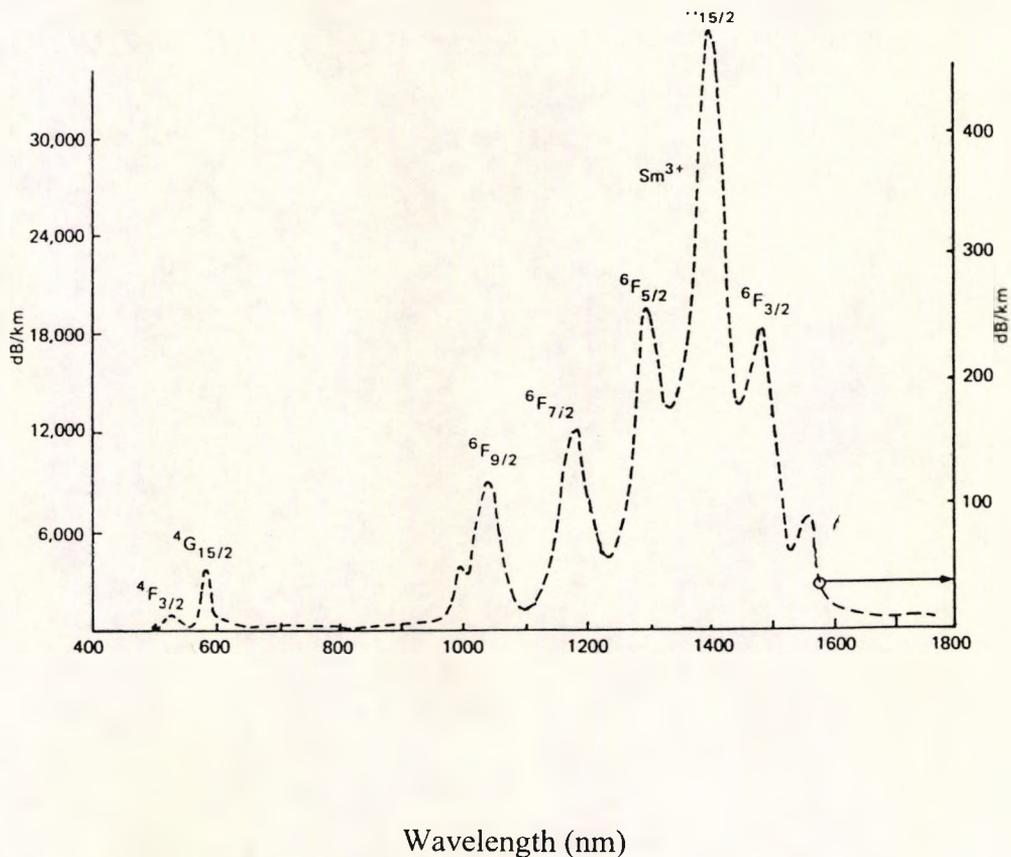
Fig.5.2 The Absorption Spectrum of Sm^{3+} in GeO_2-P_2O_5-SiO_2 [3]
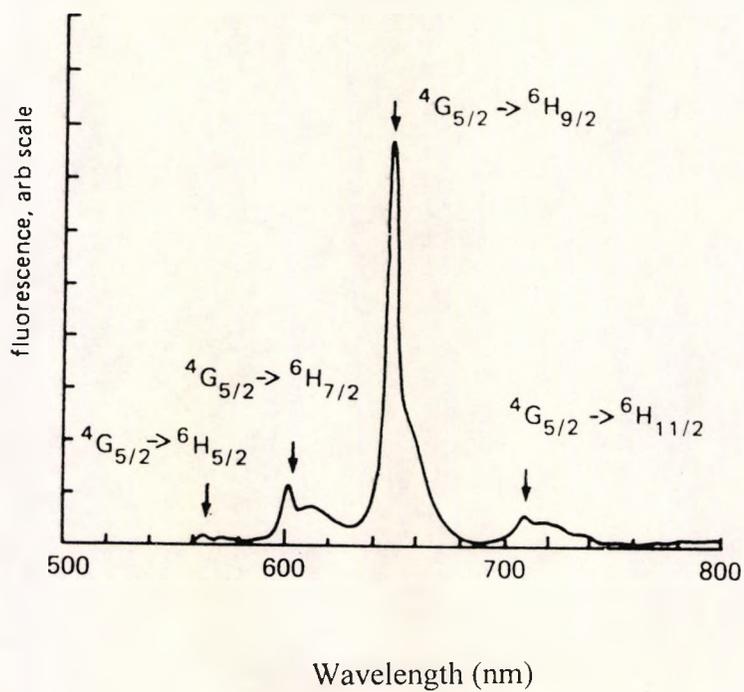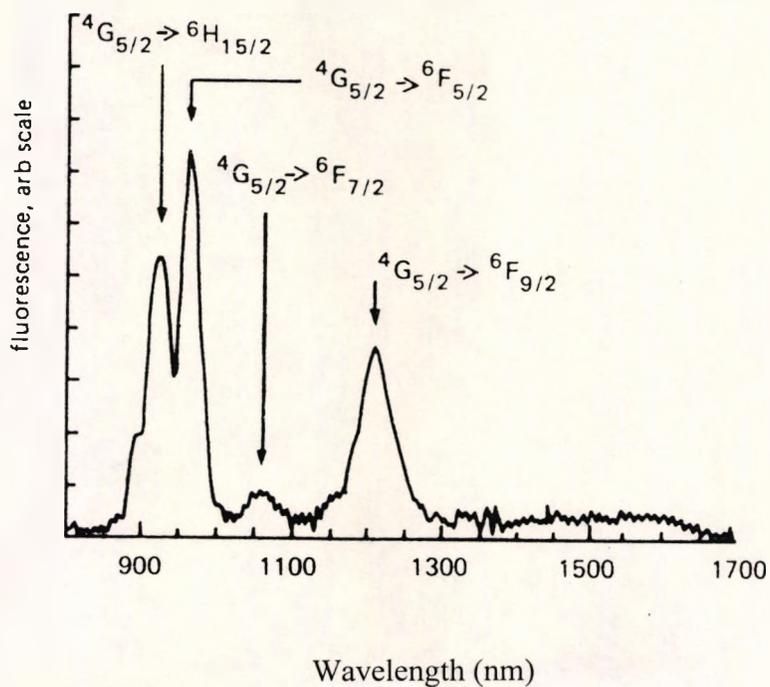
Fig.5.3 The Fluorescence Spectrum of Sm^{3+} in GeO_2-P_2O_5-SiO_2 [3]

(a) Over the Range 500 — 800nm

(b) Over the Range 800 — 1700nm

Fig.5.3 shows the fluorescence spectrum for Sm^{3+} in GeO_2 + P_2O_5 + SiO_2 [3]. In the visible region, at a wavelength of about 605nm and 650nm, two fluorescence peaks can be found, corresponding to the energy level transitions, $^4G_{5/2} \rightarrow {}^6H_{7/2}$ and $^4G_{5/2} \rightarrow {}^6H_{9/2}$ respectively.

Therefore, by the use of a pumping source emitting near the wavelength peak centred over the 525nm wavelength region, the electrons in the ground level $^6H_{5/2}$ will absorb the energy of incident photons and be excited to a higher energy level $^4F_{3/2}$, where they experience a non-radiative decay to the energy state $^4G_{5/2}$, followed by a decay to the lower levels by emitting longer wavelength fluorescence, i.e. for the fluorescence emission at 650nm wavelength, the electrons drop to the energy level $^6H_{9/2}$ and in the case of 605nm wavelength, to the level $^6H_{7/2}$.

5.3 Experimental Results of Using Sm^{3+}-Doped Fibre as a two Wavelength Combination Source

The Sm^{3+}-doped fibre used in this work [22], had a core glass fabricated of SiO_2 + GeO_2, doped with samarium with the concentration of 70ppm, the fiber core diameter was about 13μm. The cladding composition was SiO_2 + F + P_2O_5. The fibre length used was 13 meters.

5.3.1 Experimental Arrangement

The schematic experimental arrangement used in this investigation is shown in Fig.5.4. The pumping source, an Ar-ion laser, was operated at a wavelength of 514.5nm. In order to prevent possible damage to the fibre, the launching power into the Sm^{3+}-doped fibre was limited to below the 150mW level, on the advice of the

manufacturer. As shown in Fig.5.4(a), the output beam from the fibre was input to a spectrophotometer of measuring range between 200 to 800nm, to enable the fluorescence spectrum to be analyzed. In Fig.5.4(b), the output beam was launched into a Michelson interferometer for sensor application purposes. One of the mirrors in the interferometer was mounted on a micrometer, in order to mechanically scan the optical path imbalance, and the other was driven by a loudspeaker, to produce the phase modulated signals. The input beam in the interferometer was divided by a beam splitter into two and then, after balancing by the positions of the two mirrors in the interferometer, the recombined beam was detected and the interference fringe pattern obtained was observed using an oscilloscope.
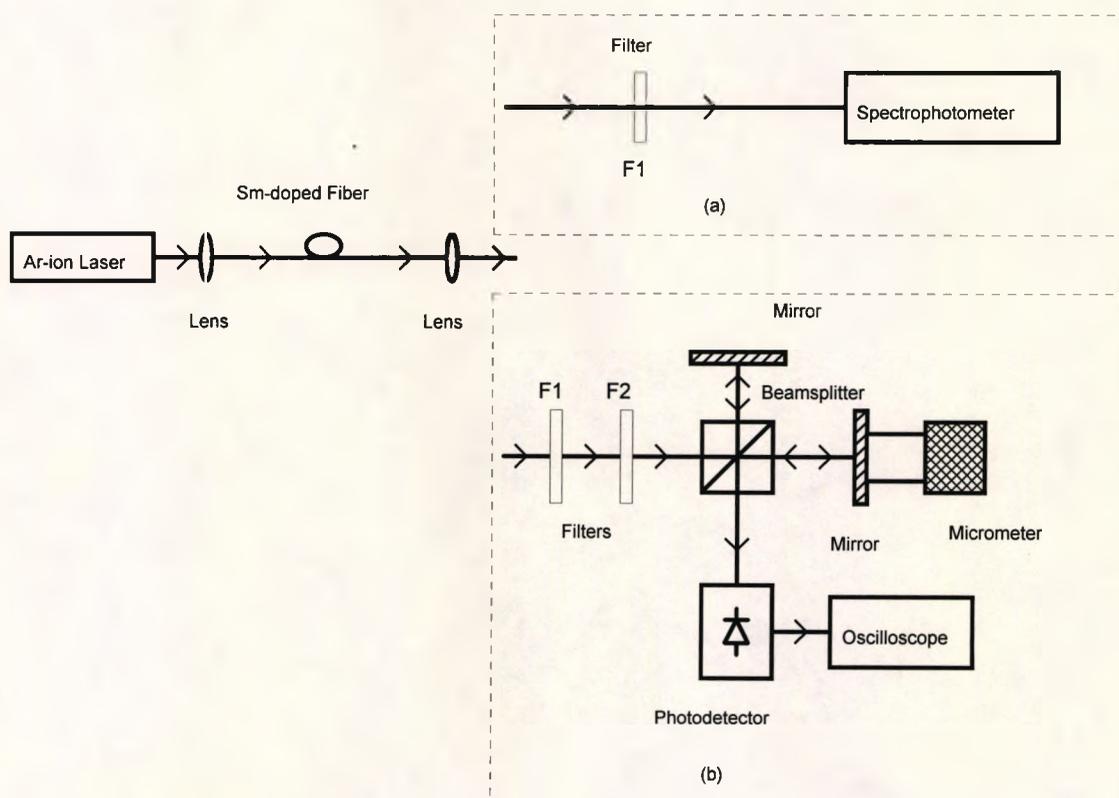
Fig.5.4 Experimental Arrangement
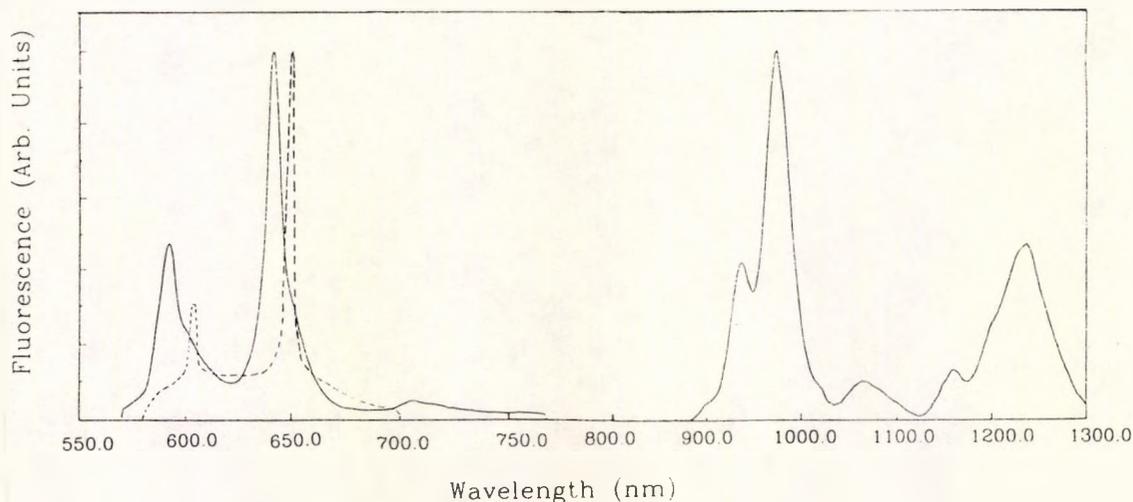
Fig.5.5 The Fluorescence Spectrum of Sm^{3+}-Doped Fibre [22]

Solid Line — Manufacturers' Data (Pump Wavelength: 530nm)

Dashed Line — Experimentally Obtained Data (Over the Visible Wavelength

Range only, Pump Wavelength: 514.5nm, 580nm $\leq \lambda \leq$ 700nm)

5.3.2 Experimental Results of Using Sm^{3+}-Doped Fibre as a two Wavelength Combination Source

A typical fluorescence spectrum recorded from the fiber is shown in Fig.5.5 where the solid line corresponds to the manufacturers' data at the pump wavelength of 530nm, and the dashed line represents the experimentally obtained data from a spectrophotometer when pumped by an Ar-ion laser of 514.5nm wavelength. Since the output from the Ar-ion laser may include some other spectral elements such as at wavelengths of 496nm, 488nm and 476nm which could pass through the fiber [23], and the optical power of the 514.5nm wavelength may not have been completely absorbed.

A substantial amount of blue and green light emission was present in the fiber output in addition to the fluorescence. In order to suppress this undesireable long coherence light beam, a long-pass spectral filter, F1 was used in the system, to transmit the wavelengths above 580nm, and the corresponding fluorescence spectrum recorded in the figure (dashed line), showing a close agreement with the solid line produced by the manufacturer, although a small wavelength shift was observed which was possibly due to the different pump wavelength and also the different pump power and temperature environment employed in the two cases [19]. From the experimentally obtained fluorescent spectrum it can be seen that there are two peaks in the red spectral region, at 603nm and 650nm respectively, which can be utilized to form a two wavelength combination source. Other peaks at the infrared region were not used in this preliminary investigation, but they may also be used to generate a multiwavelength combination source.

In order to select the two red spectral peaks and form a two wavelength combination source, two spectral filters were used in the experimental system where one filter, F1, can pass the wavelengths above 580nm with approximately an equal transmission intensity for both wavelengths of 603 and 650nm and the other being a short-pass filter, F2, having a transmission of 55% at the wavelength of 603nm and 17% at 650nm. From Fig.5.5 however, the relative fluorescence intensity was 0.31 at 603nm and 0.99 at 650nm, hence the corresponding fluorescence intensities observed at the two different wavelengths became similar, being 0.17 and 0.168 respectively. As a result, the fringe visibility in the output fringe pattern could be increased.

The experimentally obtained "beat fringe" pattern is shown in Fig.5.6(a), in which it can be seen that the central fringe identification becomes easier than the case of using only a single wavelength source, as discussed before, and the equivalent coherence length of such a source (i.e. 1/e of the central fringe packet width) now becomes only about 6μm, representing a significant coherence length reduction when compared with the commonly used low coherence light sources such as LEDs and superluminescent

diodes. Therefore, an efficient and convenient way of producing a visible, low coherence and two wavelength combination source can be realized with this fiber.
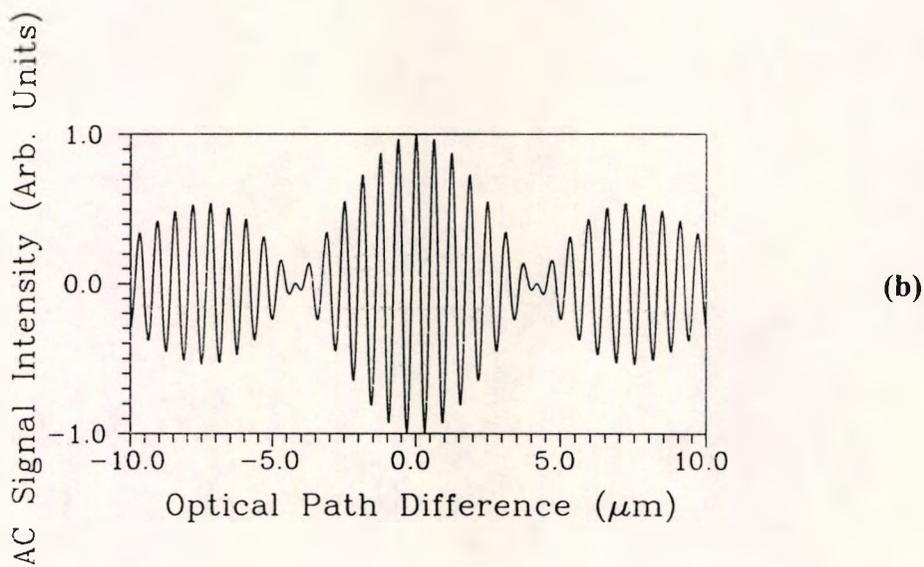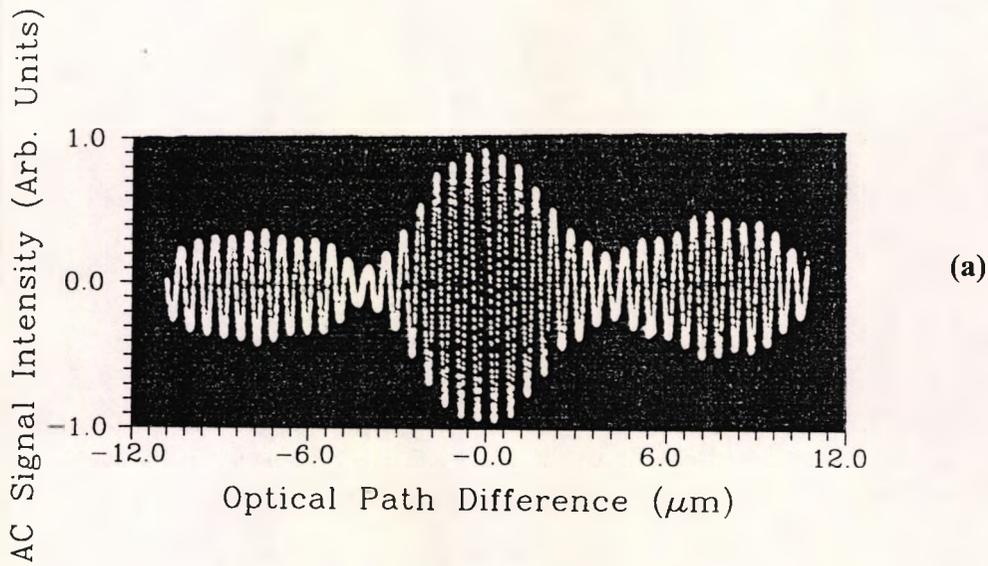
Fig.5.6 Interference Fringe Patterns for a two Wavelength Combination Source

$(\lambda_1 = 603nm, \lambda_2 = 650nm)$

(a) Experimental;

(b) Computer Simulated

In order to compare the result obtained from the experiment with that from theory, a computer simulated interference fringe pattern corresponding to a two wavelength combination source of wavelengths 603nm and 650nm respectively is demonstrated in Fig.5.6(b), in which a Gaussian spectrum was assumed for both light sources and the corresponding coherence length of each source was taken as 20μm. By comparing the two fringe patterns, a close similarity can be found, and the equivalent coherence length has reduced to ~ 6μm, although the actual spectral lineshape of the fluorescent emission may not be an exact Gaussian function. The asymmetry observed in the experimentally-obtained fringe pattern may be caused by the slight misalignment of the beam splitter and the mirrors in the interferometer.
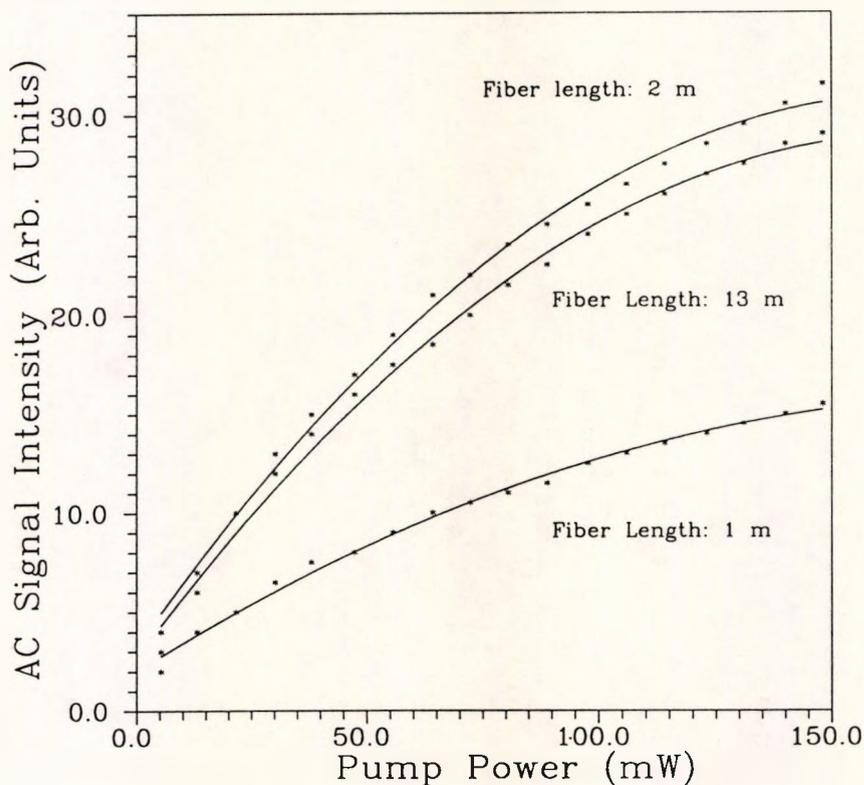
Fig.5.7 Interference ac Signal Intensity as a Function of Pump Power

It is also possible, by the use of an appropriate band-pass filter, to choose only one (usually the highest) fluorescence peak and form a single wavelength fibre light source,

in which case a relatively large signal intensity may be obtained, but as the corresponding coherence length would be increased, the central fringe identification becomes more difficult as previously discussed.

The other possible wavelength combinations which could be obtained using the red fluorescence peak with an infrared peak, may improve both the signal intensity and the minimum signal-to-noise ratio required in a white light interferometric system when used to perform central fringe identification as discussed in Chapter 3 and Chapter 4, when using the appropriate filters and photodetectors. In addition, a multiwavelength combination source may be also obtained by selecting several fluorescence peaks to provide further signal-to-noise ratio improvement as discussed in Chapter 4.

It has also been observed that the output ac signal intensity can be increased with an increase of the pump power and the corresponding relationship between them is depicted in Fig.5.7. Hence the pump power should be as large as possible without reaching the fibre damage limit. In addition, the ac signal intensity obtained also varies with the values of fibre length, for instance, when the pump power was 140mW and the fibre length was 2 meters, a relatively higher ac signal intensity of 31 units (on the scale used) can be observed. However, at the same pump power, if the fibre length was increased to 13 meters or inversely, reduced to 1 meter, the signal intensities were found to be decreased in both cases, to 29 units and 15 units respectively. This fact suggests an optimum fibre length corresponding to the highest possible ac signal intensity does exist, at a given pump wavelength and power.

5.4 Discussion

It has been demonstrated that a rare-earth-doped fibre, exemplified by a Sm^{3+}-doped fibre, when pumped by an Ar-ion laser, can be used as an effective low coherence,

visible light source. It provides a flexible means to produce a two wavelength combination source and potentially a multiwavelength combination source without causing the additional alignment difficulty of several separate sources, and hence it is suitable for high precision white light interferometric measurements. As a fibre fluorescent light source, it is compatible with other fibre components, and shows excellent coupling efficiency into optical fibres and high spatial coherence. The fluorescence power obtained in the experiment was still low, ~9μW from a fiber (of 13 meters length) output when pump power was 125mW and filter F1 was used. However, when both filters F1 and F2 were used, the red fluorescence power was only a few microwatts. There is clearly some potential to increase the output power, through optimization of the pump wavelength, the host glass and the concentration of the Sm^{3+}-ion used [6] and the choice of filter and fiber length itself must also be optimized for a given fiber and pump wavelength. However, this investigation does show that the Sm^{3+}-doped fibre exhibits a significant potential as a promising low coherence light source for white light interferometric sensor applications, especially as a laser diode-pumped system may be realized in the near future, offering a greater degree of compactness of the system. In addition, other rare-earth-elements such as praseodymium (Pr^{3+}) may be also explored as fibre fluorescent sources [3] [10].

Various kinds of low coherence light sources have been investigated, so far, in order to enhance the capability of central fringe identification which is important for high precision and absolute measurement in a white light interferometric system. However, to perform such a measurement, a scanning mechanism has to be introduced in either a single interferometer or a remote sensing white light interferometric system in order that the measurand induced OPD change in the sensing interferometer can be followed, as discussed in Chapter 1 and Chapter 2. An optical scanning technique is presented in the next Chapter as an alternative to the current scanning mechanisms for white light interferometric sensor applications.

References

1. D. J. Webb, J. D. C. Jones and D. A. Jackson, "Extended-Range Interferometry Using a Coherence-Tuned, Synthesized Dual-Wavelength Technique with Multimode Fibre Links", Electronics Letters, Vol.24, No.18, pp.1173-1175, 1st September 1988

2. V. Gusmeroli and M. Martinelli, "Two-Wavelength Interferometry by Superluminescent Source Filtering", Optics Communications, Vol.94, No.5, pp.309-312, 1 December 1992

3. B. J. Ainslie, S. P. Craig and S. T. Davey, "The Absorption and Fluorescence Spectra of Rare Earth Ions in Silica-Based Monomode Fiber", IEEE/OSA Journal of Lightwave Technology, Vol.6, No.2, pp.287-292, February 1988

4. R. Mears, L. Reekie, I. M. Jauncey and D. N. Payne, "Low-Noise Erbium-Doped Fibre Amplifier Operating at 1.54μm", Electronics Letters, Vol.23, No.19, pp.1026-1028, 10th September 1987

5. E. Desurvire, J. R. Simpson and P. C. Becker, "High-Gain Erbium-Doped Travelling-Wave Fiber Amplifier", Optics Letters, Vol.12, No.11, pp.888-890, November 1987

6. K. Liu, M. Digonnet, H. J. Shaw, B. J. Ainslie and S. P. Craig, "10mW Superfluorescent Single-Mode Fibre Source at 1060nm", Electronics Letters, Vol.23, No.24, pp.1320-1321, 19th November 1987

7. M. C. Farries, P. R. Morkel and J. E. Townsend, "Samarium[3+]-Doped Glass Laser Operating at 651nm", Electronics Letters, Vol.24, No.11, pp.709-710, 26th May 1988

8. I. N. Duling III, W. K. Burns and L. Goldberg, "High-Power Superfluorescent Fiber Source", Optics Letters, Vol.15, No.1, pp.33-35, January 1990

9. H. Fevrire, J. F. Marcerou, P. Bousselet, J. Auge and M. Jurczyszyn, "High Power, Compact 1.48μm Diode-Pumped Broadband Superfluorescent Fibre Source at 1.55 μm", Electronics Letters, Vol.27, No.3, pp.261-263, 31st January 1991

10. R. G. Smart, D. C. Hanna, A. C. Tropper, S. T. Davey, S. F. Carter and D. Szebesta, "CW Room Temperature Upconversion Lasing at Blue, Green and Red Wavelength in Infrared-Pumped Pr^{3+}-Doped Fluoride Fibre", Electronics Letters, Vol.27, No.14, pp.1307-1309, 4th July 1991

11. E. Desurvire, "Lightwave Communications: The Fifth Generation", Scientific American, pp.96-103, January 1992

12. W. A. Gambling, "Optical Fibres, Lasers, and Amplifiers", Endeavour, New Series, Vol.16, No.1, pp.17-22, 1992

13. R. J. Mears and S. R. Baker, "Erbium Fibre Amplifiers and Lasers", Optical and Quantum Electronics, Vol.24, No.5, pp.517-538, May 1992

14. A. V. Belov, G. G. Devyatykh, E. M. Dianov, A. N. Guryanov, D. D. Gusovskiy, V. F. Khopin and A. S. Kurkov, "Sm^{3+}-Doped Fibre Application to Spectral Filtration in the Range 1.53-1.57μm", Soviet Lightwave Communications, Vol.2, No.3, pp.265-268, August 1992

15. N. S. Kwong, "High-Power, Broad-Band 1550nm Light Source by Tandem Combination of a Superluminescent Diode and an Er-Doped Fiber Amplifier", IEEE Photonics Technology Letters, Vol.4, No.9, pp.996-999, September 1992

16. D. N. Payne, "Active Fibres and Optical Amplifiers", Fiber and Integrated Optics, Vol.11, No.3, pp.191-219, 1992

17. W. A. Gambling, "Fiber Lasers and Amplifiers in Distributed Sensors", Proceedings of the 9th International Optical Fiber Sensors Conference, pp.49-53, Firenze, Italy, May 4-6, 1993

18. E. Desurvire, "The Golden Age of Optical Fiber Amplifiers", Physics Today, pp.20-27, January 1994

19. P. F. Wysocki, M. J. F. Digonnet, B. J. Kim and H. J. Shaw, "Characteristics of Er-Doped Superfluorescent Fiber Sources for Interferometric Sensor Applications", IEEE/OSA Journal of Lightwave Technology, Vol.12, No.3, pp.550-567, March 1994

20. D. A. Chapman, "Erbium-doped Fibre Amplifiers: The Latest Revolution in Optical Communications", Electronics & Communication Engineering Journal, pp.59-67, April 1994

21. J. R. Armitage, "Introduction to Glass Fibre Lasers and Amplifiers", in "Optical Fibre Lasers and Amplifiers", Edited by P. W. France, pp.14-49, Blackie, 1991

22. Sm^{3+}-Doped fiber Data Sheet, Oxford Electronics Limited, 1994

Chapter 6

An Optical Scanning Technique for
White Light Interferometry

In this Chapter, an optical scanning technique is presented as an alternative to the current scanning mechanisms for white light interferometric sensor use. This technique utilizes the characteristics of an interference fringe pattern generated by a two wavelength combination source of which one light source is wavelength tunable. The operating principle of optical scanning is explained in the course of the theoretical analysis and a set of computer simulated fringe patterns, and further confirmed by experimentally obtained results carried out using a laser diode in combination with a wavelength tunable dye laser. This optical scanning technique offers the possibility to eliminate the receiving interferometer in some circumstances and the potential of an alternative simple, stable and compact white light interferometric sensor system.

6.1 Introduction

As described in Chapter 1 and Chapter 2, for a remote sensing white light interferometric system, an extra receiving interferometer is required, thus increasing the complexity of the system configuration. In such a system where the two interferometers are connected in tandem or a single interferometer white light system, a scanning mechanism has to be introduced to allow the OPD change in the sensing interferometer, induced by the variation of the physical measurand, to be retrieved by matching the

OPDs in the two interferometers or in the case of the single interferometer system, balancing the two arms of the interferometer.

The main scanning techniques currently used in white light interferometry are mechanical and electronic [1-3], as discussed in Chapter 2. The mechanical scan is usually achieved by scanning the mirror mounted on a translation stage while the electronic scan is realized by the use of a CCD array. In the mechanical scanning technique, a large operating range is readily available, but the mechanical stability and the accuracy of the moving components are critical for a high precision measurement and the system has a relatively large configuration. The electronic scan exhibits a high stability as no moving elements are involved, a small system physical dimension as well as a high scanning speed. However, its operating range may be rather limited [2] [4-5].

Another scanning mechanism reported is a thermally scanned polarimetric interferometric system where the receiving interferometer consists of two equal lengths of polarization maintaining fibre, spliced with orthogonal polarization axes. The OPD between the two polarization modes in the interferometer is dependent on the temperature difference between the two fibre lengths, hence by scanning their temperature difference, an OPD can be produced and controlled between the two modes, which can match that of the sensing interferometer [6]. The system is also compact and stable as it is without any moving elements, but its scanning time is relatively long (e.g. ten seconds), limited by the speed of temperature change that can be achieved.

An acoustic scanning technique has also been proposed [7], which is based on the group velocity difference between two modes in an optical fibre and performed by the use of an acoustic pulse travelling along the optical fibre, inducing coupling between the two modes and hence producing a corresponding OPD. Although the mechanical moving elements can be avoided by the use of this technique, the measurement precision is limited as the position of acoustic pulse is difficult to be accurately determined in the system.

In [8], a static polarimetric interferometer with a fixed OPD value was used as the receiving interferometer and from which four outputs were arranged to provide phase

information through the use of an electronic assembly which was connected to a personal computer. Two LEDs were utilized as the light sources in order to extend the operating range by means of a dual wavelength interferometric method [9-10], as explained in Chapter 1. The major drawback is the complexity of the system as four detectors, a number of polarizing beam splitters and fibre couplers, an electronic device as well as a computer are involved.

From the above discussion, it may be seen that current scanning techniques in white light interferometry have limitations and the receiving interferometer employed for remote sensing purpose increases the number of optical components involved and hence the system complexity and thus may be inconvenient to use in some applications.

In this chapter, an optical scanning technique, combining the use of a two wavelength combination source [11] and the wavelength tuning method [12-13] discussed in Chapter 1, is presented as an alternative to white light interferometric sensor use [14-15]. This optical scanning mechanism can be achieved without using moving mechanical elements, and by tuning one wavelength in the two wavelength combination source, the beat interference fringe pattern observed will be changed accordingly and hence an effective scanning mechanism can be realized. In addition, the measurement may be achieved without the receiving interferometer, thus making the whole system potentially simple, stable and compact.

6.2 Theoretical Analysis

6.2.1 Characteristics of the two Wavelength Combination Source

As discussed in Chapter 3, for an interferometer illuminated by a two wavelength combination source of wavelengths λ_1 and λ_2, and with coherence lengths L_{c1} and L_{c2} respectively, the normalized output interference signal intensity has the form:

where x is the OPD introduced by the interferometer, and the other terms are as previously defined.

If the two laser sources have similar coherence lengths, i.e. $L_{c1} = L_{c2} = L_c$, then

$$I_{ac}(x) = (1/2)\exp[-(2x/L_c)^2][\cos(2\pi x/\lambda_1) + \cos(2\pi x/\lambda_2)]$$

$$= \exp[-(2x/L_c)^2]\cos(2\pi x/\lambda_a)\cos(2\pi x/\lambda_m) \qquad (3.2.6)$$

where $\lambda_a = 2\lambda_1\lambda_2/(\lambda_1 + \lambda_2)$ is the average wavelength and $\lambda_m = 2\lambda_1\lambda_2/|\lambda_2 - \lambda_1|$ is the modulation wavelength of the two wavelength combination source.

The output signal is actually a cosine function of wavelength λ_a, modulated by another cosine function of wavelength λ_m, and the overall envelope is modulated by a Gaussian visibility profile, of the form $\exp[-(2x/L_c)^2]$ which becomes 1 when $L_c \gg 2x$.
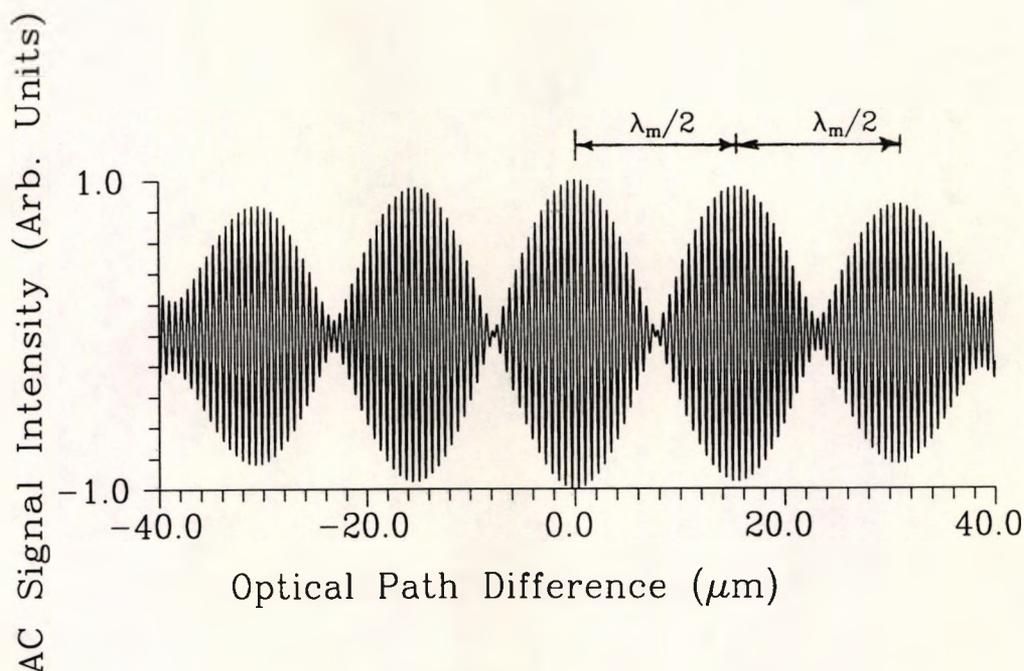
Fig.6.1 Typical Interference Fringe Pattern of the two Wavelength

Combination Source Discussed

A typical interference fringe pattern obtained from such a source is shown in Fig.6.1, where the central fringe in the central fringe packet is situated at the zero OPD position, the profile peak position in the first side fringe packet is at $\lambda_m/2$, and the second side

the profile peak position in the first side fringe packet is at $\lambda_m/2$, and the second side peak position is a further $\lambda_m/2$ away, i.e. λ_m away from the central fringe position. In general, the distance between the nth side peak and the central fringe is given by:

$$x_n - x_0 = (n/2)\lambda_m$$

$$= n\lambda_1\lambda_2/|\lambda_2 - \lambda_1| \qquad (n = \pm 1, \pm 2, \ldots) \qquad (6.2.1)$$

where a positive n value is set to correspond to an OPD increase. It can be noticed from this equation that if the wavelength of one of the laser sources is changed, all the side peak positions in the fringe pattern will be changed as a consequence, and this fact can be used to form an optical scanning technique as will be seen later.

6.2.2 Operating Principles of the Optical Scanning Technique

Assuming that in a two wavelength combination source, one laser source has a given wavelength, λ_1, and the other is wavelength tunable, then by tuning the wavelength λ_2 to a new value, λ_2', the nth side peak position will move from x_n to x_n', and the equivalent scanning distance in this process is

$$d_n = -(x_n' - x_n)$$

$$= (n\lambda_m/2 + x_0) - (n\lambda_m'/2 + x_0)$$

$$= (n/2)(\lambda_m - \lambda_m')$$

$$= n\lambda_1^2 (1/|\Delta\lambda| - 1/|\Delta\lambda'|) \qquad (6.2.2)$$

where $\lambda_m' = 2\lambda_1\lambda_2'/(\lambda_2' - \lambda_1)$, $\Delta\lambda = \lambda_2 - \lambda_1$ and $\Delta\lambda' = \lambda_2' - \lambda_1$, and the relation $sgn(\Delta\lambda) = sgn(\Delta\lambda')$ is also assumed, in which $sgn(x)$ is the sign function defined by:

$$sgn(x) = -1, \qquad \text{when } x < 0;$$

$$0, \qquad \text{when } x = 0;$$

$$1, \qquad \text{when } x > 0.$$

A positive d_n value also means an OPD increase in this case.

If the **wavelength change** $\lambda_2' - \lambda_2$ is denoted by $\delta\lambda$, then

132

$$\delta\lambda = \lambda_2' - \lambda_2 = \Delta\lambda' - \Delta\lambda \qquad (6.2.3)$$

i.e. $\delta\lambda$ is also the wavelength difference change. From equation (6.2.2), it follows that

$$d_n = n\lambda_1^2 \, (1/|\Delta\lambda| - 1/|\Delta\lambda + \delta\lambda|)$$

$$= n\lambda_1^2 \, \delta\lambda \, \text{sgn}(\Delta\lambda)/[\Delta\lambda(\Delta\lambda + \delta\lambda)] \qquad (6.2.4)$$

Hence, for a given two wavelength combination source, the wavelength change, $\delta\lambda$, in a tunable laser source can be transformed into an equivalent scanning distance of the given n^{th} side peak in the output fringe pattern, this performance thus constituting the operating principle of the proposed optical scanning technique.

For an interferometer illuminated by a two wavelength combination source, the central fringe in the central fringe packet and the nth side peak positions in the output fringe pattern are situated at the position x_0 and x_n respectively. If an OPD change of d is generated in the interferometer by the variation of the measurand, the whole fringe pattern will shift a distance d, and the corresponding position for the central fringe and the nth side peak will become $x_0 + d$ and $x_n + d$ respectively. Introducing an appropriate wavelength change of $\delta\lambda$ of the tunable laser source, the nth side peak can be made to move backward to an equivalent scanning distance, d_n, and return to its initial position, x_n (the central fringe in the central fringe packet will remain unchanged during this optical scanning process, as no further OPD change is involved). The OPD change, d, hence is equal to the equivalent scanning distance, d_n, so that

$$d = d_n = n\lambda_1^2 \, \delta\lambda \, \text{sgn}(\Delta\lambda)/[\Delta\lambda(\Delta\lambda + \delta\lambda)] \qquad (6.2.5)$$

i.e. the OPD change can be calculated from the corresponding wavelength change, $\delta\lambda$. In this technique, since the OPD change induced by the measurand in the sensing interferometer can be recovered by a corresponding wavelength change in the tunable laser source, the receiving interferometer normally associated with the remote sensing white light interferometry for absolute measurement becomes unnecessary. If the operating range of optical scan can fulfil the requirement of the system, this fact thus can be used to simplify the sensing system configuration.

6.2.3 Characteristics of the Optical Scanning Technique

In order to evaluate this optical scanning technique, its main characteristics, such as the operating range, measurement resolution and dynamic range, should be determined.

Supposing that the values of n, $\Delta\lambda$ and $\delta\lambda$ are all positive, then from equation (6.2.5), it follows that

$$d = d_n = n\lambda_1^2 \, \delta\lambda \, / \, [\Delta\lambda(\Delta\lambda + \delta\lambda)]$$

$$= n\lambda_1^2[1/\Delta\lambda - 1/(\Delta\lambda + \delta\lambda)] \qquad (6.2.6)$$

the partial derivatives are given as

$$\partial d/\partial(\delta\lambda) = n\lambda_1^2 \, / \, (\Delta\lambda + \delta\lambda)^2 \, > 0 \qquad (6.2.7)$$

and

$$\partial d/\partial(\Delta\lambda) = - \, n\lambda_1^2 \, \delta\lambda \, (2\Delta\lambda + \delta\lambda)/\Delta\lambda^2 \, (\Delta\lambda + \delta\lambda)^2 \, < 0 \qquad (6.2.8)$$

Thus, the OPD change is a monotonically increasing function of the wavelength change, $\delta\lambda$, and a monotonically decreasing function of the initial wavelength difference, $\Delta\lambda$. As a result, the OPD change increases with the increase of the given wavelength λ_1, the order of the side fringe packet peak chosen, n, and the wavelength change, $\delta\lambda$, and with the decrease of initial wavelength difference, $\Delta\lambda$. Other different situations can also be elucidated by the use of the same analysis. For example, if n > 0, $\delta\lambda$ < 0 and $\Delta\lambda$ < 0, then $\partial d/\partial(\delta\lambda)$ < 0 and $\partial d/\partial(\Delta\lambda)$ > 0, then the relationship between the OPD change and $\delta\lambda$ and $\Delta\lambda$ turns out to be contrary to that obtained above.

Obviously, in this technique, the system operating range, d_{max}, is limited by the maximum variation of the tuning wavelength, $\delta\lambda_{max}$, and this can be written as:

$$d_{max} = |n\lambda_1^2 \, \delta\lambda_{max}/[\Delta\lambda(\Delta\lambda + \delta\lambda_{max})]| \qquad (6.2.9)$$

where $\delta\lambda_{max}$ is the maximum wavelength change allowed.

In addition, the operating range is also restricted by the coherence length, L_c, i.e. $d_{max} \leq L_c$ is required as indicated by equation (3.2.6). Hence it is desirable that L_c, be

large, as long as the order of the selected side peak can be easily identified in an "initialization" process, as will be described later.

On the other hand, the measurement resolution of this technique, d_{min}, may also be determined by the factors n, λ_1, $\Delta\lambda$ and more critically, the wavelength resolution of the tunable laser source, $\delta\lambda_{min}$, and hence

$$d_{min} = |n\lambda_1^2 \, \delta\lambda_{min}/[\Delta\lambda(\Delta\lambda + \delta\lambda_{min})]| \qquad (6.2.10)$$

For a given wavelength resolution, $\delta\lambda_{min}$, in order to maximize the system measurement resolution, the smallest possible value of n should be set and the value of the given wavelength λ_1 also has to be chosen to be as low as possible. However, the value of the initial wavelength difference, $\Delta\lambda$, ought to be set high in this case. If a value n = 1 is assumed and the condition: $\delta\lambda_{min} \ll \Delta\lambda$ can be satisfied, equation (6.2.10) then gives:

$$d_{min} \approx (\lambda_1/\Delta\lambda)^2 \, \delta\lambda_{min} \qquad (6.2.11)$$

i.e. a simple linear relation between the measurement resolution and the wavelength resolution may be obtained, which may facilitate the interpretation of the measurement results.

By choosing a particular side peak of the interference fringe pattern, the dynamic range of the system, D, can be expressed as:

$$D = d_{max}/d_{min}$$

$$= |\delta\lambda_{max}/\delta\lambda_{min}| |(\Delta\lambda + \delta\lambda_{min})/(\Delta\lambda + \delta\lambda_{max})| \qquad (6.2.12)$$

In general, the maximum wavelength change, $\delta\lambda_{max}$, and the wavelength resolution, $\delta\lambda_{min}$, have given values which are determined by the characteristics of the tunable laser source.

In practice, the selection of the values of $\Delta\lambda$, n and λ_1 should be in accordance with any particular system requirement, in order to achieve either a large operating range or a high system resolution or alternatively, to obtain an appropriate dynamic range for the system.

6.3 Computer Simulations of the Optical Scanning Technique
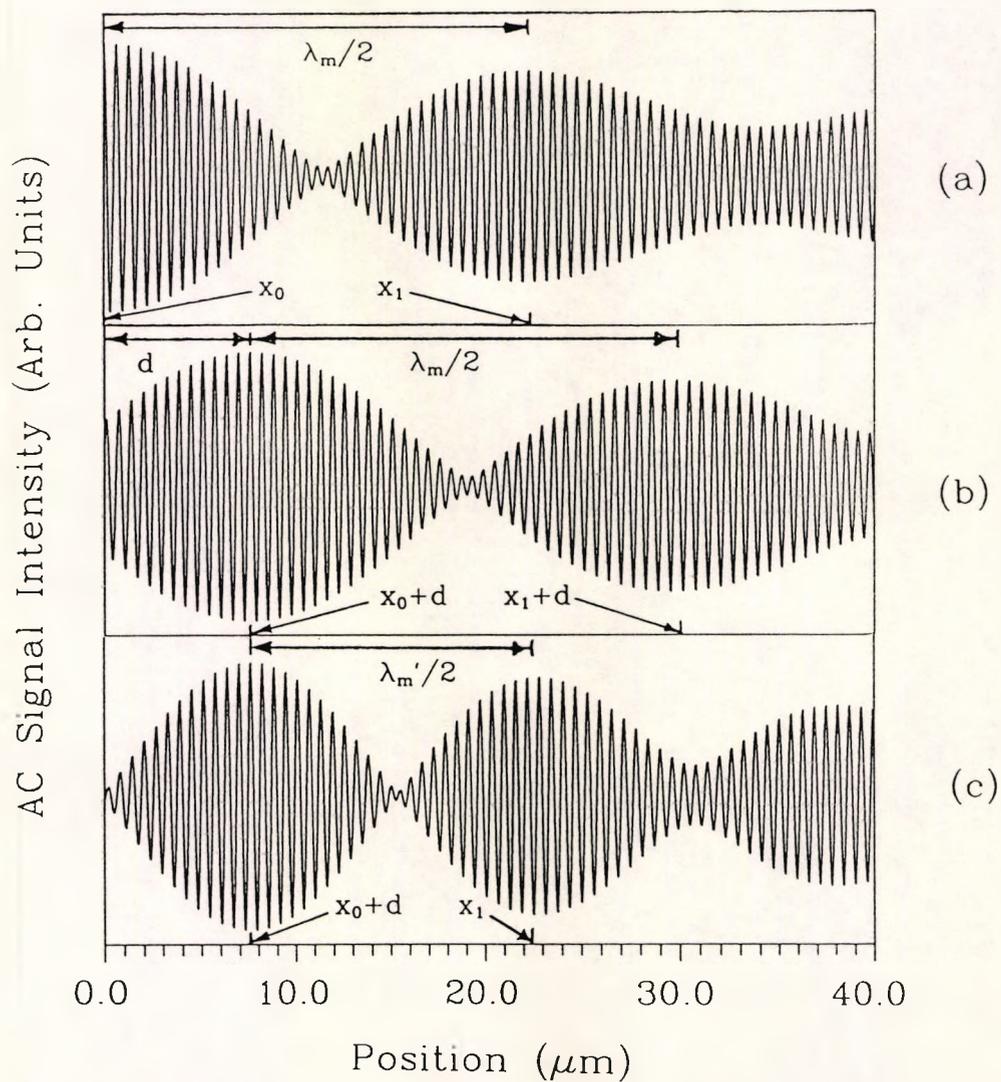
Fig.6.2 Computer Simulated Interference Fringe Patterns

(a) $\lambda_1 = 635nm$, $\lambda_2 = 618nm$, $x_0 = 0$

(b) $\lambda_1 = 635nm$, $\lambda_2 = 618nm$, $x_0 + d = 7.6\mu m$

(c) $\lambda_1 = 635nm$, $\lambda_2 = 610nm$, $x_0 + d = 7.6\mu m$

Computer simulation is a valuable tool to generate theoretical interference fringe patterns and to analyze their characteristics. In this Section, the operating principle and the characteristics of the optical scanning technique are studied with the help of computer simulation results.

The operating principle of the optical scanning technique can be easily explained by a set of computer simulated fringe patterns, as illustrated in Fig.6.2. Fig.6.2(a) demonstrates the fringe pattern of $I_{ac}(x - x_0)$ where $x_0 = 0$ is the central fringe position and the first side peak position is at $x_1 = \lambda_m/2$. The given wavelength, λ_1, and the initial wavelength difference, $\Delta\lambda$, are assumed to be 635nm and -17nm respectively, and the coherence lengths of the two laser sources are chosen as $L_{c1} = 60\mu m$ and $L_{c2} = 75mm$, corresponding to values typical of a commercial laser diode and a dye laser respectively that will be used in the later experimental investigations. When an OPD change of $d = 7.6\mu m$ is introduced, as shown in Fig.6.2(b), the whole fringe pattern shifts a distance of d and is given by: $I_{ac}[x - (x_0 + d)]$. The first side peak is now situated at $x_1 + d$. However, if $\Delta\lambda$ is changed by a value of $\delta\lambda = -8nm$, i.e. λ_2 becomes 610nm, then it can be seen from Fig.6.2(c) that the first side peak will move back to its original position. The central fringe (in the central fringe packet) position remains unchanged throughout this wavelength tuning process. An equivalent optical scanning distance of $d_1 = 7.6\mu m$ can also be obtained from equation (6.2.5) by substituting the corresponding values, i.e. $\lambda_1 = 635nm$, $\Delta\lambda = -17nm$, $\delta\lambda = -8nm$ and $n = 1$.

In order to determine the scanning distance, the relations between the wavelength difference and the side peak positions in a typical two wavelength combination source are depicted in Fig.6.3, where the given wavelength $\lambda_1 = 635nm$ is assumed and the wavelength difference, $\Delta\lambda$, varies from 1 to 50nm. The curves obtained correspond to the different orders of the side peak, $n = 1, 2$ and 3 respectively. It can be seen from this figure that for a small initial wavelength difference, the value of x_n is large, and when the initial wavelength difference is increased, the value of x_n becomes small, and therefore a large scanning distance or in other words, a large system operating range, is possible. Furthermore, it also shows that for the same initial wavelength difference, $\Delta\lambda$,

and a wavelength change, $\delta\lambda$, different scanning distances can be achieved by choosing a different order of the side peaks. The higher order of the side peak means a larger scanning distance. For instance, if the initial wavelength difference is 5nm and the wavelength difference change is 15nm, then a scanning distance $d_1 = 60.5\mu m$ can be obtained when using the first side peak. However, by choosing the second or the third side peak, the scanning distance becomes $d_2 = 121.0\mu m$ or $d_3 = 181.5\mu m$, i.e. 2 or 3 times higher respectively. Therefore, a large n value is required in order to increase the system operating range.
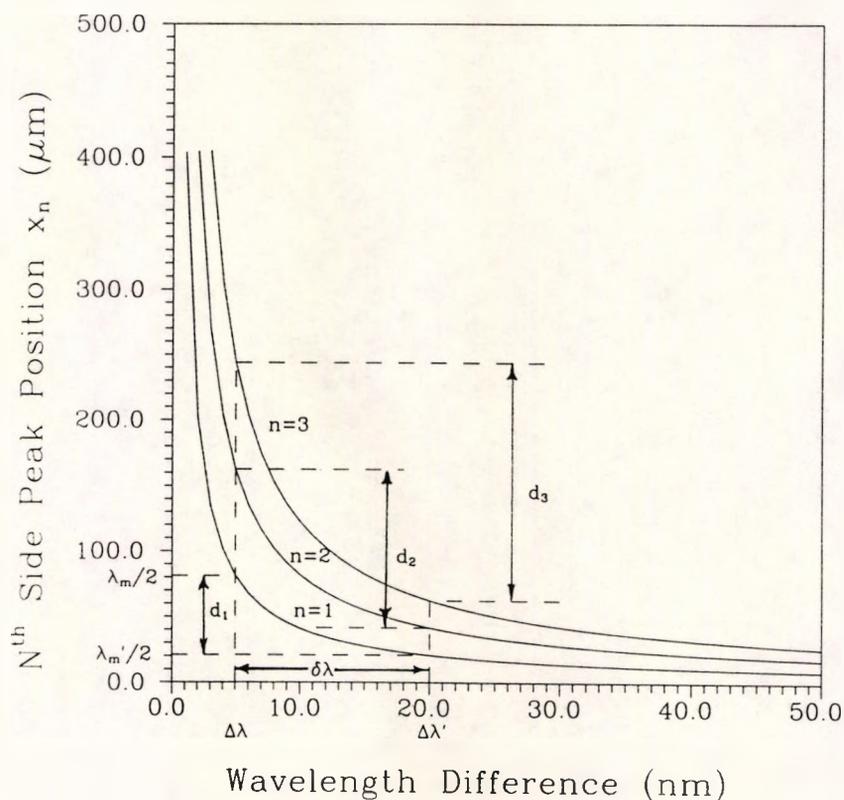
Fig.6.3 The Variation of the Nth Side Packet Peak Position
with the Initial Wavelength Difference, $\Delta\lambda$

A typical relationship between the dynamic range, D, and the initial wavelength difference, $\Delta\lambda$, is demonstrated in Fig.6.4, where the values of the maximum wavelength change $\delta\lambda_{max} = 100nm$ and the wavelength resolution, $\delta\lambda_{min} = 0.5nm$ are assumed to be positive and to have been given realistic values for a practical system. It

can be seen from this figure that when the initial wavelength difference, $\Delta\lambda$, is increased, the system dynamic range will also be increased, and become closer to the value $|\delta\lambda_{max}/\delta\lambda_{min}|$. To obtain a large dynamic range, the ratio $|\delta\lambda_{max}/\delta\lambda_{min}|$ and the value $\Delta\lambda$ should be selected as high as possible, as indicated by equation (6.2.12)
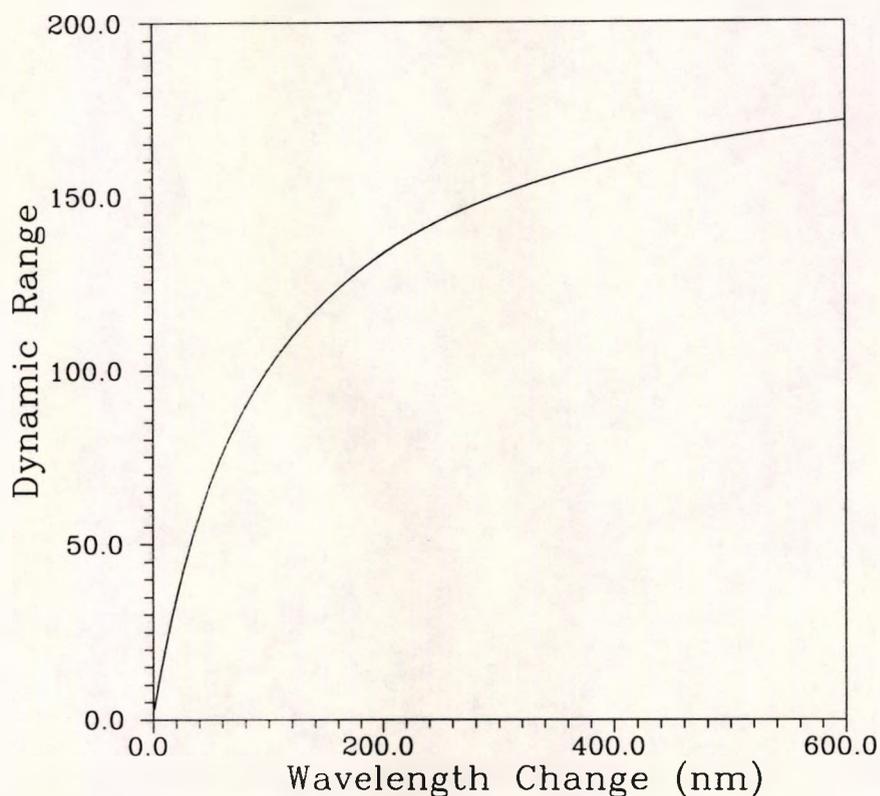
Fig.6.4 The Variation of the Dynamic Range with the Initial Wavelength

Difference, $\Delta\lambda$ ($\delta\lambda_{max} = 100$nm and $\delta\lambda_{min} = 0.5$nm)

6.4 Experimental Results of the Optical Scanning Technique

6.4.1 Experimental Arrangement

Fig.6.5 shows schematically an experimental arrangement for verifying the operating principle discussed and computer simulation results obtained and described.
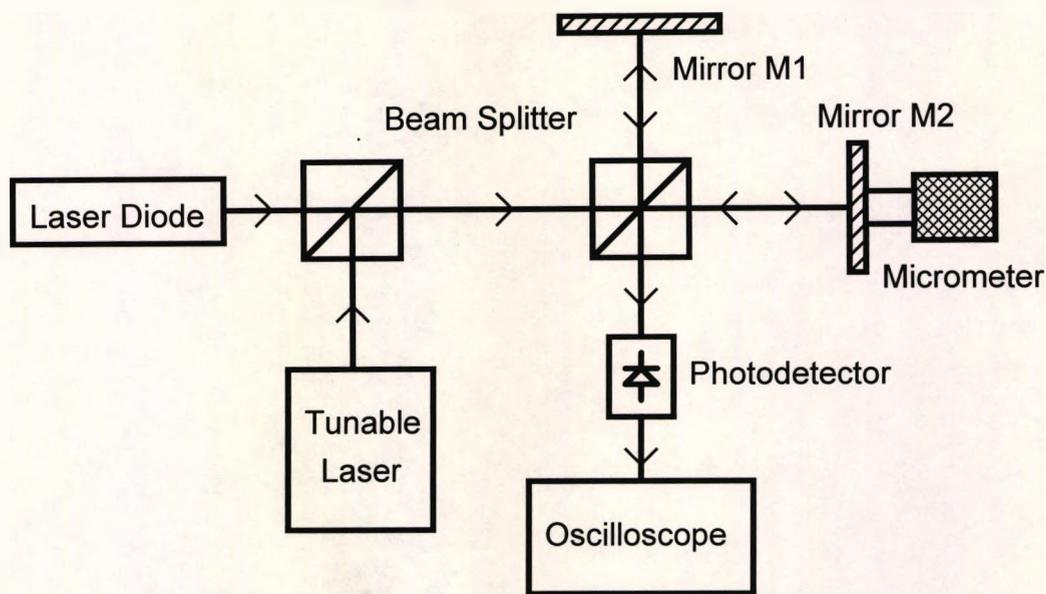
Fig.6.5 Experimental Arrangement

In the experiments carried out, in order to calculate the OPD change introduced in the system according to equation (6.2.5), the first procedure is to "initialize" the interferometer, i.e. the initial position of the nth side peak in the fringe pattern of a two wavelength combination source of given wavelength, λ_1, and the initial wavelength difference, $\Delta\lambda$, is determined, and then, an OPD change introduced in the interferometer can be compensated by an appropriate wavelength change, $\delta\lambda$, of the tunable laser.

A typical laser diode of wavelength $\lambda_1 = 635$nm was operated just close to the threshold (106.2mA) where it exhibits a short coherence length ($L_c = 40\mu$m), thus showing clearly the central fringe packet obtained and the distinguishable n^{th} side peak in the output interference fringe pattern during the "initialization" of the interferometer. After this initialization process is completed, the laser diode can also be operated above its threshold to obtain a relatively long coherence length, thus providing a relatively large operating range. A long coherence length (75mm) dye laser with a wavelength tuning range from 604nm to 642nm, this being the only tunable laser available in the laboratory with such a wide range, was used as the tunable laser source in the

experiment in order to demonstrate the operating principle of the system at this preliminary stage, in spite of such a laser being a high cost option for use in such a system. However, other light sources such as tunable laser diodes and fibre lasers are likely to be more suitable in terms of their compactness or potential low costs in future work beyond this "proof-of-principle". Thus the value of the technique can be seen more clearly with the use of these lower cost sources to compete with a conventional white light interferometric system, and prove the validity of the system. The light beams from the two laser sources were first combined by a beam splitter to illuminate a bulk optic Michelson interferometer. One of the mirrors in the interferometer, M_1, was driven by a loudspeaker to allow fine control of the optical path imbalance, thus generating a phase modulation, and the other, M_2, was mounted on a micrometer in order to introduce a known OPD change during the investigation. The output from the interferometer was detected directly by a photodetector. The fringe pattern can then be observed on an oscilloscope connected to the photodetector.
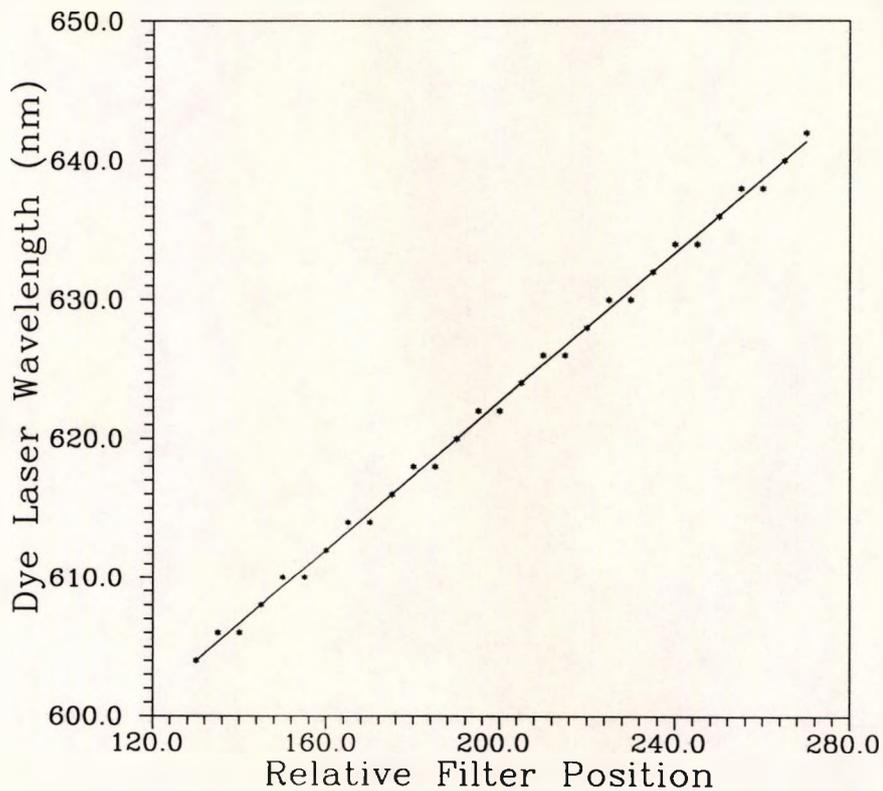
Fig.6.6 Dye Laser Wavelength Versus The Filter Calibration

In this "proof-of-principle" experiment, the wavelength variation in the dye laser is controlled through a filter inside the laser cavity. By rotating the angle between the laser beam inside the cavity and the filter surface thus the wavelength of the output laser beam from the dye laser can be changed. The variation of the wavelength as a function of the filter calibration was measured and is depicted in Fig.6.6.

6.4.2 Experimental Results of the Optical Scanning Technique
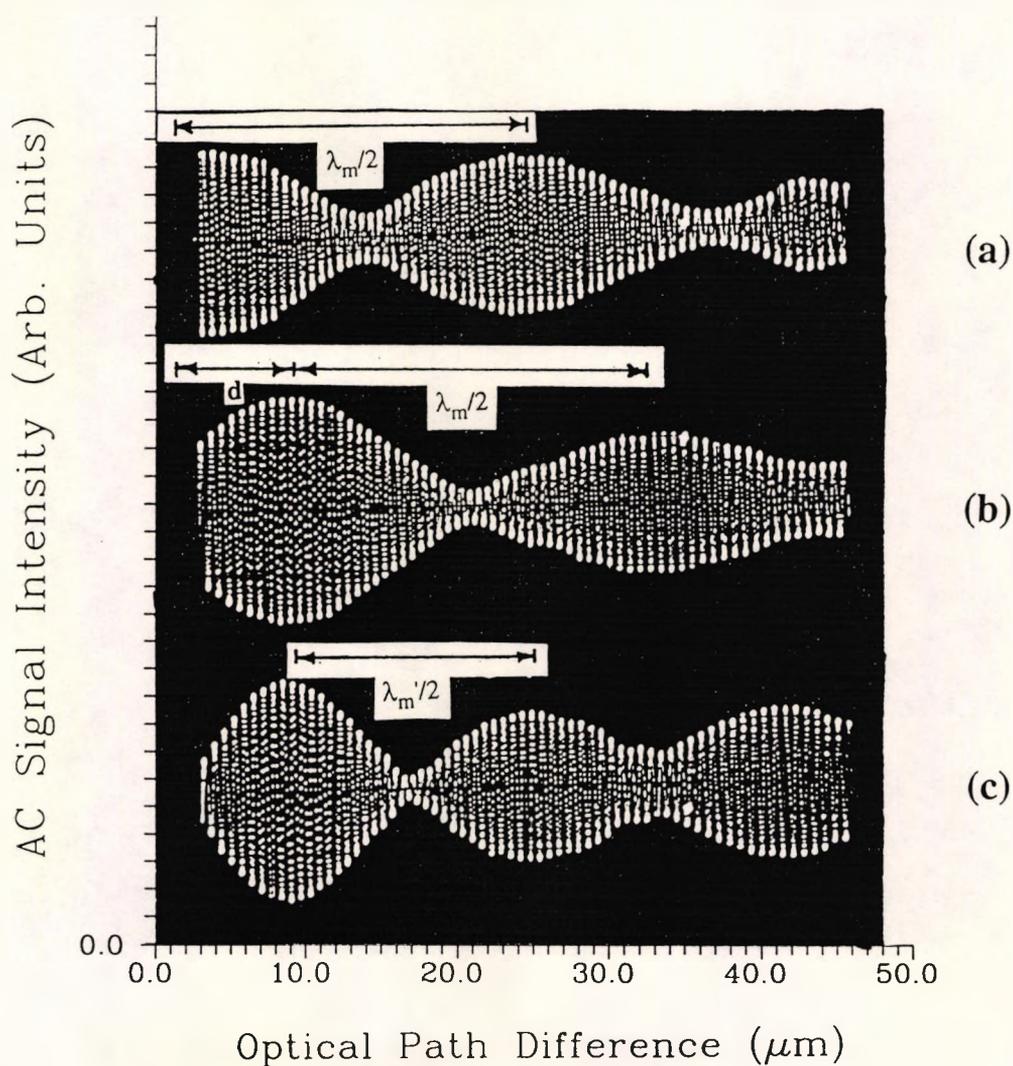
Fig.6.7 Experimentally obtained Interference Fringe Patterns

(a) $\lambda_1 = 635$nm, $\lambda_2 = 618$nm, $x_0 = 0$

(b) $\lambda_1 = 635$nm, $\lambda_2 = 618$nm, $x_0 = 8\pm0.5\mu$m

(c) $\lambda_1 = 635$nm, $\lambda_2 = 610$nm, $x_0 = 8\pm0.5\mu$m

The first side peak was selected to demonstrate the operating principle of the optical scanning technique through the experiment and the interference fringe pattern obtained is shown in Fig.6.7. A given wavelength of λ_1 = 635nm and an initial wavelength difference of $\Delta\lambda$ = -17nm, were chosen and the results are shown on Fig.6.7(a). The fringe pattern movement caused by the OPD change of 8±0.5μm in Fig.6.7(b) can be compensated by imposing a wavelength change of $\delta\lambda$ = -8nm in the tunable laser as indicated in Fig.6.7(c), where the first side peak returned to its initial position. The wavelength values used were similar to those in the computer simulations and the interference fringe patterns obtained have also shown good agreement with those in Fig.6.2, thus confirming experimentally the operating principle of the optical scanning technique.
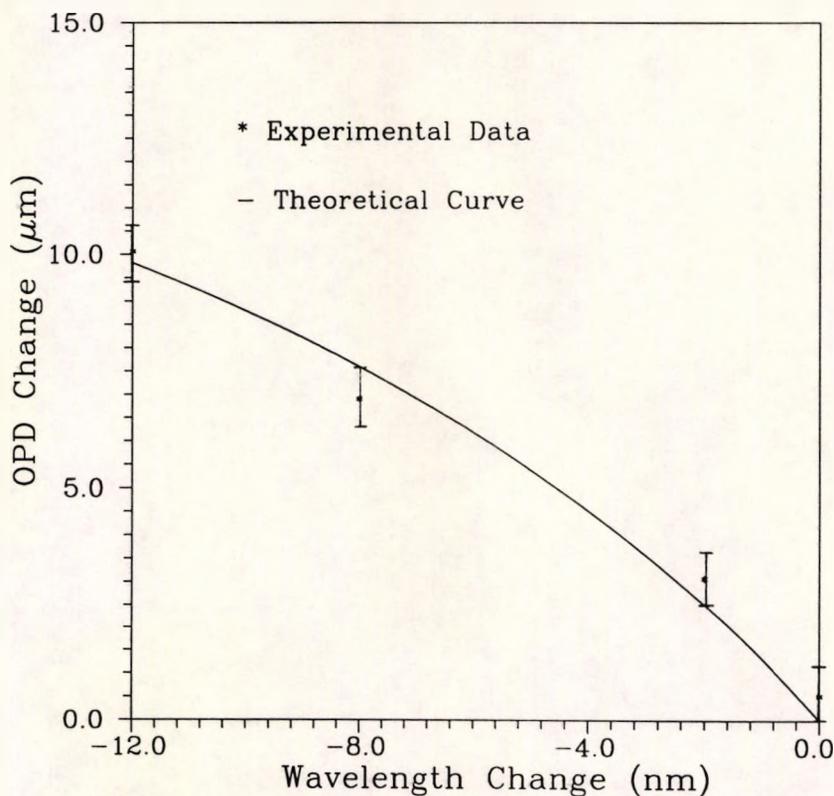
Fig.6.8 The Variation of the OPD Change with the Wavelength Change, $\delta\lambda$

In the optical scanning technique, the OPD change in the interferometer is tracked by the use of a wavelength change. A series of measurements have been made and the results give the relationship between the variation of the wavelength change and the OPD change in the interferometer. The corresponding data points obtained are plotted in Fig.6.8, where the first side peak position was taken as the reference and the given wavelength, λ_1 was still 635nm. The initial wavelength difference, $\Delta\lambda$ = -17nm was used, i.e. λ_2 = 618nm in this case. The wavelength changes introduced were -2nm, -8nm and -12nm, corresponding to the wavelengths of the tunable laser at 616nm, 610nm and 606nm respectively. When compared with the theoretical curve also plotted in Fig.6.8, the results appear to show a close correlation within reasonable experimental error of less than 1μm.

The measurement resolution achieved was 1.4 μm, which was limited by the wavelength resolution, about 1nm in this case, and it also depends on the initial wavelength difference chosen. When $\Delta\lambda$ is increased, a higher resolution can be expected as shown by equation (6.2.11).

6.5 Discussion

An optical scanning technique as an alternative to white light interferometric sensing has been developed theoretically and verified experimentally. By adopting this alternative, it is possible to eliminate the receiving interferometer which is otherwise essential to a remote sensing white light interferometric system when the path imbalance is greater than the coherence length of the light source. Thus a simple, stable and compact interferometric sensor operation may be realized.

In this technique, the system operating range, defined by equation (6.2.9), may become very large if either the value of $\Delta\lambda$ or $\Delta\lambda + \delta\lambda_{max}$ is close to zero, and a typical operating range of 1mm can be readily achieved, As an example, when λ_1 = 635nm, $\Delta\lambda$

= 51nm, $\delta\lambda_{max}$ = -50nm and n = 3, the operating range is about 1.2mm. This value is better than the electronic scanning method can usually offer [2] [4]. The operating range of this technique is restricted by the optical path imbalance control device such as a loudspeaker used to drive mirror M_1 in Fig.6.5. If, for instance, when n = 1, λ_1 = 635nm, $\Delta\lambda$ = 2nm and $\delta\lambda$ = 18nm, the operating range is about 181.5 μm, it should be ensured that the optical path imbalance control device has at least a moving range of larger than 363 μm.

The measurement resolution of this technique, usually given by equation (6.2.11), is determined by the wavelength resolution that can be achieved, $\delta\lambda_{min}$, and the initial wavelength difference chosen, $\Delta\lambda$. A high measurement resolution can be realized by the use of this technique if $\delta\lambda_{max}$ is small and a large value of $\Delta\lambda$ can be chosen. For instance, when λ_1 = 635nm, λ_2 = 830nm, i.e. $\Delta\lambda$ = 195nm, a measurement resolution of 10.6nm can be achieved for the wavelength resolution of 1nm and can be further reduced to 5.3nm if the wavelength resolution of 0.5nm becomes a reality. The measurement resolution may be affected by the intensity noise in the system and the wavelength stability of the light source.

It can be seen from equation (6.2.9) and (6.2.11) that there is a trade off between the operating range and the measurement resolution. To increase the operating range, a higher order of side peak, n, a large value of λ_1 and a small value of $\Delta\lambda$ are needed, but for a high measurement resolution, the requirement turns out to be the contrary. To overcome this difficulty, a flexible approach and a reliable measurement can be obtained by tracking several peaks during the experimental process, in which the lower order side peaks give a better resolution and the higher order peaks provide a larger operating range as discussed in Section 6.2, thus optimizing the information which may be obtained. Hence, a large operating range, high resolution and hence large dynamic range become possible by the use of this optical technique.

Since the actual position of the side peak does not necessarily correspond to the maximum fringe intensity position in the side fringe packet, some difficulties may exist in determining the side peak position during the operation and consequently, an

ambiguity range of $\lambda_a/2$, typically less than 0.4μm, may be introduced. However, for a more accurate measurement an electronic envelope detector can be employed to enhance the resolution that can be achieved.

Another difficulty which may arise in the use of this technique is when multiple reflections of similar intensities are involved in the system, which may cause some problems in the determination of the central and the order of the side fringe packet, and reduce the system operating range. However, if the uncontrolled or unintentional reflection is weak, the measurement results would not be seriously affected, as long as a careful "initialization" process is ensured, as described previously.

In conclusion, the "proof-of-principle" alternative optical scanning technique shows advantages over the conventional mechanically scanned system by offering the potential of a simple, stable and compact alternative to white light interferometric system operation and when compared with the electronic scanning method, a large operating range can be easily realized. Although the industrial use of this technique is subject to the availability of low cost tunable laser sources which are being developed, it represents a promising alternative for some situations, to white light interferometric sensing.

From Chapter 3 to this Chapter, different kinds of light sources and an optical scanning technique have been investigated, in order to enhance the capability of white light interferometry as a tool for high precision measurement and with a potentially compact system configuration. Further efforts are still necessary to employ such a tool for practical applications, and as will be shown in Chapter 7, a white light interferometric sensor is explored for eye length measurement.

References

1. H. C. Lefèvre, "White Light Interferometry in Optical Fiber Sensors", Proceedings of the 7th International Optical Fiber Sensors Conference, pp.345-351, Sydney, Australia, December, 1990

2. A. Koch and R. Ulrich, "Fiber-Optic Displacement Sensor with 0.02μm Resolution by White-Light Interferometry", Sensors and Actuators A, 25-27, pp.201-207, 1991

3. D. Trouchet, B. Laloux and P. Graindorge, "Prototype Industrial Multi-Parameter F. O. Sensor Using White Light Interferometry", Proceedings of the 6th International Optical Fiber Sensors Conference, pp.227-233, Paris, 1989

4. S.Chen, B. T. Meggitt and A. J. Rogers, "Electronically-Scanned White-Light Interferometry with Enhanced Dynamic Range", Electronics Letters, Vol.26, No.20, pp.1663-1665, 27th September, 1990

5. W. J. Bock and W. Urbanczyk, "Electronically Scanned White-Light Interferometric Sensor for High Hydrostatic Pressure Measurements", Proceedings of the 9th International Optical Fiber Sensors Conference, pp.135-138, Firenze, Italy, May 4-6, 1993

6. M. G. Xu, M. Johnson, M. Farhadiroushan and J. P. Dakin, "Novel Polarimetric Fibre Device for Interrogating 'White-Light' Interferometers", Electronics Letters, Vol.29, No.4, pp.378-379, 18th February 1993

7. E. Kolltveit and K Bløtekjær, "Acoustically Scanned Delay for White-Light Interferometry", Proceedings of the 8th International Optical Fiber Sensors Conference, pp.189-192, Montery, USA., January 29-31, 1992

8. M. Lequime, C. Lecot, H. Giovannini and S. J. Huard, "A Dual-wavelength Passive Homodyne Detection Unit for Fiber-coupled White Light Interferometers", Proceedings of SPIE., Vol.1267, pp.288-297, 1990

9. C. Polhemus, "Two Wavelength Interferometry", Applied Optics, Vol.12, No.9, pp.2071-20774, September 1973

10. A. D. Kersey and A. D. Dandridge, "Dual-Wavelength Approach to Interferometric Sensing", proceedings of SPIE., Vol.798, pp.176-181, 1987

11. D. N. Wang, Y. N. Ning, K. T. V. Grattan, A. W. Palmer and K. Weir, "The Optimized Wavelength Combinations of Two Broadband Sources for White Light Interferometry", IEEE/OSA Journal of Lightwave Technology, Vol.12, No.5, pp.909-916, May 1994

12. H. Kikuta, K. Iwata, and R. Nagata, "Distance Measurement by the Wavelength Shift of Laser Diode Light", Applied Optics, Vol.25, No.177, pp.2976-2980, 1 September 1986

13. E. Gelmini, U. Minoni and F. Docchio, "Tunable, Double-Wavelength Heterodyne Detection Interferometer for Absolute-Distance Measurements", Optics Letters, Vol.19, No.3, pp.213-215, February 1, 1994

14. D. N. Wang, Y. N. Ning, K. T. V. Grattan, A. W. Palmer and K. Weir, "An Optical Scanning Technique in a White Light Interferometric System", IEEE Photonics Technology Letters, Vol.6, No.7, pp.855-857, July 1994

15. D. N. Wang, Y. N. Ning, K. T. V. Grattan, A. W. Palmer and K. Weir, "Scanning in a White Light Interferometer Using a Tunable Laser", Proceedings of the 10th International Optical Fiber Sensors Conference, pp.592-595, Glasgow, U.K., October 1994

Chapter 7

A White Light Interferometric Sensor

for Eye Length Measurement

An exciting application of white light interferometry is in eye length measurement, a subject important to optometrists in diagnosis and treatment and for which present ultrasonic method have limitations. This Chapter presents a white light interferometric sensor for such an application, which utilizes two Michelson interferometers, each of which locates one of the surfaces of the eye, the cornea and the retina respectively. A simultaneously determination of the two surface positions of the eye will give the value of eye length. The results obtained were carried out on a simulated eye due to the University's policy of not permitting experimentation on human or animal subjects, and show that the proposed system is simple, easy to align, suitable for measuring different kinds of eyes, tolerant to transverse eye movement and worth further exploration.

7.1 Introduction

It has become clear from the previous discussions that white light interferometry is a powerful tool in performing unambiguous, high precision and absolute measurement, and as an optical technique, the measurement can also be implemented in a non-contact and non-invasive manner. Consequently, the white light interferometric method has been used in the investigation of biological systems, such as the tissue thickness [1-2]

and eye structures [3-7]. One of the major developments in this aspect is the axial eye length measurement [8-16].

In this Chapter, the use of optical techniques for eye length measurement is reviewed, a simple white light interferometric sensor for such an application is investigated, the operating principle of the system is explained, the preliminary experiments carried out on a simulated eye are presented and finally, the main characteristics of the proposed sensor system are discussed.

7.2 The Human Eye

The human eye can be considered as an optical system which forms a real image of an object on its back surface.
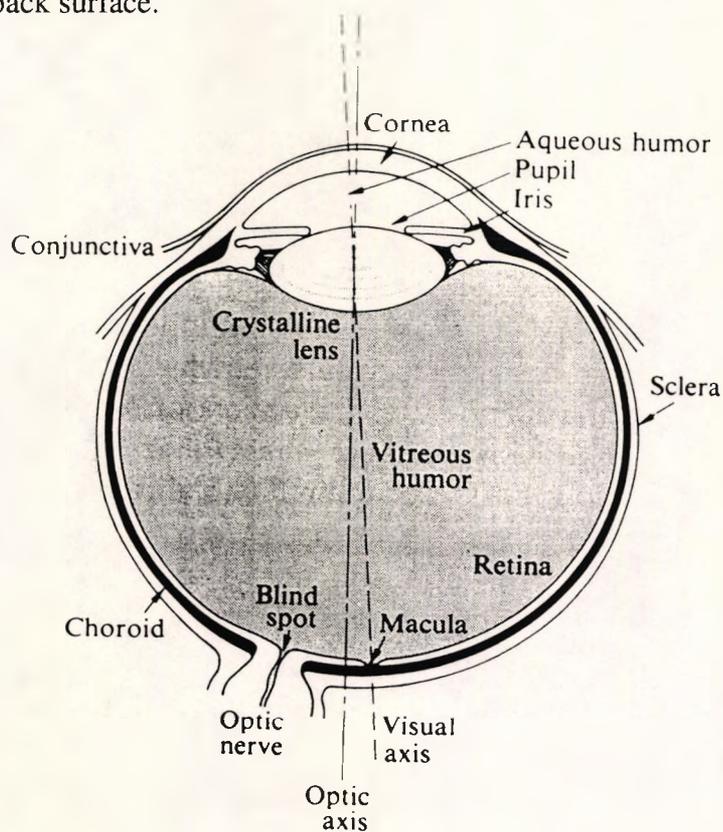
Fig.7.1 The Human Eye [17]

A sketch of the structure of the human eye is shown in Fig.7.1 [17], where the **sclera** is a tough shell and the **cornea**, i.e. the front surface of the eye, is the transparent part of the sclera. The cornea plays the main role as the focusing element; behind the cornea, the **crystalline lens** provides the fine control of the focal length by changing its shape. The **iris**, as the aperture stop of the eye, can regulate the size of the pupil and hence determine the light flux. The **retina** is essentially an array of light-sensitive cells at the back surface of the eye, connected with the brain via a complex nerve cell network.

The two most important parts of the eye are the cornea, and the retina: the cornea can focus an image on the retina and the retina can record the image. The distance between the cornea and the retina is defined as the **axial eye length**.

7.3 Optical Techniques for Eye Length Measurement

Intraocular distances such as cornea thickness and axial eye length are important parameters in ophthalmic investigations. An accurate knowledge of eye length is essential for the determination of the refractive power of an implanted intraocular lens after cataract surgery [18]. A number of eye length measurement methods have been explored previously [8-16]. In order to prevent the possible harmful effects on the human eye and in an attempt to reduce the unacceptable error level, the method of radiography is no longer used. The standard eye length measurement method at present is the ultrasonic echo-impulse technique [8-9] [18]. In this technique, a quick and easy means of measurement can be realized: however, the drawbacks are also severe. The ultrasonic measurement process requires a direct mechanical contact between the eye and the transducer; usually anaesthesia is needed or, alternatively, the eye has to be immersed in saline in order to facilitate the acoustic wave transmission. In neither case will the patient feel comfortable, and extra hygienic measures have to be taken. In addition, this technique has only a limited transverse resolution [8-9] and the

compression on the cornea by the direct contact of the transducer may also cause eye length reading errors. Consequently, the overall measurement accuracy can rarely be better than 100μm [8].

Recently, optical techniques have emerged as the strongest candidate to replace the ultrasonic detection method and to provide a non-contact, non-invasive and high accuracy intraocular distance measurement. Obviously, this technique is more comfortable for the patient involved as no anaesthesia is needed and hence it is in principle simpler to implement.
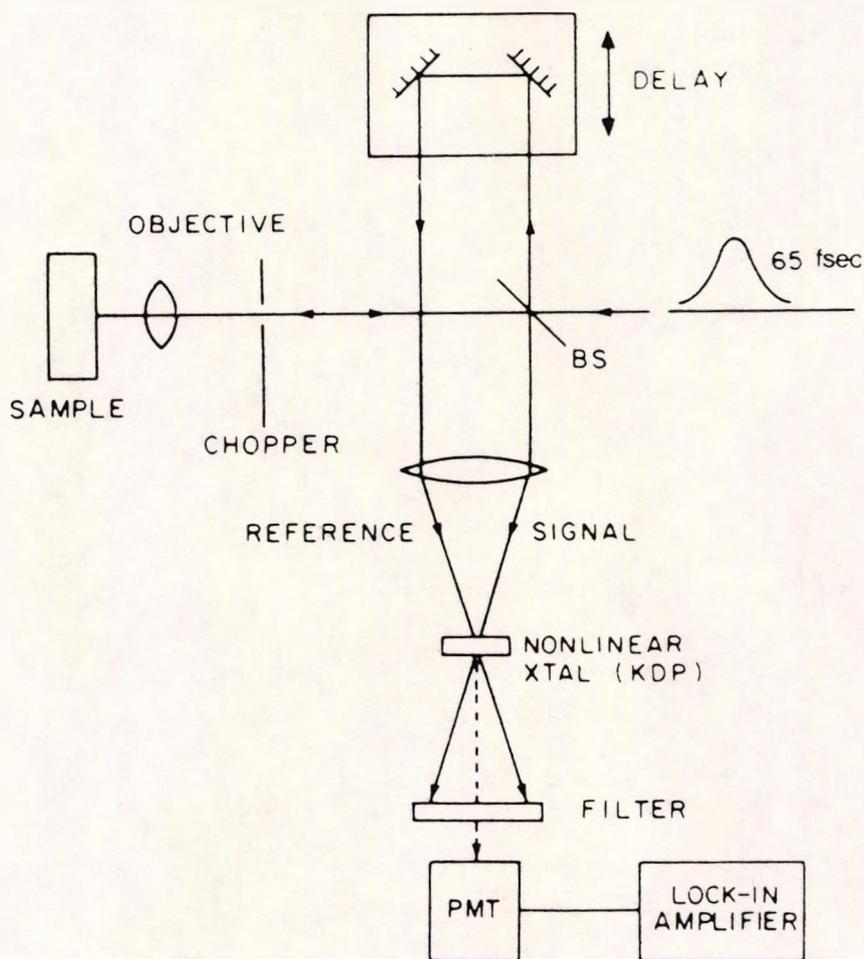
BS: Beam Splitter; PMT: Photomultiplier Tube; XTAL: Nonlinear Crystal

Fig.7.2 Schematic of Femtosecond Optical Ranging Experiment,

after Fujimoto *et al* [19]

152

Fujimoto *et al* [19] have used femtosecond optical ranging technique to measure the corneal thickness of anesthesized rabbit eyes *in vivo*. In this technique, as shown in Fig.7.2, the femtosecond pulse train generated by a dye laser is divided by a beam splitter into two, one travels along the signal path and the other is fed into the reference path which is controlled by a stepping motor mechanical stage to introduce an optical delay. The signal and reference pulse trains are then focused by a lens into an angle-phase-matched KDP crystal, to generated a second harmonic signal whose intensity is proportional to the intensity product of the signal beam and the reference beam. A high resolution (15μm) can be achieved by the use of this technique, but the laser source and the signal processing employed in the system are large, complex and expensive, rendering this non-viable for most measurement situations.

In contrast, optical coherence domain reflectometry (OCDR) uses a continuous wave light source for optical ranging without the need for an ultrashort pulse laser source [20]. In an OCDR system, the output beam from a low coherence light source is split into two paths, one of which is taken as the reference and the other is incident on and reflected by the sample surface, both beams being then recombined and collected by a photodetector. Because of the low coherence property of the light source, the interference fringes can be observed only when the OPD between the two beams is less than the coherence length of the light source, and the fringe will disappear if the OPD exceeds the coherence length. Therefore, the distance information can be determined from the relative position between which the interference fringes exist, by scanning the reference arm of the interferometer.

The OCDR technique has been used for a number of intraocular distance measurements and eye structure investigations in the past few years [3-5] [7]. A reported system for measuring cornea thickness etc. is shown schematically in Fig.7.3 from the work of Huang *et al* [3], where the low coherence light source is a superluminescent diode, a He-Ne laser is used as a visible light source to facilitate the system alignment and a reference mirror is mounted on a computer-controlled stepping motor translation stage with a 0.1μm resolution. In the measurement, the probe light

beam is focused on the corneal surface, and reflections are produced at the air-cornea boundary and the cornea-aqueous boundary. When the reference mirror is scanned step-by-step so that its position can match that of the corresponding boundaries, the interference signal can be observed and hence the distance between the boundaries can be determined.
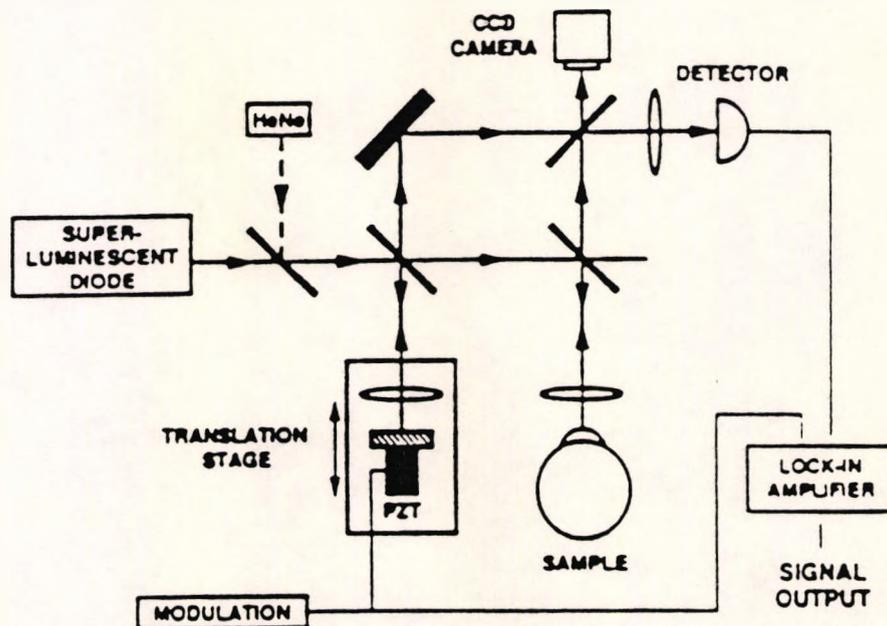
Fig.7.3 Schematic of Optical Coherence Domain Reflectometer

Setup for Ranging Experiments, after Huang *et al* [17]

The OCDR technique also offers superior resolution (longitudinal and transverse) which is limited only by the coherence length of the light source and high detection sensitivity. Furthermore, it employs only the simple, compact and economic light sources now available such as LEDs and multimode laser diodes. For this reason and the associated absence of complexity, it is more attractive than femtosecond technique.

It can be seen from the above description that an OCDR system is essentially a simple white light interferometric system where only one interferometer is employed, and in such a system, different sample surface positions can be located separately. Since, a simultaneous determination of the two surface positions is required in order to realize the eye length measurement, a dual interferometer white light interferometric

system has been used. In some of these systems, the eye itself may play the role as an interferometer [8-10] [13-14].

Fercher *et al* [8] were the first to use white light interferometric technique for measuring the axial length of the human eye *in vivo,* and the corresponding system is shown in Fig.7.4. In the measurement process, a He-Ne laser is firstly used to align the patient's eye and interferometer, and if the eye is in the correct position, the interference fringe pattern of a ring structure can be observed through an infrared scope, the output of which is demonstrated in Fig.7.5. Subsequently, the light beam from a multimode laser diode passes through a Fabry-Perot interferometer to illuminate the patient's eye. If the OPD produced by the two beams reflected by the cornea and the retina respectively is compensated by the optical interval of the Fabry-Perot interferometer, the interference fringe pattern can be seen. The optical eye length can then be determined as the distance between the two plates of the Fabry-Perot interferometer. An accuracy of 30μm has been achieved by using this approach: however, the experimental procedure is tedious as one of the plates of the Febry-Perot interferometer has to be moved step by step, with a careful examination at each step to ensure if the interference fringe pattern occurs. The whole measurement process takes a long time and thus is not convenient for the patient. In addition, the operator is also required to be particularly skilful and this may reduce the popularity of this technique for more general use.
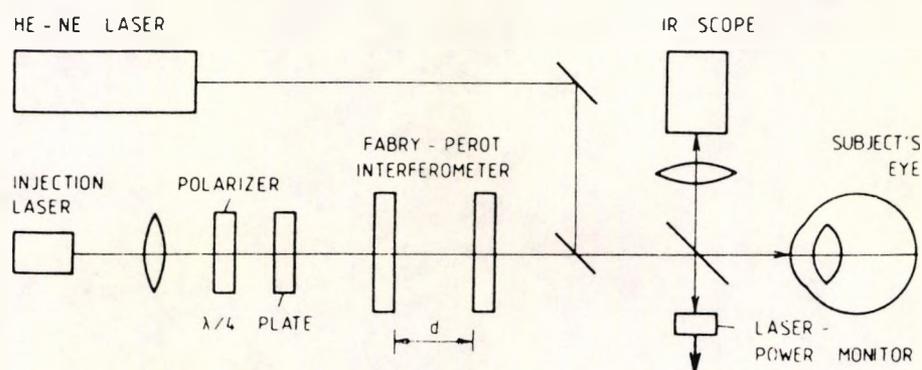
Fig.7.4 Optics of the Interferometer Used to Measure the Length of the Optic

Axis of the Human Eye *In Vivo*, after Fercher *et al* [8]

Fig.7.5 Interference Phenomenon Used to Match the Fabry-Perot Plate Distance

with the Optical Length of the Eye, after Fercher *et al* [8]

An improved version of the above approach as shown in Fig.7.6 was used by Hitzenberger to determine the axial length of the human eye *in vivo* [9]. Instead of observing the static interference fringe patterns, a phase modulated signal is created by scanning one of the plates of Febry-Perot interferometer with a constant speed, and if the OPD produced by the interferometer can match that generated by the reflected beams of the cornea and the retina, the interference fringes can be observed. In this system, two additional lasers are included to facilitate the alignment. A He-Ne laser is first used for the coarse alignment of the patient's eye, then a single mode laser diode of long coherence length is operated in order to find the centre of the interference pattern

in the infrared scope and finally, a multimode laser diode of short coherence length is switched on to perform the practical measurement.
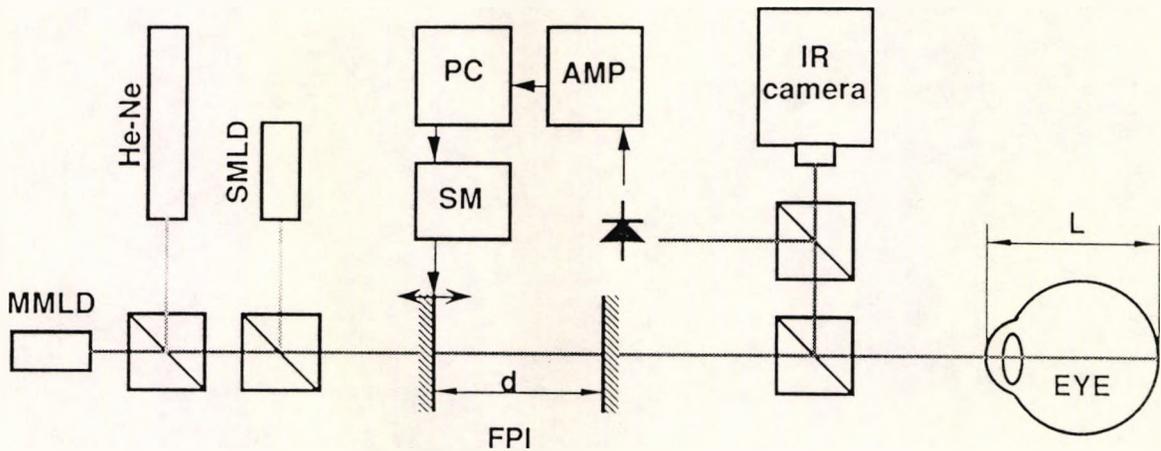
SMLD: Single Mode Laser Diode;   MMLD: Multimode Laser Diode;

BSC: Beam Splitter Cube: FPI: Fabry-Perot Interferometer;

PD: Photodetector;   AMP: Amplifier;   PC: Personal Computer;

SM: Stepper Motor;   IR: IR-Scope

Fig.7.6 Block Diagram of the Laser Doppler Interferometer for Measuring
the Axial Length of the Eye, after Hitzenberger [9]

The system has the distinct advantage of being insensitive to longitudinal eye movement. However, as it can be seen from Fig.7.6, the whole system is relatively complicated as three lasers have to be used and many components are involved, which makes the alignment become so critical that any slight transverse deviation caused by the patient's eyeball movement may seriously influence the measurement results.

Another eye length measurement system using a conventional long coherence length light source and a wavelength tuning method was reported by Sekine *et al* [15]. In this system, the eye length can be obtained from the measurement of the corresponding phase shift in the interference fringe pattern, where the phase shift is induced by the wavelength shift of the light source. Fig.7.7 shows the schematic of the system.
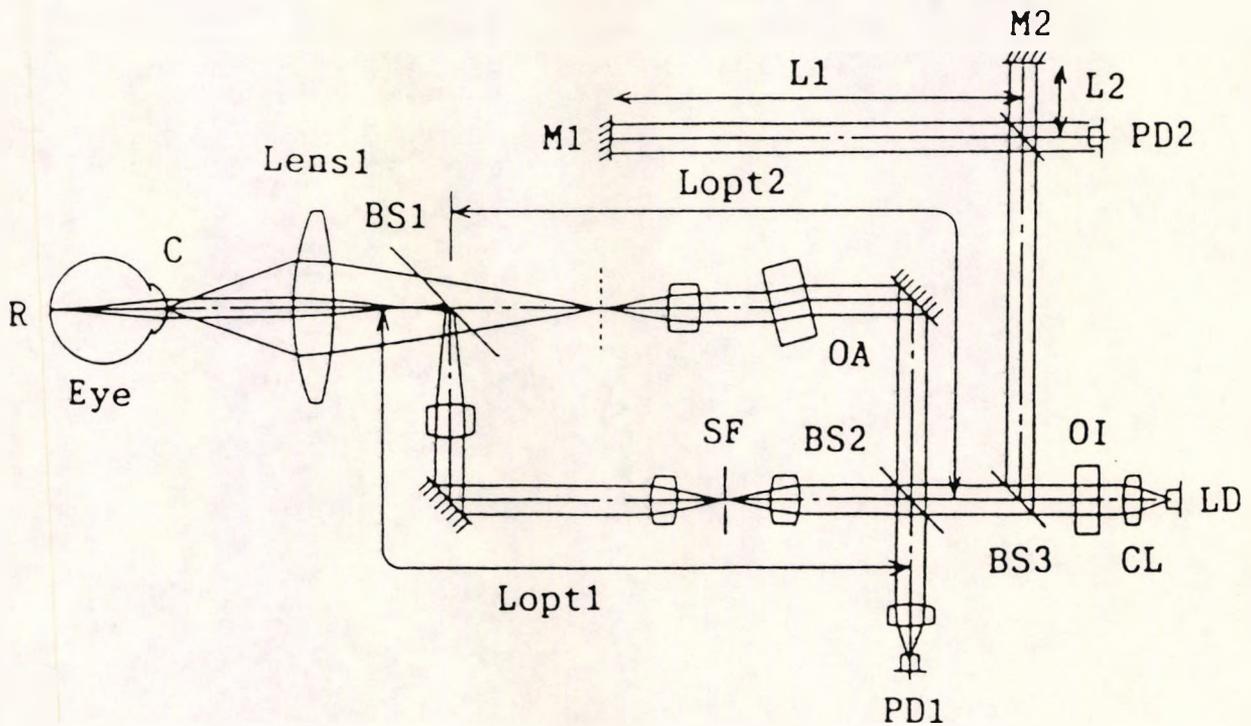
BS: Beam Splitter; C: Cornea; CL: Colimator Lens; OA: Optical Path Compensator;

OI: Optical Isolator; R: Retina; SF: Spatial Filter

Fig.7.7 Scheme of the Principal Interferometric System for

Axial Eye-Length Measurement, after Sekine *et al* [15]

The light beam from a long coherence length single mode laser diode is divided by a beam splitter into two and launched into a measuring interferometer and a reference interferometer respectively. The beam that enters the measuring interferometer is split again, where the two beams obtained travel along the different paths and are focused on

the cornea and the retina respectively. The reflected beams from the cornea and the retina interfere with each other and are received by a photodetector. The beam that enters the reference interferometer is also split into two and reflected by two mirrors respectively, and the interference signals can be obtained and determined by another photodetector.

The wavelength change in the laser diode will cause a phase difference change or the OPD change in the two interferometers, which then can be calculated by means of fringe number counting. The eye length can then be obtained from the ratio of OPD changes in the two interferometers and the OPD value in the reference interferometer.

This system is reported to be capable of performing eye length measurement at a high speed (about 10 seconds on average) and have a wide measurement range (16-32mm), but the actual experimental system (Fig.2 in reference [15]) is even more complicated than the one used in the work of Heizenberger [9], the measurement accuracy is low (~ 110μm) and the signal-to-noise ratio is also relatively poor.

One of the common characteristics of the eye length measurement systems described above lies in their relative complexity, and a difficulty also arises from the fact that the interference is generated by the two reflected beams from the cornea and the retina respectively. Since the beam reflected from the cornea has a divergent wavefront and the optical power becomes weak when arriving at the photodetector, and the retina is only a partially reflecting surface so that the reflected beam is also weak and mixed with scattering light, the interference fringe pattern thus obtained has a considerable distortion when compared with the ideal ring shape. Consequently, the system has to be carefully aligned to make sure that the photodetector is situated at the centre of the fringe pattern, as the centre of the ring shape is so small as shown in Fig.7.5 [8] that the alignment becomes critical and is sensitive even to a slightly transverse movement of the patient's eyeball. In addition, the signal-to-noise ratio is also poor because of the distortion in the interference pattern.

In the next Section, results obtained from a white light interferometric sensor developed to address the above difficulties are reported. This sensor system is simple,

easy to align and can achieve a good signal-to-noise ratio as well as a wide measurement range [11].

7.4 Operating Principles of the Proposed White Light Interferometric Sensor for Axial Eye Length Measurement

The principle of the proposed eye length measurement system utilizes two Michelson interferometers to locate the position of cornea and retina simultaneously and hence determine the eye length. The schematic experimental arrangement used in this investigation is shown in Fig.7.8.

A multimode laser diode of central wavelength 670nm is used as the light source which is operated below the threshold in order to provide a short coherence length ($L_c = 20\mu m$) as well as a low output power to meet the laser safety requirement.

Two reference mirrors, M1 and M2, are mounted on the two translation stages respectively to provide a linear scan of the OPD. They are also driven by two loudspeakers to generate the phase modulated signals in the photodetectors. The two photodetectors are both connected to different channels of an oscilloscope in order to be able to observe the two interference patterns simultaneously.

The output beam coming from the multimode laser diode is first split into two beams. One is reflected by the reference mirror M1 and received by the photodetector PD1, while the other is again divided by the beam splitter BS2 into two, and one travels along the reference path, is reflected by M2 and collected by PD2. The other is reflected by the cornea and the retina separately and then received by PD1 and PD2 respectively, through the corresponding beam splitters BS2 and BS1, respectively.
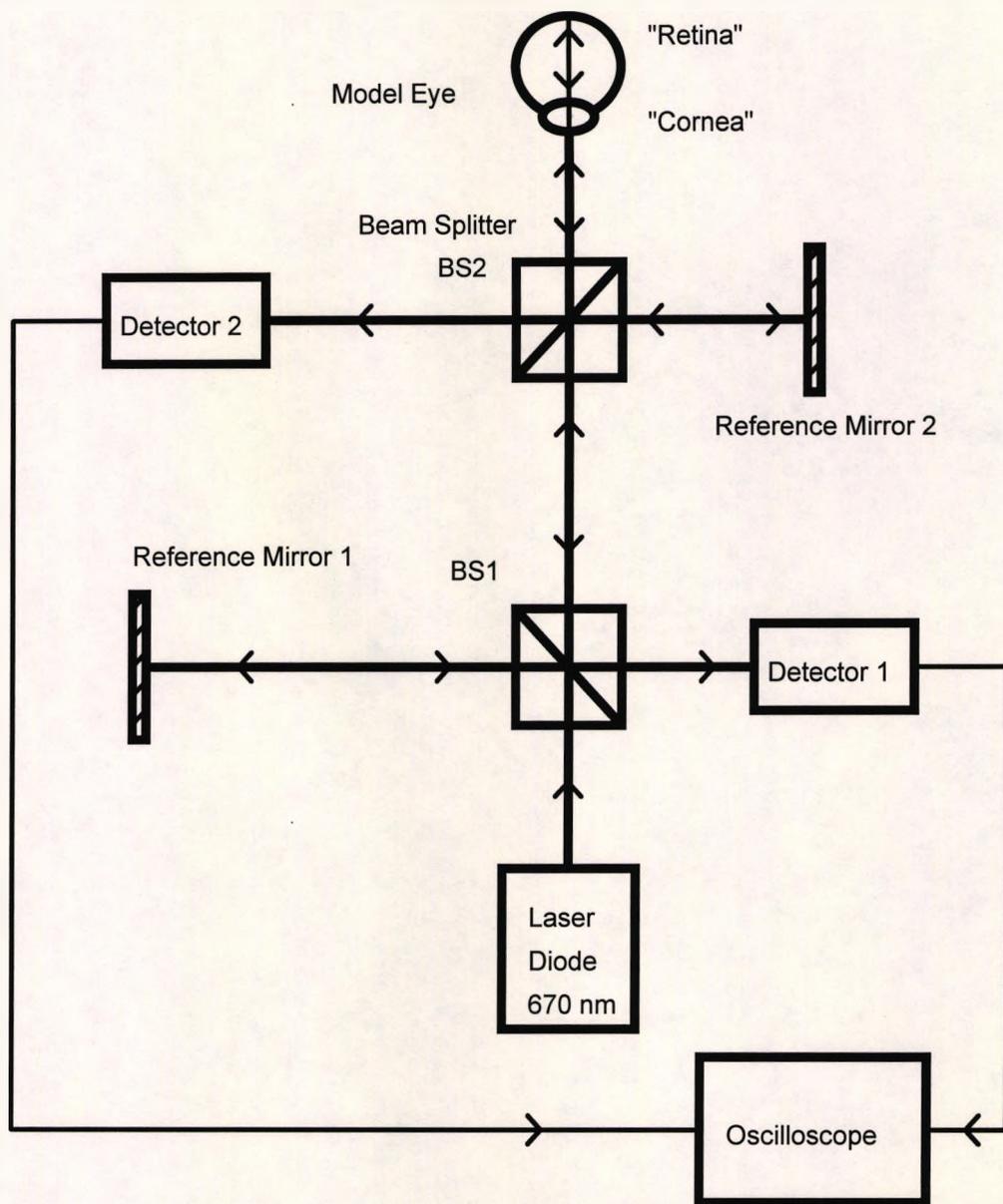
Fig.7.8 Schematic of two Michelson Interferometer System

In the operation of the system, the reference mirror M1 is used to locate the cornea

position and, by scanning the reference mirror M2, the position of the retina can also be

determined. When the interference fringes corresponding to the two positions are observed on the oscilloscope simultaneously, the eye length value can then be obtained.

In the determination of the eye length value, a correspondence between the position calibration of the two reference mirrors has to be established in advance. This can be achieved, for instance, by using a mirror in front of the system before the eye length measurement, when the interference fringes appear simultaneously, and the two reference mirrors are considered to be in the same position. As both mirrors can be controlled to follow the longitudinal movement of the eye, the system is also suitable for a practical *in vivo* measurement.

Unlike the commonly-used remote sensing white light interferometric system in which the two interferometers are connected in tandem, and the OPD generated in the sensing interferometer can be compensated by that of the receiving interferometer thus realizing the measurement, the two interferometers in the system used for this investigation are mutually "independent", as each locates a certain surface of the eye. Only a simultaneous determination of the locations of the two surfaces of the eye, the cornea and the retina respectively, can give an eye length value. The main reason for this system design is to provide an ideal, undistorted reference beam to interfere with the light beams reflected from one of the surfaces of the eye, which are usually weak and exhibit a distorted wavefront.

The system investigated has several distinct advantages over the system described previously. First, a small and visible laser diode is now used as the only source for both alignment and measurement purposes so that the system is greatly simplified in terms of configuration as well as measurement procedure. Secondly, the reflected beam from the cornea or the retina can now interfere with an ideal light beam which is reflected from a mirror, and as a result, the signal-to-noise ratio can be improved and the alignment also becomes easier. In addition, since the position of the cornea and that of the retina can be determined separately by different interferometers in the system, a wide measurement range and a good flexibility for measuring different kinds of eyes, such as those which are short sighted or far sighted can be readily achieved.

162

7.5 Experimental Results of Eye Length Measurement
on a Simulated Eye

7.5.1 The Simulated Eye
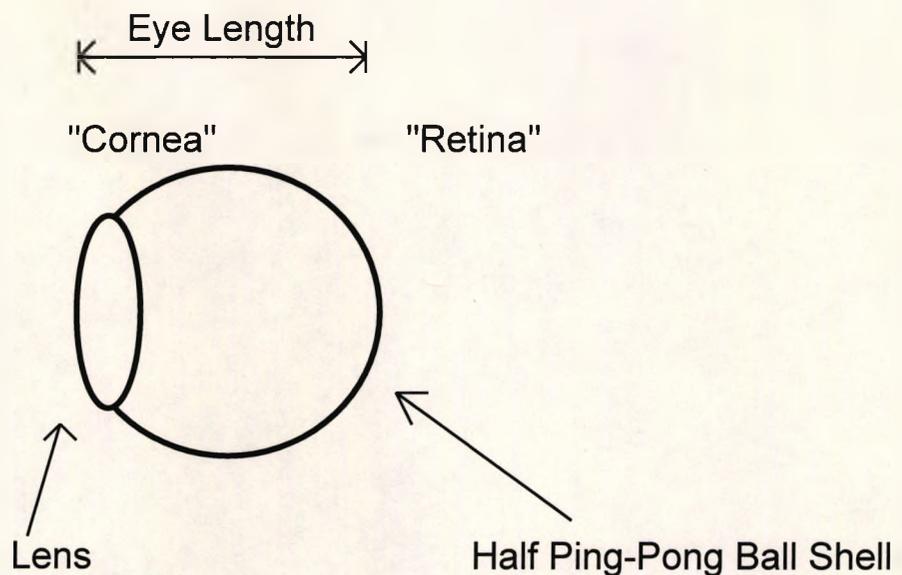
Fig.7.9 Simulated Eye

In order to evaluate the system safely before considering introducing the technique to an *in vivo* measurement, some investigatory experiments were carried out on a simulated eye which consists of a biconvex lens and a half ping-pong ball shell. Although simple, such a model represents the main optical surfaces of the eye. As shown in Fig.7.9, the front surface of the lens plays the role as the "cornea" and the inner surface of the half ping-pong ball shell represents the "retina". The distance between the "cornea" and the "retina" is adjustable, so that different kinds of eye can be simulated and investigated. Since the focal length of this lens is about 36.5mm, any eye

of axial eye length close to this value may be considered as the "normal eye". If, however, the eye length is larger or smaller than the focal length, there is a simulation of "myopia" or "hyperopia".

From Fig.7.9, the simulated eye length, d_m, can be calculated by mechanical measurement, as

$$d_m = d + (n - 1) t - t' \qquad (7.5.1)$$

where d is the distance between the front surface of the lens and the outer surface of the ping-pong ball shell, n is the refractive index of the lens and t and t' are the thicknesses of the lens and the ping-pong ball shell respectively. The corresponding values for n, t and t' were 1.51, 3.16mm and 0.5mm respectively.

7.5.2 Experimental Results of Eye Length Measurement on a Simulated Eye

A series of measurements has been carried out, both mechanically and optically, on a simulated eye, the results are shown in Table 7.1. The accuracy of the mechanical measurement is about ±0.03mm. For the eye length value, d_0, obtained by the optical measurement, the accuracy is limited by the coherence length of the light source employed in the experiment, and in this case, the multimode laser diode has a coherence length of about 20μm. Hence the optical measurement accuracy is ±0.02mm in this work.

In order to test the adaptability of this technique for different kinds of eyes, the position of the "retina" was varied by more than 10% from the normal focal point, representing extreme cases of short and far sightness and distinct interference fringes were still clearly observed at these extremes.

A typical interference fringe pattern obtained in a simulated eye is shown in Fig.7.10, corresponding to the situation of the normal eye, i.e. the eye length is 37.54 ± 0.02mm, corresponding to the focal length value. In Fig.7.10, the upper trace fringe pattern is obtained by the reflected beams from the cornea, and the lower trace corresponds to the retina. Since the light beam reflected from the cornea exhibits a diverging wavefront and

the optical power detected is relatively weak, the corresponding fringe intensity is usually lower than that obtained from the retina.

Table 7.1 Eye Length Measurement Results

Measurement	d	d_m (mm)	d_0 (mm)	$d_m - d_0$ (mm)
1	29.34 ± 0.03	30.45 ± 0.03	30.32 ± 0.02	0.13
2	31.84 ± 0.03	32.95 ± 0.03	32.9 ± 0.02	0.05
3	36.46 ± 0.03	37.57 ± 0.03	37.54 ± 0.02	0.03
4	39.06 ± 0.03	40.17 ± 0.03	40.15 ± 0.02	0.02
5	45.04 ± 0.03	46.15 ± 0.03	46.41 ± 0.02	- 0.26
6	49.24 ± 0.03	50.35 ± 0.03	50.33 ± 0.02	0.02

It was found from the results shown in Table 7.1 that the system is capable of measuring different kinds of subjects without seriously affecting the measurement accuracy. Another encouraging point is that the system possesses a certain degree of transverse movement tolerance, where the fringe can still be observed for a transverse movement of up to 0.5mm. For instance, when a transverse displacement of 0.2mm was introduced, the fringe pattern is shown in Fig.7.11 (the scale is the same as that in Fig.7.10) from which may be seen that the fringe pattern corresponding to the cornea is still similar to that in Fig.7.10: however, a significant intensity reduction can be observed from the fringe pattern generated by the retina, as the reflecting point at the retina is deviated from the focal point.

"Cornea"
(Channel 1)
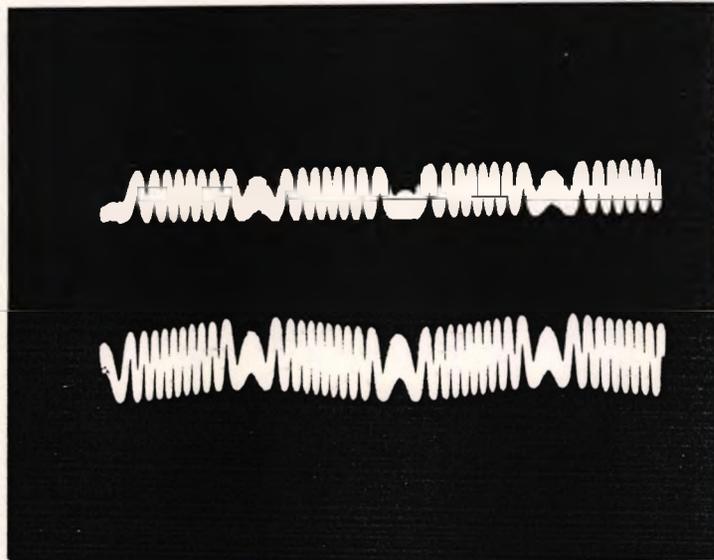
"Retina"
(Channel 2)

Fig.7.10 Fringe Patterns of a Simulated Eye

"Cornea"
(Channel 1)
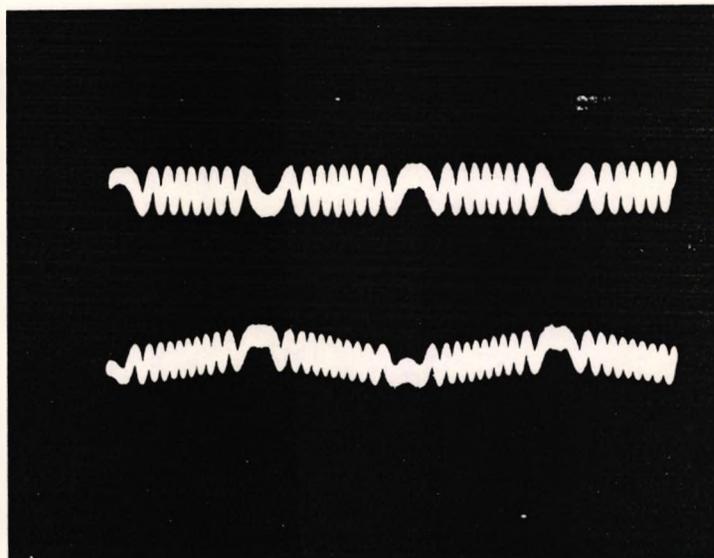
"Retina"
(Channel 2)

Fig.7.11 Fringe Patterns of a Simulated Eye with a Transverse Movement of 0.2mm

In order to further investigate the adaptability of this technique for measuring different kinds of eyes, another set of experiments was carried out, in which a number of auxiliary lenses were inserted between the main biconvex lens and the imaging screen (half ping-pong ball shell). The main lens used in this case was 26D, where D is the unit of diopter, m^{-1}, and the diopter is the reciprocal of the focal length, and the auxiliary lenses applied in turn were -1D, +1D and +6D, to simulate different kinds of eyes. The position of retina corresponds the refractive error in each case. The equation (7.5.1) now becomes

$$d_m = d + (n - 1) t + (n_a - 1)t_a - t' \qquad (7.5.2)$$

where n_a and t_a are the refractive index and the thickness of the auxiliary lens respectively. In this set of experiments, the corresponding values used were: n = 1.527, n_a = 1.52, t_a = 1.208, 2.293 and 4.08 respectively and t' = 0.344. The measurement results are demonstrated in Table 7.2.

Table 7.2 Eye Length Measurement Results with a Auxiliary Lens

Eye Type	Main Lens (D)	Auxiliary Lens (D)	Refractive Error (D)	d (mm)	d_m (mm)	d_0 (mm)	d_m - d_0 (mm)
A	26	0	0	39.00 ± 0.03	40.34 ± 0.03	40.34 ± 0.02	0
B	26	+1	-1	39.00 ± 0.03	41.53 ± 0.03	41.56 ± 0.02	- 0.03
C	26	-1	+1	39.00 ± 0.03	40.97 ± 0.03	40.99 ± 0.02	- 0.02
D	26	+6	0	34.0 ± 0.03	37.47 ± 0.03	37.49 ± 0.02	- 0.02

It has been further confirmed from these results that the proposed sensor system is suitable for various eye length measurement, and the results obtained from both the mechanical and optical means can be accurately matched.

7.5.3 Laser Safety Consideration

Laser safety is one of the major concerns in the eye length measurement. According to the American National Standard [21], for an intra beam viewing, a maximum power of $77\mu W$ is permitted to illuminate the eye for 25 minutes by a laser source of wavelength 670nm. In the above experiments, the probing power arriving at the simulated eye was only $15\mu W$ at maximum and the whole measuring process took about 1 minute at maximum, and thus this level is well below the safety limit.

7.6 Discussion

As a non-contact and high precision technique, white light interferometry provides a more comfortable and suitable means for axial eye length measurement when compared with the use of the ultrasonic method. The proposed white light interferometric sensor system utilizes two Michelson interferometers, each of which locates one of the surfaces of the eye and both can work together to determine simultaneously the positions of the front and the back surfaces of the eye and hence the eye length value. The advantages of this system include simple arrangement, ease of alignment, wide measurement range, various subject suitability, a tolerance to transverse eye movement and, as the result of utilizing an undistorted reference light beam to interfere with the reflected beam from the surfaces of the eye, the signal-to-noise ratio can be improved when compared with that obtained by interfering two light beams reflected from different surfaces of the eye respectively.

However, since the simultaneous measurement from the cornea and the retina are required, a reference mirror control mechanism has to be built to ensure that automatic tracking of the longitudinal movement of the eye may be achieved, before the system can be developed into a compact, hand-set device to implement *in vivo* eye length measurement.

Unfortunately, due to the strict regulations preventing animal tests at City University, the investigation could not reach the *in vivo* measurement stage. However, the system described has shown the potential for the non-contact, non-invasive and accurate eye length measurement and is worth further exploration in the future.

Thus far in the work, a systematic investigation of a white light interferometric sensor system has been carried out, in which different kinds of low coherence light sources and an alternative scanning mechanism for white light interferometry have been developed, followed by an exploration of a simple sensor system for eye length measurement applications. It is now necessary to summarize the main results and to suggest future research work in order to continue further to improve the performance of the white light interferometric sensor system.

References

1. X. Clivaz, F. Marquis-Weible, R. P. Salathé. R. P. Novàk and H. H. Gilgen, "High-Resolution Reflectometry in Biological Tissues", Optics Letters, Vol.17, No.1, pp.4-6, January 1, 1992

2. M. R. Hee, J. A. Izatt, J. M. Jacoson, J. G. Fujimoto and E. A. Swanson, "Femtosecond Transillumination Optical Coherence Tomograph", Optics Letters, Vol.18, No.12, pp.950-952, 1993

3. D. Huang, J. Wang, C. P. Lin, C. A. Puliafito and J. G. Fujimoto, "Micron-Resolution Range of Cornea Anterior Chamber by Optical Reflectometry", Laser in Surgery and Medicine, Vol.11, pp.419-425, 1991

4. D. Huang, E. A. Swanson, C. P. Lin, J. S. Schuman, W. G. Stinson, W. Chang, M. R. Hee, T. Flotte, K. Gregory, C. A. Puliafito and J. G. Fujimoto, "Optical Coherence Tomography", Science, Vol.254, pp.1178-1181, 22 November 1991

5. E. A. Swanson, D. Huang, M. R. Hee, J. G. Fujimoto, C. P. Lin and C. A. Puliafito, "High-Speed Optical Coherence Domain Reflectometry", Optics Letters, Vol.17, No.2, pp.151-153, January 15, 1992

6. C. K. Hitzenberger, "Measurement of Cornea Thickness by Low-Coherence Interferometry", Applied Optics, Vol.31, No.31, pp.6637-6642, 1 November 1992

7. E. A. Swanson, J. A. Izatt, M. R. Hee, D. Huang, C. P. Lin, J. S. Schuman, C. A. Puliafito and J. G. Fujimoto, "*In Vivo* Retinal Imaging by Optical Coherence Tomography", Optics Letters, Vol.18, No.21, pp.1864-1866, November 1, 1993

8. A. F. Fercher, K. Mengedoht and W. Werner, "Eye-Length Measurement by Interferometry with Partially Coherent Light", Optics Letters, Vol.13, No.3, pp.186-188, March 1988

9. C. K. Hitzenberger, "Optical Measurement of the Axial Eye Length by Laser Doppler Interferometry", Investigative Ophthalmology & Visual Science, Vol.32, No.3, pp.616-624, March 1991

10. A. F. Fercher, C. K. Hizenberger and M. Juchem, "Measurement of Intraocular Optical Distances Using Partially Coherent Laser Light", Journal of Modern Optics, Vol.38, No.7, pp.1327-1333, 1991

11. D. N. Wang, S. Chen, K. T. V.Grattan, A. W. Palmer and G. Dick, "A Simple Optical Sensor with Potential Applications in Eye Length Measurement", Proceedings of the Applied Optics Conference, Pub. IOP, pp.56-58, Leeds, U.K., September 1992

12. D. N. Wang, G. Dick, S. Chen, K. T. V. Grattan and A. W. Palmer, "The Use of Short Coherence Length Laser Light for Eye Length Measurement", Proceedings of the 14th Annual International Conference of the IEEE Engineering in Medicine and Biology Society, pp.340-341, Paris, France, October 1992

13. S. Chen, D. N. Wang, K. T. V. Grattan, A. W. Palmer and G. L. Dick, "An Optical Fibre Sensor for Eye Length Measurement", Proceedings of the 9th International Optical Fiber Sensors Conference, pp.321-324, Firenze, Italy, May 1993

14. S. Chen, D. N. Wang, K. T. V. Grattan, A. W. Palmer and G. L. Dick, "A Compact Optical Device for Eye Length Measurement", IEEE Photonics Technology Letters, Vol.5, No.6, pp.729-731, June 1993

15. A. Sekine, I. Minegishi and H. Koizumi, "Axial Eye-Length Measurement by Wavelength-Shift Interferometry", Journal of Optical Society of America A, Vol.10, No.7, pp.1651-1655, July 1993

16. W. J. O. Boyle, G. L. Dick, K. T. V. Grattan, A. W. Palmer, D. N. Wang and K. Weir, "Optical Instrumentation for Eye Length Measurement Using a Short Coherence Length Laser-Based Interferometer Approach", Review of Scientific Instruments, Vol.64, No.11, pp.3082-3087, November 1993

17. E. Hecht and A. Zajac, "Optics", Second Edition, p.178, Addison-Wesley, Publishing Company, 1987

18. M. P. Snead, M. P. Rubinstein, S. Hardmanlea and S. M. Haworth, "Calculated Versus A-Scan Result for Axial Length Using Different Types of Ultrasound Probe Tip", Eye, Vol.4, pp.718-722, 1990

19. J. G. Fujimoto, S. De Silvestri, E. P. Ippen, C. A. Puliafito, R. Margolis and A. Oseroff, "Femtosecond Optical Ranging in Biological System", Optics Letters, Vol.11, No.3, pp.150-152, March 1986

20. R. C. Youngquist, S. Carr and D. E. N. Davies, "Optical Coherence-Domain Reflectometry: A New Optical Evaluation Technique", Optics Letters, Vol.12, No.3, pp.158-160, March 1987

21. "American National Standards Institute: Safe Use of Lasers", ANSI Z136.1.New York, American National Standards Institute, 1986

Chapter 8

Conclusions

Optical fibre sensor technology has been a booming research area over the last decade, by offering great advantages such as small size, light weight, compactness, high flexibility, immunity of electromagnetic interference and adaptability to hazardous environments. During that time, various kinds of optical fibre sensors have been explored. Among them, the interferometric type sensors have received much attention because of their high sensitivity and measurement resolution and their large dynamic range. A conventional interferometric optical fibre sensor utilizes monochromatic, long coherence length light sources such as a He-Ne laser, the output interference signals thus possessing only a limited unambiguous range, due to the periodic nature of the interferometer transfer function. As a result, the system operating range is also limited, which actually reduces the possibility of a wide range of applications. As has been shown, by using some techniques, such as dual wavelength interferometry and the wavelength tuning method, the unambiguous range can be greatly extended, but a difficulty remains from the fact that there is no absolute position which can be taken as a reliable reference and useful information may be lost in the case of the system interruption or power failure.

White light interferometry has successfully overcome the above difficulty and provides an unambiguous, high precision and absolute measurement for sensor use which has become the topic of this research work.

The theoretical basis of white light interferometry is on the coherence theory which deals with the interference effect generated by using a non-monochromatic light source,

and from which the relationship between the interference signal intensity and the light source power spectrum can be deduced.

An interferometer can be considered as a spectral filter and its output spectrum is the product of the source spectrum and the interferometer spectral transmission function. A typical remote sensing white light interferometric system consists of two unbalanced interferometers of which the sensing interferometer encodes the measurand into the periodicity of its spectral transmission function and the receiving interferometer decodes the signals by matching the periodicities of the two spectral transmission functions through a scanning mechanism. As a result, white light inteferometry offers the great advantages of unambiguous, high precision and absolute measurement and the results obtained will not be disturbed by the source wavelength drift and power fluctuation and fibre transmission and connection losses.

In white light interferometry, broadband, low coherence light sources have to be used and in this aspect, multimode laser diodes become more and more competitive, because of their large output power, good coupling efficiency into optical fibres, high spatial coherence and reasonable price. However, multimode laser diodes have a relatively large coherence length, which causes a major difficulty in the determination of the central fringe position in the output interference pattern and thus reducing the possibility of white light interferometry to perform a high precision measurement. An efficient way to overcome this difficulty is the use of two multimode laser diodes of different wavelengths as a combination source: however, the method of selecting the appropriate wavelength combinations was not investigated prior to this work.

By the efforts made in Chapter 3, it has been revealed that, with a two wavelength combination source, the interference fringe pattern varies regularly with the wavelength difference between the two laser diodes and for a given laser diode, there exists an optimum wavelength combination, by the use of which the central fringe can much more easily be identified. Hence the appropriate laser diodes can be selected according to the optimum wavelength combination and the corresponding commercial availability, to achieve efficient white light interferometric operation.

As shown in Chapter 4, a further clear improvement in the central fringe identification can be made by the use of a multiwavelength combination source, especially when the wavelengths are optimized, as only one fringe, the central fringe, becomes particularly dominant. With the help of computer simulation, the optimum wavelength combination can be obtained, thus giving a guide to the appropriate laser diode selections. This multiwavelength technique provides a highly efficient central fringe detection and large signal power and hence is very attractive in high precision measurement and coherence multiplexed interferometric sensor system.

The price paid for the two wavelength and multiwavelength combination source is the increased system complexity and alignment difficulty. In Chapter 5, a Sm^{3+}-doped fibre provides a flexible means to produce a two wavelength and multiwavelength combination source with relatively easy alignment. As a fibre fluorescent source, it exhibits an excellent coupling efficiency into optical fibres and shows a significant potential as a promising light source for white light interferometric sensor applications, especially as a laser diode pumped system may be employed, offering a simple system configuration.

In a remote sensing white light interferometric system, the receiving interferometer has to be scanned to recover the physical measurand. The main scanning techniques currently used are the mechanical and electronic, suffering the disadvantages of either a large system configuration and possible mechanical instability, or only a small operating range.

An alternative scanning technique was developed and discussed in Chapter 6, by using a two wavelength combination source, of which one laser source is wavelength tunable, and the OPD generated in the sensing interferometer can be compensated by a corresponding wavelength change imposed in the tunable source, thus realizing an optical scanning mechanism. By the use of this technique, it is possible to eliminate the receiving interferometer, and hence a simple, stable and compact interferometric operation may be achieved, showing advantages over the mechanical scanning system. When compared with the electronic scan, a large operating range can be readily

achieved. This technique is a promising alternative to white light interferometric sensing.

White light interferometry has been applied to a wide range of applications, one of which is the axial eye length measurement. Several systems have been explored in this aspect, and one of their common features is the system complexity. The alignment is also difficult and the signal-to-noise ratio obtained is poor, due to the fact that the two interference light beams, reflected from the cornea and the retina respectively, are either weak or exhibit a distortion. In Chapter 7, a simple white light interferometric sensor is demonstrated within which, two interferometers are in parallel, each to locate one of the eye surfaces, the cornea or the retina respectively, and a simultaneously determination of the two surface positions can make for the eye length measurement. As a result of using an ideal, undistorted beam to interfere with one reflected beam from the eye surface, the signal-to-noise ratio can be improved and the system alignment becomes relatively easy. Although the capability of automatic tracking the longitudinal eye movement remains to be built up before any practical test, this system is competitive in terms of its simple structure, easy alignment, wide measurement range, various subject suitability as well as the tolerance to the transverse eye movement.

In summary, the work shown in this thesis has contributed to the field of white light interferometry in the three aspects: the use of different kinds of white light sources, an optical scanning mechanism and a simple optical sensor for eye length measurement.

As a suggestion, future research work may be pursued in the following aspects:

(1) Since a highly efficient multiwavelength combination source has been developed, where only one fringe, the central fringe, becomes dominant, representing an extremely short equivalent coherence length and good signal-to-noise ratio, an immediate application of this source is the coherence multiplexed interferometric system, the advantage of using such a source is that the number of multiplexing units can be significantly increased and as a result the efficiency of multiplexing will be enhanced.

(2) The Sm^{3+}-doped fibre fluorescent source needs to be further investigated, such as to optimize the laser wavelength, pump power and the fibre length in order to maximize

the output fluorescent power which is important for a practical white light interferometric sensor application. Other rare-earth-doped fibre sources such as Pr^{3+} can also be explored for such a use.

(3) Since the suitability of optical scanning technique to white light interferometry depends on its capability to perform efficiently a practical parameter measurement, a detailed investigation of such a technique should be carried out, to explore the efficient means for fringe packet tracking, signal demodulation and processing, to increase the operating range experimentally.

(4) By the use of a simple white light interferometric sensor system, the eye length measurement has been carried out on a simulated eye with encouraging results. It now becomes necessary to implement *in vivo* eye length measurement in order to examine this system in practice, and the proposed sensor system also needs to be developed into a compact, flexible and easily operated device before any further practical applications can be advanced.

Appendix A

Fringe Intensity Function $I_{10n}(\Delta\lambda)$

As stated in Chapter 3, if the wavelength difference, $\Delta\lambda$, can be divided into a series of sections $[2\lambda_1/n, 2\lambda_1/(n-1)]$, where n is an integer, then the normalized central fringe intensity in the first side fringe packet, $I_{10n}(\Delta\lambda)$, as a function of $\Delta\lambda$, is a monotonic increasing function for the end points: $2\lambda_1/n$, $2\lambda_1/(n-1)$, ... , and within a particular section, i.e. when

$$\Delta\lambda \in [2\lambda_1/n_0, 2\lambda_1/(n_0-1)]$$

where n_0 is a given integer, and $I_{10n}(\Delta\lambda)$ appears as a convex curve. The following is the proof of such a statement.

In the analysis, first, consider the end points of a section $[2\lambda_1/n, 2\lambda_1/(n-1)]$ of $\Delta\lambda$, at the left end, $\Delta\lambda = 2\lambda_1/n$, then from equation (3.2.15) and (3.2.17)

$$\lambda_a = 2\lambda_1[1 - \lambda_1/(2\lambda_1 + \Delta\lambda)]$$

$$= (n + 2)\lambda_1/(n +1) \tag{A.1}$$

$$\lambda_m/\lambda_a = 1 + 2\lambda_1/\Delta\lambda = n + 1 \tag{A.2}$$

from equation (3.2.53)

$$I_{10}(2\lambda_1/n) = \left| I_{ac}[(n + 1)\lambda_a/2] - I_{ac}[(n + 2)\lambda_a/2] \right|$$

$$= \exp\{-[(n + 2)\lambda_1/L_c]^2\} + \exp\{-[(n + 2)^2\lambda_1/(n + 1)L_c]^2\}\cos[\pi/(n + 1)] \tag{A.3}$$

Similarly, at the right end, $\Delta\lambda = 2\lambda_1/(n - 1)$, and

$$\lambda_a = 2\lambda_1[1 - \lambda_1/(2\lambda_1 + \Delta\lambda)]$$

$$= (n + 1)\lambda_1 / n \tag{A.4}$$

$$\lambda_m/\lambda_a = 1 + 2\lambda_1/\Delta\lambda = n \tag{A.5}$$

$$I_{10}[2\lambda_1/(n - 1)] = \left| I_{ac}(n\lambda_a/2) - I_{ac}[(n + 1)\lambda_a/2] \right|$$

$$= \exp\{-[(n + 1)\lambda_1/L_c]^2\} + \exp\{-[(n + 1)^2\lambda_1/nL_c]^2\}\cos(\pi/n) \tag{A.6}$$

Hence

$$I_{10}[2\lambda_1/(n - 1)] - I_{10}(2\lambda_1/n)$$

$$= \exp\{-[(n + 1)\lambda_1/L_c]^2\} + \exp\{-[(n + 1)^2\lambda_1/nL_c]^2\}\cos(\pi/n)$$

$$- \exp\{-[(n + 2)\lambda_1/L_c]^2\} - \exp\{-[(n + 2)^2\lambda_1/(n + 1)L_c]^2\}\cos[\pi/(n + 1)]$$

$$(A.7)$$

When the normalized fringe intensity is considered, then

$$I_{00} = I_{ac}(0) - I_{ac}(\lambda_a)$$

$$= 1 + \exp[-(\lambda_a/L_c)^2] \cos(\pi\lambda_a/\lambda_m) \qquad (A.8)$$

thus

$$I_{00}[2\lambda_1/(n - 1)] = 1 + \exp\{-[(n + 1)\lambda_1/nL_c]^2\}\cos(\pi/n) \qquad (A.9)$$

$$I_{00}(2\lambda_1/n) = 1 + \exp\{-[(n + 2)\lambda_1/(n + 1)L_c]^2\}\cos[\pi/(n + 1)] \qquad (A.10)$$

so that

$$I_{10n}[2\lambda_1/(n - 1)] = \{\exp\{-[(n + 1)\lambda_1/L_c]^2\} +$$

$$\exp\{-[(n + 1)^2\lambda_1/nL_c]^2\}\cos(\pi/n)\}/I_{00}[2\lambda_1/(n - 1)] \qquad (A.11)$$

and

$$I_{10n}(2\lambda_1/n) = \{\exp\{-[(n + 2)\lambda_1/L_c]^2\} +$$

$$\exp\{-[(n + 2)^2\lambda_1/(n + 1)L_c]^2\}\cos[\pi/(n + 1)]\}/I_{00}(2\lambda_1/n) \qquad (A.12)$$

therefore

$$I_{10n}[2\lambda_1/(n - 1)] - I_{10n}(2\lambda_1/n)$$

$$= R\{S + T\cos(\pi/n) + U\cos[\pi/(n + 1)] + V\cos(\pi/n)\cos[\pi/(n + 1)]\} \qquad (A.13)$$

where

$$R = 1/ I_{00}[2\lambda_1/(n - 1)]I_{00}(2\lambda_1/n) \qquad (A.14)$$

$$S = \exp\{-[(n + 1)\lambda_1/L_c]^2\} - \exp\{-[(n + 2)\lambda_1/L_c]^2\} \qquad (A.15)$$

$$T = \exp\{-[(n + 1)^2\lambda_1/nL_c]^2\} - \exp\{-\{[(n + 1)/n]^2 + (n + 2)^2\}(\lambda_1/L_c)^2\} \qquad (A.16)$$

$$U = \exp\{-[(n + 1)^2 + (n + 2)^2/(n + 1)^2](\lambda_1/L_c)^2\} -$$

$$\exp\{-[(n + 2)^4/(n + 1)^2](\lambda_1/L_c)^2\}\cos[\pi/(n + 1)] \qquad (A.17)$$

$$V = \exp\{-\{[(n + 1)^4/n^2 + (n + 2)^2/(n + 1)^2](\lambda_1/L_c)^2\} -$$

$$\exp\{-[(n + 1)^2/n^2 + (n + 2)^4/(n + 1)^2](\lambda_1/L_c)^2\} \qquad (A.18)$$

Obviously, for any $n \geq 2$

$$\cos[\pi/(n + 1)] > \cos(\pi/n) > 0 \qquad (A.19)$$

and

$$S > 0 \tag{A.20}$$

from

$$(n+1)^2/n^2 + (n+2)^4/(n+1)^2 - (n+1)^4/n^2 - (n+2)^2/(n+1)^2$$

$$= 1/[n(n+1)]^2 \, [(n+1)^4 + n^2(n+2)^4 - (n+1)^6 - n^2(n+1)^2]$$

$$= (n+2)(2n^2 + 3n - 1)/n$$

$$> 0 \tag{A.21}$$

thus

$$V > 0 \tag{A.22}$$

Similarly, from

$$(n+2)^4/(n+1)^2 - (n+1)^2 - (n+2)^2/(n+1)^2$$

$$= [1/(n+1)^2][4n^3 + 17n^2 + 24n + 11]$$

$$> 0 \tag{A.23}$$

it has

$$U > 0 \tag{A.24}$$

Therefore

$$I_{10n}[2\lambda_1/(n-1)] - I_{10n}(2\lambda_1/n)$$

$$= R\{S + T\cos(\pi/n) + U\cos[\pi/(n+1)] + V\cos(\pi/n)\cos[\pi/(n+1)]\}$$

$$\geq R\{S + T\cos(\pi/n) + U\cos[\pi/(n+1)]\}$$

$$\geq R\cos(\pi/n)\,(S + T + U) \tag{A.25}$$

Since

$$S + T + U$$

$$= \exp[-(n+1)^2 A] + \exp[-(n+1)^4/n^2 A] + \exp\{-[(n+1)^2 + (n+2)^2/(n+1)^2]A\} -$$

$$\exp[-(n+2)^2 A] - \exp\{-[(n+1)^2/n^2 + (n+2)^2]A\} - \exp[-(n+1)^4/(n+1)^2 A]$$

$$= \exp[-(n^2+2n+1)A]\{1+\exp[-(2n+5+4/n+1/n^2)A]+ \exp\{-[1 + 2/(n+1) + 1/(n+1)^2]A\}\} -$$

$$\exp[-(n^2+4n+4)A]\{1+ \exp[-(1 + 2/n + 1/n^2)] +\exp\{-[2n+7+4/(n+1)+1/(n+1)^2]A\}\}$$

$$\tag{A.26}$$

where $A = (\lambda_1/L_c)^2$, and by the fact that

$$1 + 2/n + 1/n^2 > 1 + 2/(n+1) + 1/(n+1)^2 \tag{A.27}$$

$$2n + 7 + 4/(n+1) + 1/(n+1)^2 > 2n + 5 + 4/n + 1/n^2 \tag{A.28}$$

$$n^2 + 4n + 4 > n^2 + 2n + 1 \tag{A.29}$$

thus

$$S + T + U > 0 \tag{A.30}$$

therefore

$$I_{10n}[2\lambda_1/(n-1)] - I_{10n}(2\lambda_1/n) > 0 \tag{A.31}$$

i.e. $I_{10n}(\Delta\lambda)$ is a monotonically increasing function about the discrete value of $\Delta\lambda$, where $\Delta\lambda = 2\lambda_1/(n-1)$ and $n \geq 2$.

Second, consider the situation that when $\Delta\lambda \ni [2\lambda_1/n, 2\lambda_1/(n-1)]$, in this case

$$\lambda_m/\lambda_a = 1 + 2\lambda_1/\Delta\lambda = n + \delta \tag{A.32}$$

where $0 < \delta < 1$, is a real and

$$\lambda_a = 2\lambda_1[1 - \lambda_1/(2\lambda_1 + \Delta\lambda)]$$

$$= [1 + 1/(n+\delta)]\lambda_1 \tag{A.33}$$

$$I_{10n}(\Delta\lambda) = I_{10n}(\delta)$$

$$= [1/I_{00}(\delta)]\{\exp[-(n\lambda_a/L_c)^2]\cos[\pi\delta/(n+\delta)] + \exp\{-[(n+1)\lambda_a/L_c]^2\}\cos[\pi(1-\delta)/(n+\delta)]\}$$

$$= [1/I_{00}(\delta)]\{\exp\{-[1+1/(n+\delta)]^2(n\lambda_1/L_c)^2\}\cos[\pi\delta/(n+\delta)] +$$

$$\exp\{-[1+1/(n+\delta)]^2[(n+1)\lambda_1/L_c]^2\}\cos[\pi(1-\delta)/(n+\delta)]\} \tag{A.34}$$

where

$$I_{00}(\delta) = 1 + \exp\{-[1+1/(n+\delta)]^2(\lambda_1/L_c)^2\}\cos[\pi/(n+\delta)] \tag{A.35}$$

When $n \gg \delta$, then $n + \delta \approx n$, it follows that

$$I_{10n}(\Delta\lambda) = I_{10n}(\delta)$$

$$= [1/I_{00}(\delta)]\{\exp[-(1+1/n)^2(n\lambda_1/L_c)^2\}\cos(\pi\delta/n) +$$

$$\exp\{-(1+1/n)^2[(n+1)\lambda_1/L_c]^2\}\cos[\pi(1-\delta)/n]\}$$

$$= M\{\cos(\pi\delta/n) + N\cos[\pi(1-\delta)/n]\}$$

where

$$M = \exp[-(1+1/n)^2(n\lambda_1/L_c)^2 / I_{00}(\delta)$$

$$= \exp[-(1+1/n)^2(n\lambda_1/L_c)^2] / \{1 + \exp[-(1+1/n)^2(\lambda_1/L_c)^2]\cos(\pi/n)\} \tag{A.36}$$

$$N = \exp[-(2n+1)(1+1/n)^2(\lambda_1/L_c)^2] \tag{A.37}$$

since

$$\partial I_{10n}(\delta)/\partial\delta = (M\pi/n)\{-\sin(\delta\pi/n) + N\sin[\pi(1-\delta)/n]\} \tag{A.38}$$

$$\partial^2 I_{10n}(\delta)/\partial^2\delta = (M\pi^2/n^2)\{-\cos(\delta\pi/n) - N\cos[\pi(1-\delta)/n]\} < 0 \tag{A.39}$$

so that $I_{10n}(\Delta\lambda) = I_{10n}(\delta)$ is a convex curve in the section $[2\lambda_1/n, 2\lambda_1/(n-1)]$.

Appendix B

Computer Programs for the Determination of the Largest Side Fringe

B.1. Two Wavelength Combination Source:

In order to determine the peak-to-peak values of the normalized fringe intensity I_{01n} and I_{10n}, the computer program was designed first to locate a series of fringe peak positions and calculate the corresponding fringe intensity values. This was achieved by continuously comparing the intensity values of three consecutive points separated by a small given OPD difference. If the intensity value at the middle point of the group was the largest, this point was considered to be the positive fringe peak position. On the other hand, if such a intensity value appeared to be the smallest, a negative fringe peak position was thus located. Hence the noramalized peak-to-peak values of the side fringes can be subsequently calculated. Furthermore, the value of I_{01n} can be easily found as it corresponds to the first side fringe next to the central fringe. From the variation of the fringe intensity values obtained in operating the computer program, the intensity value of the central fringe in the first side fringe packet, I_{10n}, can also be readily determined.

B.2. Multiwavelength Combination Source:

In a two wavelength combination source, the largest side fringe obtained is either I_{01n}, if the wavelength difference between the two laser diode sources is small, or I_{10n}, when the wavelength difference is relatively large. However, such a fact may not be the case for a multiwavelength combination source system, as any side fringe may become the largest one.

In a multiwavelength source, it is assumed there are wavelengths λ_1, λ_2 and λ_3, where $\lambda_1 \leq \lambda_2 \leq \lambda_3$, $\lambda_1 = \lambda$, $\lambda_2 = a\lambda$ and $\lambda_3 = b\lambda$. In order to select the optimum wavelength combination source (corresponding to the minimum signal-to-noise ratio required to identify the central fringe, SNR_{min}), the following procedures were adopted in the computer program.

1. For a given wavelength λ, an initial guess of the normalized value of the largest side fringe intensity, I', was made. The wavelength coefficients values a and b were chosen (b = a + nd, where n is an integer and d > 0, is a given small difference).

2. For each wavelength combination, all the side fringe intensity values were calculated. If the absolute value of the side fringe intensity was less than the predetermined value, I', then the corresponding wavelength coefficient values of a and b were printed out.

3. The values of b and then the value of a were changed step by step and at each step, the above process was repeated. The values of a were changed from 1 to 2 in 100 steps within which the valuea of b were increased from a to a + 1 in a similar manner.

4. If more than one pair of wavelength coefficients were found, I' was reduced.

5. The same procedure was repeated until only one pair of coefficients a_{opt} and b_{opt} satisfied the condition, i.e. all the side fringe intensities were less than the predetermined value, I'.

The wavelength conffieient pair obtained can be determined as the optimum wavelength coefficients and the corresponding wavelength combination λ, $a_{opt}\lambda$ and $b_{opt}\lambda$ was the selected optimum wavelength combination.

Appendix C

Publications by the Author

1. D. N. Wang, S. Chen, K. T. V. Grattan, A. W. Palmer and G. Dick, "A simple optical sensor with potential applications in eye length measurement", Proceedings of the Applied Optics Conference, Pub. IOP. Bristol, pp.56-58, Leeds, U.K., September 1992

2. D. N. Wang, G. Dick, S. Chen, K. T. V. Grattan and A. W. Palmer, "The use of short coherence length laser light for eye length measurement", Proceedings of the 14th Annual International Conference of the IEEE Engineering in Medicine and Biology Society, Pub. IEEE., pp.340-341, Paris, France, October 1992

3. S. Chen, D. N. Wang, K. T. V. Grattan, A. W. Palmer and G. L. Dick, "An optical fibre sensor for eye length measurement", Proceedings of the 9th International Optical Fiber Sensors Conference, pp.321-324, Firenze, Italy, May 1993

4. S. Chen, D. N. Wang, K. T. V. Grattan, A. W. Palmer and G. L. Dick, "A compact optical device for eye length measurement", IEEE Photonics Technology Letters, Vol.5, No.6, pp.729-731, June 1993

5. W. J. O. Boyle, G. L. Dick, K. T. V. Grattan, A. W. Palmer, D. N. Wang and K. Weir, "Optical instrumentation for eye length measurement using a short coherence length laser-based interferometer approach", Review of Scientific Instruments, Vol.64, No.11, pp.3082-3087, November 1993

6. Y. N. Ning, D. N. Wang, K. T. V. Grattan, A. W. Palmer and K. Weir, "A detailed study of synthesized light Sources for white-light interferometric systems", Proceedings of the second International Symposium on Measurement Technology and Intelligent Instruments, SPIE Vol. 2101, pp.19-27, Wuhan, P. R. China, October 29- November 5, 1993

7. D. N. Wang, Y. N. Ning, K. T. V. Grattan, A. W. Palmer and K. Weir, "Characteristics of synthesized light sources for white light interferometric systems", Optics Letters, Vol.18, No.22, pp.1884-1886, November 15, 1993

8. D. N. Wang, Y. N. Ning, K. T. V. Grattan, A. W. Palmer and K. Weir, "Three wavelength combination sources for white light interferometry", IEEE Photonics Technology Letters, Vol.5, No.11, pp.1350-1352, November 1993

9. D. N. Wang, Y. N. Ning, K. T. V. Grattan, A. W. Palmer and K. Weir, "The optimized wavelength combinations of two broadband sources for white light interferometry", IEEE/OSA Journal of Lightwave Technology, Vol.12, No.5, pp.909-916, May 1994

10. D. N. Wang, Y. N. Ning, A. W. Palmer, K. T. V. Grattan and K. Weir, "Multi-wavelength combination source — a novel technique for white light interferometry", Abstracts of IEEE/IEE International Conference on Applications of Photonic Technology: sensing, signal processing and communications, Toronto, Ontario, Canada, June 21-23, 1994

11. D. N. Wang, Y. N. Ning, K. T. V. Grattan, A. W. Palmer and K. Weir, "An optical Scanning Technique for White Light Interferometric System", IEEE Photonics Technology Letters, Vol.6, No.7, pp.855-857, July 1994

12. D. N. Wang, Y. N. Ning, K. T. V. Grattan, A. W. Palmer and K. Weir, "Scanning a White Light Interferometer Using a Tunable Laser", Proceedings of the 10th International Optical Fiber Sensors Conference, SPIE. Vol.2360, pp.592-595, 11-13 October, Glasgow, U.K. 1994

13. D. N. Wang, Y. N. Ning, K. T. V. Grattan, A. W. Palmer and K. Weir, "Optimized multiwavelength combination sources for interferometric use", Applied Optics, Vol.33, No.31, pp.7326-7333, 1 November 1994

14. D. N. Wang, Y. N. Ning, K. T. V. Grattan, A. W. Palmer and K. Weir, "An Alternative to White Light Interferometric Sensing", IEEE/OSA Journal of Lightwave Technology, Vol.13, No.5, pp.961-966, May 1995

15. D. N. Wang, B. T. Meggitt, K. T. V. Grattan, A. W. Palmer and Y. N. Ning, "Use of a Sm^{3+}-doped Fiber as a Low Coherence Light Source", IEEE Photonics Technology Letters, Vol.7, No.6, pp.620-622, June 1995

16. D. N. Wang, B. T. Meggitt, K. T. V. Grattan, A. W. Palmer and Y. N. Ning, "A two Wavelength Fiber Fluorescent Source", Presented in the 10th International Conference on Integrated Optics and Optical Fibre Communication, Hong Kong, June 26-30, 1995